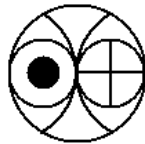


**QUATERNARY GEOCHRONOLOGY AND
PALAEOCLIMATOLOGY OF THE INDIAN
OCEAN**

MANISH TIWARI

Ph.D. Thesis

February 2005



Physical Research Laboratory

Ahmedabad – 380009, India

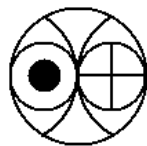
Quaternary Geochronology and Palaeoclimatology of the Indian Ocean

Thesis submitted to
**The Maharaja Sayajirao University of Baroda,
Vadodara, India**

For the degree of
Doctor of Philosophy in Geology

By
Manish Tiwari

February 2005



Planetary & Geosciences Division
Physical Research Laboratory
Ahmedabad – 380009, India

Certificate

I hereby declare that the work presented in this thesis is original and has not formed the basis for the award of any degree or diploma by any university or institution.

Manish Tiwari (author)

Planetary and Geosciences Division
Physical Research Laboratory
Ahmedabad – 380009, India

Certified by:

Prof. R. Ramesh (Guide)

Planetary and Geosciences Division
Physical Research Laboratory
Ahmedabad – 380009, India

Prof. P.P. Patel (Co-guide)

Department of Geology
The M.S. University of Baroda
Vadodara – 390002, India

To

My family

Their belief in me is my strength

This thesis is dedicated

Acknowledgement

At this stage of my career, I am short of words to express my feelings for the many persons who have shaped my life, work and personality. First of all I fondly remember the care and attention showered on me by my guide Prof. R.Ramesh. His analytical approach and attention towards minor details are a quality to be imbibed. He patiently taught me the nuances of paleoclimatology and is one of the best teachers I have come across. I thank him from the bottom of my heart for all he has done for me. In the same breath I remember Prof. B.L.K. Somayajulu who introduced me to the science of studying past climates. His erudite discourses on various topics were always a treat to hear and his enthusiasm towards life in general and science in particular never failed to lift the veil of gloom and recharged me. Thank you, Soma.

I am indebted to Drs. A.J.T.Jull, G.S.Burr and M.S.Sheshshayee for carrying out supporting measurements during the course of this study. Help and encouragement provided by Prof. P.P. Patel and Prof. L.S. Chamyal is duly acknowledged.

I owe special thanks to Prof. S. Krishnaswami whose intelligent remarks, critical comments and scientific approach made me strive for better. I am grateful to Prof. S.K. Bhattacharya who was instrumental in teaching me the intricacies of mass spectrometry and taking special interest in my work. Many thanks to Prof. M.M. Sarin for his constant support and valuable inputs during my work in the chemistry lab. I thank the members of the Academic Committee for reviewing my work from time to time and providing their constructive inputs. Sincere thanks are due to Prof. J.N. Goswami, Prof. N. Bhandari, Prof. A.K. Singhvi, Prof. S.V.S. Murthy, Prof. Kanchan Pande, Dr. S. K. Gupta, Dr. P.N. Shukla, Dr. G. Srinivasan, Dr. J.S Ray, Dr. S. Singh (Jyoti and Sunil for me) and Dr. D. Banerjee for their words of encouragement and critical comments during the area seminars.

I express my sincere gratitude to Prof. M.S. Srinivasan who initiated me into micropaleontology and oceanography. He has been a steady source of inspiration for me. I am thankful to Dr. Devesh Kr. Sinha for generating my interest in Geology and taking personal interest in my career. Thanks are due to Dr. Rahul Mohan for helping me choose the right direction after my masters and for being there whenever I need

him. With affection I remember Dr. Ashish Sarkar from whom I learnt the art of the isotopic analysis of foraminifera. Thanks a lot, Ashish da.

No amount of words is sufficient to express my love and respect for Ravi da and Yadav ji. They personally ensured that I get best of the facilities, were always there whenever I needed them and went out of the way to help me. My sincere thanks to Jani ji and Sanyal who made the isotopic measurements possible. Due thanks to Padia ji, Kamlesh, Bhavsar bhai, Vaghela bhai and V.G. Shah for helping me during the course of various experiments.

I gratefully acknowledge the help extended by Library staff, Computer Center personnel, Workshop, Glass blowing and Liquid Nitrogen section. Without their support this journey would not have been so smooth.

Friends are like flowers in the garden of life and by the God's grace I am blessed with many flowers who always keep my garden full of their aroma. They are too many to name here but some of the names that flash in mind are Manoj (chiku and very cool), Pathak (unsatisfied with the world), Sudhir (the coolest one), Prashanto (opposite to his name), Santosh (the great entertainer), Neeraj (something different), Sanjeev (born lucky but frastu), Thakur, PK, Gere and Das babu. I also remember with warmth the company provided by other members of the PRL farmhouse tea club meeting unfailingly at 10 o' clock, 3.30 and 5.30 pm weekdays. Without them life will loose half of its charm. God bless them.

I thank my parents, nani ji, sanu and bunny for standing by me for the duration of this work and always encouraging me to be a paragon in my field. I am indebted to my soul mate Kiran who was a pillar of support for me during the draining period of thesis writing. Her belief in me is my greatest asset.

I am very much thankful to ISRO-GBP for supporting this work.

Abstract

This study is an endeavor in paleoclimatic reconstruction of the Northern Indian Ocean with a special emphasis on deciphering the variations in Southwest (SW) Monsoon intensity during the Late Quaternary (~35,000 a BP to the present). Earlier, many studies regarding paleomonsoon variations were carried out in the Arabian Sea but most of them were confined to the western/northern Arabian Sea with little attention paid to other regions such as eastern and equatorial Arabian Sea, which are equally important. This thesis is an improvement over the previous work in the following ways:

- i. I have selected three sedimentary cores from three different locations of the Arabian Sea viz. western Arabian Sea off the Somalian coast (near the mouth of the Gulf of Aden), eastern Arabian Sea off the western Indian coast and the southern/equatorial Arabian Sea, east of Maldives. Thus I could study various processes that are manifestations of SW monsoon at different locations and delineate local versus regional responses.
- ii. Paleomonsoon studies from the western Arabian Sea invariably looked at proxies for the SW monsoon wind strength and not the monsoon precipitation. The response of these might differ significantly. By the study of equatorial and eastern Arabian Sea cores I have attempted to document the past variations in the SW monsoon precipitation.
- iii. The resolution of many of the previous studies in India was poor (typically ~2000 years/cm) because of which high-frequency/rapid changes were not detected. I have carried out high-resolution analysis on sub-centennial to centennial timescales that will facilitate the documentation of past monsoon variation in great detail.
- iv. Most of the earlier studies from India were based on the bulk radiocarbon chronology (e.g. Sarkar et al, 1990) that might be relatively inaccurate due to possible dead carbon contribution. I have obtained a large number of AMS dates on selected species of foraminifera that provide better chronological control.
- v. Further, a few studies relied on a single proxy (e.g. Gupta et al, 2003) that might mislead, as the observed variations might be an interplay of many competing processes. I have carried out multi-proxy chemical and isotopic analysis that corroborate each other and hence provide better confidence on the inferences.

The specific aims of this study are:

- 1) To document past monsoon variations on millennial to centennial scales by high-resolution sampling on accurately dated sediment cores.
- 2) To assess the strengthening of Northeast monsoon relative to SW monsoon by determining the past variations in the transport of low salinity water from the Bay of Bengal via the North East Monsoon Current using the equatorial core.
- 3) To assess how different locations/proxies respond to the same climatic forcing on different time scales by comparing the proxy data for wind strength from the western Arabian Sea with the proxy data for precipitation from the eastern Arabian Sea.
- 4) The proxies for SW monsoon precipitation were compared with the polar ice core records to assess the similarity of the low and high latitude climates.
- 5) The winds known as Indian Ocean Equatorial Westerlies (IEW) are strongest during the intermonsoon periods in the equatorial region and cause wind-induced mixed-layer deepening that enhances productivity. IEW exhibit a positive correlation with the Southern Oscillation index, which in turn is positively correlated with the SW monsoon, East African rains and negatively with El Nino frequency. Thus study of paleoproductivity variations in the equatorial core can trace the fluctuations in the IEW intensity and related phenomena.
- 6) The proposed solar connection with the SW monsoon has also been tested by comparing high-resolution $\delta^{18}\text{O}$ record with the reconstructed Total Solar Irradiance (TSI) curve along with the spectral analysis of various SW monsoon proxies.

To achieve the above objectives, various chemical (such as CaCO_3 , C_{org}) and isotopic proxies e.g. $\delta^{15}\text{N}$ in the sedimentary organic matter and $\delta^{18}\text{O}$, $\delta^{13}\text{C}$ of selected planktonic foraminiferal species were measured. The following inferences regarding the past monsoon fluctuation have been drawn by analyzing both the western and equatorial Arabian Sea cores. SW monsoon exhibits a decreasing trend since ~35 ka BP with a minimum at LGM. SW monsoon weakens during the early deglacial period as well and a sudden intensification is observed at ~14.5 ka BP, which coincides with the first step of deglaciation (T IA) that can be attributed to albedo changes over central Asia and Tibetan plateau. The glacial to Holocene transition period is

characterized by several millennial to centennial scale fluctuations in SW monsoon precipitation with higher precipitation during the periods of global warmth and reduced precipitation during cooler times. During 10 – 9 ka BP, another episode of monsoon intensification takes place that occurs just after the maximum summer insolation at ~10 ka BP between 20⁰N and 35⁰N. Thereafter SW monsoon strengthens during the Holocene as indicated by multi-proxy isotopic and chemical data. Monsoon does not appear to have decreased during the Holocene as proposed by some of the earlier single-proxy results from this region.

By high-resolution analysis of the eastern Arabian Sea core, we find a widespread arid period at ~2000 a BP as exhibited by the decline in precipitation on the southwest Indian landmass. Thereafter several arid periods are observed at ~1500 a BP, ~1100 a BP, ~850 a BP and ~500 a BP. A comparison with another study from the western Arabian Sea (Gupta et al, 2003) indicates that SW monsoon wind intensity exhibits an excellent correlation with the SW monsoon precipitation over southwestern coastal India on centennial scale. The weak winds were accompanied by reduced precipitation whereas stronger winds corresponded to enhanced precipitation. But this relation is not linear as minimum precipitation is found at ~2000 a BP while minimum SW monsoon winds is recorded at ~1500 a BP.

The equatorial core reveals that the effect of low salinity Bay of Bengal water is experienced during early deglacial period (~19 to ~17 ka BP) at the core site as Northeast Monsoon Current and hence the NE monsoon appear to strengthen during that time and not during LGM as proposed earlier based on bulk ¹⁴C dates (Sarkar et al, 1990).

Comparison with studies from the eastern Arabian Sea (Agnihotri, 2003 a) and western Arabian Sea (this study) has shown that IEW and SW monsoon winds declined and strengthened in tandem indicating a common forcing factor on a millennial scale, most probably insolation, at least during the last 35 ka.

Variations in the SW monsoon precipitation correspond very well with the polar $\delta^{18}\text{O}$ record with enhanced monsoons during interstadials and reduced precipitation during the stadials. This indicates that low latitudes could be instrumental in bringing about high latitude climatic changes by greenhouse gases or *vice versa* by albedo feedback.

This study has shown that IEW declined from ~35 ka BP to LGM with minimum values at LGM signifying decreasing SW monsoon and East African rains. A sudden intensification in IEW intensity is observed at ~14.5 ka BP and since then to the core top (~2.2 ka BP) including the Holocene, calcareous productivity exhibits a uniformly increasing trend. This implies a uniform strengthening of IEW (and perhaps the Southern oscillation index) and hence strengthening SW monsoon and east African rains along with a possibly declining El Nino frequency.

The high-resolution record from the eastern Arabian Sea was compared with the reconstructed Total Solar Irradiance curve for the past 1000 years. Broadly, the periods of lower TSI are accompanied by reduced SW monsoon precipitation whereas during the periods of higher TSI, the precipitation increases indicating a possible solar forcing on the SW monsoon on centennial timescale. Spectral analyses show that on Milankovitch timescales the SW monsoon is influenced by the insolation changes induced by precessional cycle of the earth's orbit. A common periodicity of $\sim 1400 \pm 500$ years is exhibited both by the monsoon proxies and the high latitude climatic proxies indicating perhaps a common linking mechanism. On centennial timescale the solar forcing seems to control the SW monsoon variations as exhibited by the common quasi-periodicity of ~200 yrs exhibited both by the monsoon proxies as well as solar activity proxy *viz.* TSI.

Thus this thesis in addition to documenting past variations in SW monsoon in great detail, provides a new and comprehensive data set for testing paleoclimate models. Further it raises several important points such as SW monsoon strengthening during the Holocene, NE monsoon intensification during the early deglacial period, good correlation exhibited by SW monsoon precipitation intensity with SW monsoon wind and high latitude climate. Moreover this study indicates that solar forcing appears to govern the SW monsoon on centennial and Milankovitch timescales.

Contents

	List of figures	(iv)
	List of tables	(vii)
Chapter 1	Introduction	1-17
1.1	Monsoon and the associated oceanographic effects.....	3
1.1.1	Southwest (SW) Monsoon.....	3
1.1.2	Northeast (NE) Monsoon.....	4
1.2	A brief review of the earlier work on past monsoon.....	8
	variations	
1.2.1	Western/Northern Arabian Sea.....	8
1.2.2	Eastern Arabian Sea.....	11
1.2.3	Equatorial Arabian Sea.....	12
1.3	Aims of the present study.....	14
1.4	Thesis outline.....	16
Chapter 2	Materials & Experimental Techniques	18-43
2.1	Collection and locations of the sediment cores.....	19
2.2	Foraminifera and their separation procedure.....	21
2.2.1	Separation of foraminifera.....	22
2.3	Radiocarbon chronologies.....	23
2.4	Isotopic and chemical proxies employed in this study.....	26
2.4.1	Oxygen isotopes.....	26
2.4.2	Carbon isotopes.....	31
2.4.3	Nitrogen isotopes.....	33
2.4.4	Biogenic Proxies.....	34
2.5	Analytical scheme followed to measure various.....	35
	proxies, their precisions and accuracies	
2.5.1	$\delta^{18}\text{O}$ and $\delta^{13}\text{C}$ measurements on foraminifera.....	35
2.5.2	Calcium Carbonate and Organic Carbon measurements.....	42
2.5.3	Nitrogen isotope measurements.....	43
Chapter 3	Eastern Arabian Sea: High Resolution Monsoon	44-
66		
	Reconstruction for the Past ~2800 years	
3.1	Introduction.....	45
3.2	Core location.....	46
3.3	Oceanographic conditions at the core site.....	46
3.4	Age-Depth Model.....	48
3.5	Precipitation Signals as Manifested by Oxygen Isotopes.....	49
3.6	Temporal variation in productivity.....	54
3.6.1	Productivity as manifested by CaCO_3 and C_{org} content.....	54

3.6.2	Productivity as manifested by $\delta^{13}\text{C}$	58
3.7	Temporal variation in the stable isotopes of nitrogen.....	60
3.8	The Solar connection.....	61
3.9	Spectral analysis.....	64
3.10	Inferences.....	65
Chapter 4	Equatorial Arabian Sea: SW Monsoon, NE Monsoon and Intermonsoon Variations during the Past 35,000 years	67-97
4.1	Introduction.....	68
4.2	Core Location.....	69
4.3	Oceanographic and Climatologic conditions at the core site...	70
4.4	Age-Depth Model.....	72
4.5	Oxygen isotope Analysis.....	73
4.5.1	SW Monsoon vs. NE Monsoon.....	73
4.5.2	Correlation with the high latitude temperature record.....	78
4.6	Temporal Variations in Productivity.....	84
4.6.1	Productivity as Exhibited by Calcium Carbonate Content.....	84
4.6.2	Regional climatic evolution: comparison..... with eastern Arabian Sea	87
4.6.3	Productivity as exhibited by Sedimentary Organic Matter.....	88
4.6.4	Productivity as exhibited by the $\delta^{15}\text{N}$	90
4.6.5	Productivity as exhibited by the carbon isotopes.....	92
4.7	Spectral Analysis.....	93
4.8	Inferences.....	95
Chapter 5	Western Arabian Sea: SW Monsoon History since the Last Glacial Maximum	98-121
5.1	Introduction.....	99
5.2	Core location.....	99
5.3	Oceanographic conditions at the core site.....	100
5.4	Age – Depth model.....	103
5.4	Downcore productivity variations in the core SS 4018 G.....	104
5.4.1	Productivity as manifested by CaCO_3 and C_{org}	104
5.4.2	Productivity as manifested by $\delta^{13}\text{C}$	109
5.4.3	Productivity as manifested by $\delta^{15}\text{N}$	110
5.5	Oxygen isotopic analysis.....	113
5.6	Spectral Analysis.....	116
5.7	Inferences.....	120

Chapter 6	Conclusions	122-130
6.1	Major Conclusions.....	123
6.1.1	Past variations in the SW monsoon intensity.....	123
6.1.2	NE monsoon intensification.....	124
6.1.3	Correlation between SW monsoon wind strength..... and SW monsoon precipitation	125
6.1.4	Correlation between SW monsoon precipitation..... and high latitude climate	125
6.1.5	Past variations in the IEW and the reliable SO index,..... SW monsoon, East African rains and El Nino frequency	126
6.1.6	Regional Climatic evolution.....	127
6.1.7	The solar influence.....	127
6.1.8	Limitations of Corg, $\delta^{15}\text{N}$ and $\delta^{13}\text{C}$ at the..... equatorial core site	128
6.2	Recommendation for future studies.....	128
References		131-161

List of Figures

Figure no.		Page no.
1.1	A schematic representation of identified current branches during the Southwest monsoon.....	5
1.2	Schematic representation of surface circulation in the Indian Ocean during the NE monsoon.....	6
2.1	Locations of the sediment cores employed in this study along with the Arabian Sea bottom topography.....	20
2.2	Schematic diagram of CO ₂ preparation using CAPS and the Mass Spectrometer inlet system.....	38
3.1	Locations of the core SK145-9 and other cores with which it has been compared.....	46
3.2	September Salinity contours in the eastern Arabian Sea.....	47
3.2	Calibrated radiocarbon ages and sedimentation rates (cm/ka) for various intervals in the core SK145-9.....	48
3.4	Downcore variations of $\delta^{18}\text{O}$ of three species of foraminifera in the core SK 145-9 shown along with % <i>G.bulloides</i> data from the ODP Site 723A.....	51
3.5	Downcore variation of CaCO ₃ , C _{org} and C/N ratio in the core SK145-9 covering the last ~2800 years.....	55
3.6	Downcore variation of $\delta^{13}\text{C}$ of the three species of foraminifera in the core SK 145-9.....	58
3.7	Downcore variation of $\delta^{15}\text{N}$ of sedimentary organic matter in the core SK145-9.....	60
3.8	Comparison of the TSI data and precipitation proxies for the past 1200 years.....	63
3.9	Power spectra of oxygen isotope timeseries in 3 species of foraminifera.....	64

Figure no.	Page no.	
4.1	Locations of the core SS3827 G and other cores with which it has been compared.....	69
4.2	The inflow of low salinity water from the Bay of Bengal into the Arabian Sea along the NMC in the month of December..	71
4.3	Calibrated Radiocarbon ages and sedimentation rates for the core SS 3827G.....	72
4.4	Temporal variations in the oxygen isotope ratios ($\delta^{18}\text{O}$) of three species of foraminifera in the core SS3827 G.....	75
4.5	Comparison of the $\delta^{18}\text{O}$ record of the core SS3827 G with the GISP2 $\delta^{18}\text{O}$ record.....	78
4.6	Downcore variation of CaCO_3 (%) in the core SS3827 G for the past 35 ka.....	84
4.7	Comparative study of the core SS3827 G with other cores from eastern Arabian Sea viz. SS3104 G and SS3101 G.....	87
4.8	Downcore variations of C_{org} plotted along with CaCO_3 (%) and C/N ratio.....	89
4.9	Downcore variation of $\delta^{15}\text{N}$ in the core SS3827 G for the past 35 ka.....	90
4.10	$\delta^{15}\text{N}$ vs. Nitrogen content for all the three cores viz. SS3827 G, SS4018 G and SK 145-9 analyzed in this study.....	91
4.11	Downcore variation of $\delta^{13}\text{C}$ values of the three species of planktonic foraminifera in the core SS3827 G.....	92
4.12	Power spectra for various paleoclimatic proxies of the core SS3827 G.....	94
5.1	Locations of core SS 4018G and other cores with which it has been compared.....	100
5.2	SST contours (in $^{\circ}\text{C}$) during August.....	102
5.3	Calibrated radiocarbon ages and sedimentation rates for SS4018G....	104

Figure no.	Page no.
5.4	Downcore variations of productivity proxies in the core SS 4018 G..... 106
5.5	Downcore variation of $\delta^{13}\text{C}$ of three species of foraminifera..... 109
5.6	Plot showing the downcore variation of $\delta^{15}\text{N}$ of the sedimentary organic matter in the core SS4018 G..... 110
5.7	Downcore variation in $\delta^{18}\text{O}$ of three species of foraminifera in the core SS4018 G..... 114
5.8	Power spectra for various paleoclimatic proxies of the core SS4018 G..... 119

List of Tables

Table no.		Page no.
2.1	Particulars of the sediment cores analyzed in this study.....	20
2.2	Radiocarbon ages.....	25
2.3	Z-Carrara $\delta^{13}\text{C}$ and $\delta^{18}\text{O}$ values with respect to PDB in per mil.....	41
2.3	Ammonium sulphate standard $\delta^{15}\text{N}$ values in per mil with respect to air.....	43

Chapter 1

Introduction

Paleoclimatology of the northern Indian Ocean is very closely related to the phenomenon of monsoon. India in particular is very sensitive to fluctuations in monsoon as its economy largely depends on agriculture and a poor monsoon affects millions of lives. Similarly devastating floods and untimely intense precipitation due to an above normal monsoon episode would destroy crops and property. Moreover global warming due to increased greenhouse gases in the atmosphere with the accompanying global changes is now a reality (Houghton et al, 2001). It has been estimated that the average surface temperature of the earth has increased by 0.6°C over the twentieth century (Mann et al, 1998) that has possibly led to the reduction of snow cover and an increase in the sea level. It is estimated that during the past century the precipitation has increased by 0.5% to 1% per decade for most of the mid- and high latitudes of the northern hemisphere continents and 0.2% to 0.3% for the tropical (10°S to 10°N) land areas. It was observed that in parts of Asia and Africa, the frequency and intensity of droughts increased (Houghton et al, 2001) in the period from 1900 to 1995 AD. Potential impact of global change on water resources include enhanced evaporation due to warming, geographical changes in precipitation intensity, duration and frequency affecting the average runoff, soil moisture and the frequency and severity of droughts and floods. Future projections using climate models point to an increase in the monsoon rainfall in most parts of India with increasing greenhouse gases and sulphate aerosols (Rupa Kumar et al, 2002). Many north Indian rivers such as the Ganga, Yamuna etc. have shown a sharp decline in the summer discharge in the recent past, possibly due the shrinking of the Himalayan glaciers that feed them (Gosain and Rao, 2003). These observations lead us to an important question whether this is a consequence of global warming or only a part of the low frequency climate variability inherent in the system. To answer this would require reliably dated, high-resolution records of the past monsoonal precipitation. Monsoon is known to exhibit variance over a range of periods such as annual, decadal and centennial to millennial time scales. Annual to decadal scale variations can be studied using the recorded meteorological data, which date back to the past 150 years. But even this is available for the big cities only, where weather stations are located. For studying the low frequency variations on centennial to millennial timescales, we have to take recourse to various paleoclimatic proxies such as sediments deposited in

the Indian Ocean and various lakes, ice deposited in Tibetan/ Himalayan glaciers, speleothems etc. If suitable cores from appropriate regions (such as continental margins) are available, we can explore paleomonsoon variations on centennial to decadal time scales (comparable to human lifetime).

1.1. Monsoon and the associated oceanographic effects:

Monsoon is the one of the most important planetary scale phenomena involving atmosphere-ocean-terrestrial vegetation/albedo systems. It envelops large parts of the globe from 25°S to 35°N and 30°W to 170°E (Ramage, 1971) covering western and eastern Africa, Indian subcontinent, Southeast Asia, northern Australia and even some parts of southwestern USA. There is a lack of precise definition of monsoon as differences prevail among various workers whether it should be defined according to precipitation or wind. But broadly monsoon is described as system of winds confined to the tropics that exhibits marked seasonal shifts in their direction that persist for a long time and commence due to the differential heating of land and the sea (Webster, 1987) and the solar induced seasonal shifting of the intertropical convergence zone (ITCZ, Charney, 1969; Gadgil, 2003). Infact the word monsoon is derived from the Arabic word “Mausam”, which stands for season and was first experienced by Arab sailors traversing the Arabian Sea who noted a persistent reversal of the wind at the same time every year. The most pronounced monsoon occurs over the Indian subcontinent and is the lifeline of the countries influenced by it. The Indian monsoon is further divided into two parts:

1.1.1 Southwest (SW) Monsoon: The continents surrounding the Arabian Sea receive a large amount of heat during the summer in Northern hemisphere, as sun is directly overhead (summer solstice). Because of this a low-pressure system develops over Arabia, northwest Indian subcontinent and the Tibetan plateau with pressures as low as 994 mb. On the other hand, high atmospheric pressure exists over the relatively cold southern subtropical Indian Ocean (~25°S) with pressures upto 1020 mb (Rao, 1976) with a maximum pressure of 1026 mb observed around the so-called “Mascarene High” off the southeast coast of Madagascar. This causes the SE trade winds to rush into the low-pressure region, which become southwesterly after crossing the equator

resulting in the “summer or SW monsoon”. The major part of the rushing winds follow what is known as the “Findlater Jet”, which is a low level jet stream at a height of 1 – 1.5 km with wind speeds upto 15 m/s (Hastenrath and Lamb, 1979). This jet originates around Mauritius and Northern Madagascar and strikes the Kenyan coast at 3⁰S after which it traverses the plains of Kenya, Ethiopia, Somalia and emerges out of the Somalian coast at ~9⁰N. Thereafter it splits into two branches at ~55⁰E with one striking the western coast and the other going around the southern tip of India and over southern Sri Lanka (Findlater, 1981). These moisture-laden winds cause abundant precipitation over India from June to September and release latent heat in the troposphere, which further intensifies it (Webster, 1987). As most of the rainfall (~70 %) over India occurs during the summer months, the word monsoon in India usually refers to the Southwest monsoon precipitation.

1.1.2 Northeast (NE) Monsoon: During the northern hemisphere winter an intense surface high pressure system develops in the east Asian continent south of the Lake Baikal with pressures upto 1035 mb, whereas low pressure (~1110 mb) exists over the southern subtropical Indian Ocean due to the radiation it receives from the sun directly overhead (winter solstice). Due to the pressure difference air rushes towards the south of the equator causing intense precipitation over southeastern India, Sri Lanka, Malaysia and Indonesia. In the Indian context “winter or NE monsoon”, which extends from mid-October to January is important as it the major rainy season for the southeastern India and accounts for ~50 % of the annual rainfall over the coastal Tamilnadu (Das, 2002). Unlike the summer monsoon, which occurs more or less continuously, the NE monsoon occurs in spells of 3-4 days of heavy rains interrupted by long dry periods with little or no rain. Sometimes big cyclones form in the Bay of Bengal and cause intense precipitation/floods in peninsular India.

During the summer and winter monsoons the surface oceanic circulation in the Northern Indian Ocean including the Arabian Sea and the Bay of Bengal experiences drastic changes in direction in consonance with the changing overlying wind patterns (Wyrki, 1973) as shown in Figs. 1.1 and 1.2. The circulation patterns for the eastern,

equatorial and western Arabian Sea are further discussed in detail in sections 3.3, 4.3 and 5.3 respectively.

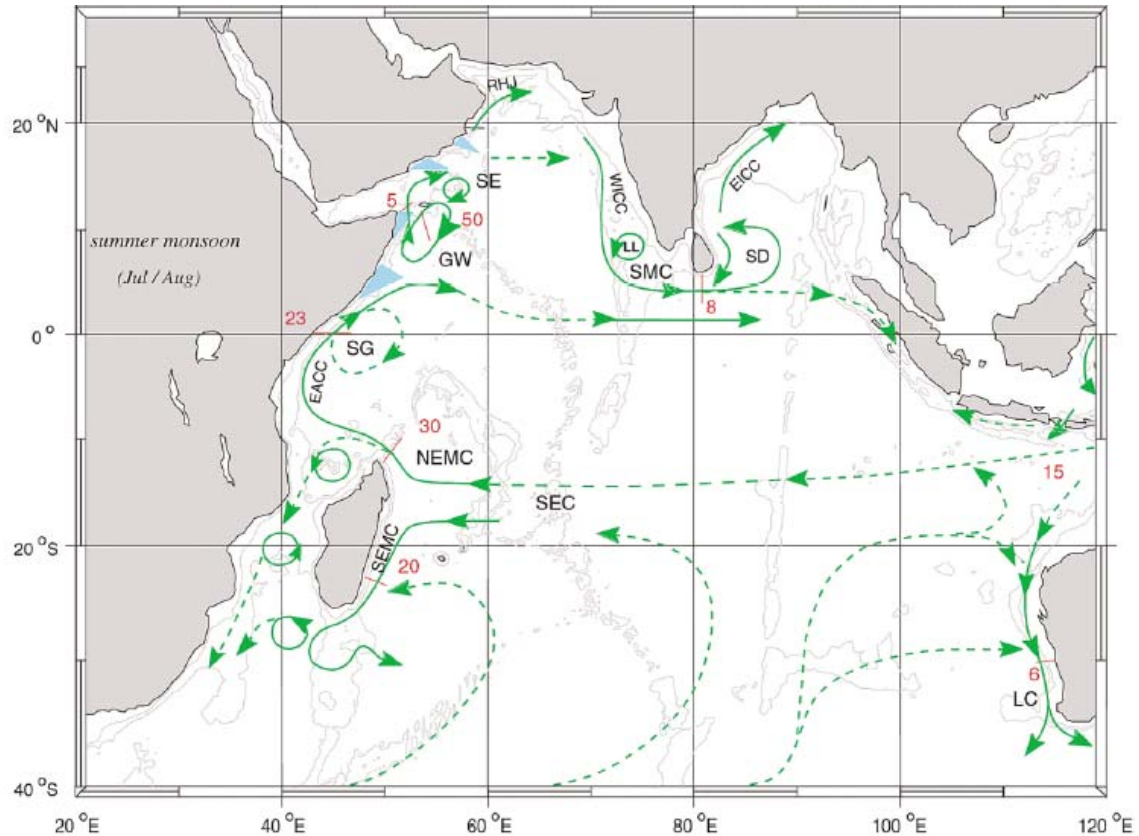


Fig. 1.1. A schematic representation of identified current branches during the Southwest monsoon, including some choke point transport numbers ($Sv = 10^6 \text{ m}^3 \text{ s}^{-1}$). Current branches indicated (see also Fig. 1.2, next page) are the South Equatorial Current (SEC), South Equatorial Countercurrent (SECC), Northeast and Southeast Madagascar Current (NEMC and SEMC), East African Coast Current (EACC), Somali Current (SC), Southern Gyre (SG) and Great Whirl (GW) and associated upwelling wedges, Socotra Eddy (SE), Ras al Hadd Jet (RHJ) and upwelling wedges off Oman, West Indian Coast Current (WICC), Laccadive High and Low (LH and LL), East Indian Coast Current (EICC), Southwest and Northeast Monsoon Current (SMC and NMC), South Java Current (JC) and Leeuwin Current (LC) (from Schott and McCreary, 2001). Shaded regions (blue) along the Somalia and Oman margins represent upwelling centers.

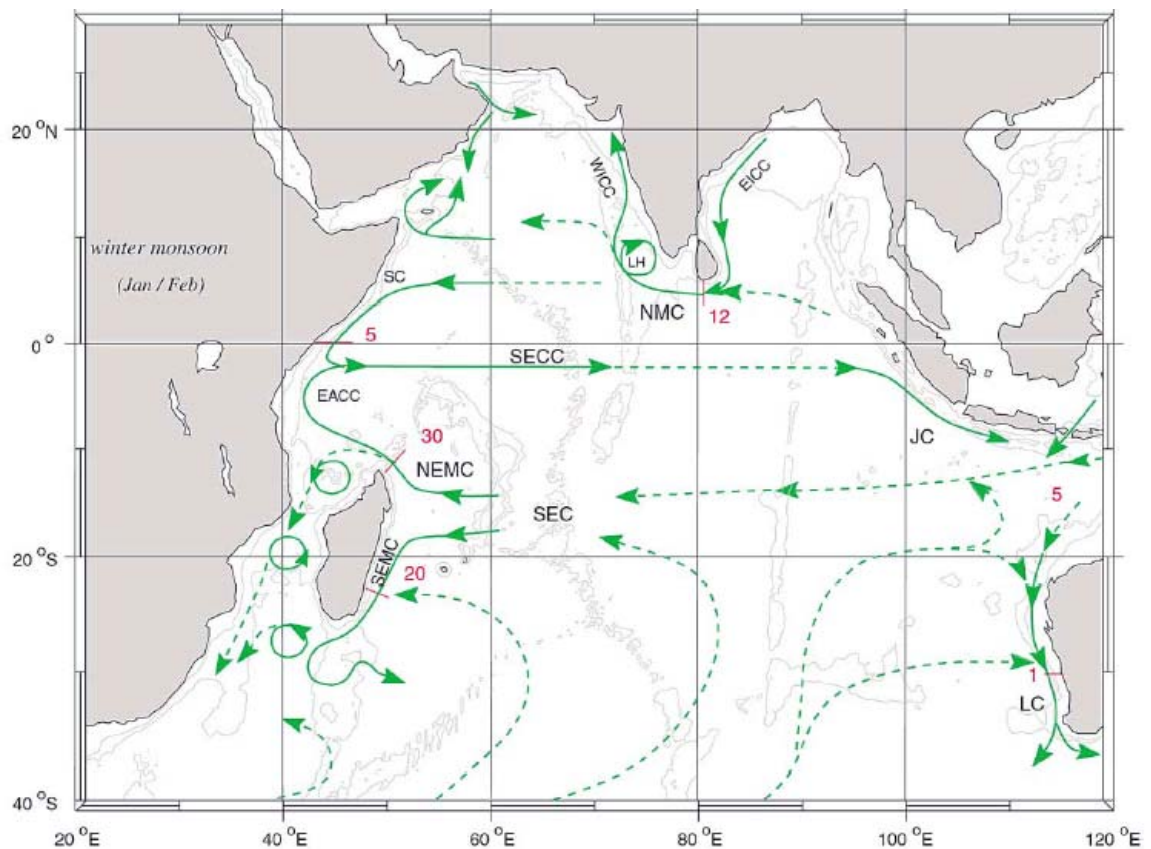


Fig.1.2. Schematic representation of surface circulation in the Indian Ocean during the NE monsoon (from Schott and McCreary, 2001). The captions for various current branches are the same as in the Fig 1.1 (see previous page).

One of the major features of the SW monsoonal circulation is the occurrence of an upwelling zone along the Somalian and Oman coasts, which causes intense biological and geochemical changes in this region with SST falling by $\sim 4^{\circ}\text{C}$ as nutrient rich deeper water surfaces that enhances the sea surface biological productivity considerably (Wyrтки, 1973; Nair et al, 1989; Haake et al, 1993 b). Weak upwelling also occurs along coastal southwest India (Wyrтки, 1973; Shetye, 1984). During the Northeast monsoon the surface circulation reverses completely with minor upwelling observed in the northeastern Arabian Sea (Wyrтки, 1973). The cold and dry NE monsoon winds causes the deepening of the mixed layer to a depth of 100 – 125 m due to convective mixing in the northern Arabian Sea, which leads to nutrient

injection and hence high productivity during winter monsoon in this region (Banse and McClain, 1986; Madhupratap et al, 1996). The typical productivity values for the western Arabian Sea are 2.0, 1.0 and 0.5 g C/m²/day for the SW monsoon, NE monsoon and the intermonsoon periods respectively (Codispotti, 1991; Barber et al, 2001). Similarly for the eastern Arabian Sea the typical productivity values are 0.6, 0.3 and 0.2 g C/m²/day for the SW monsoon, NE monsoon and the intermonsoon periods respectively (Bhattathiri et al, 1996). Along the west coast of India lies a chain of hills (with a typical altitude of 1000 – 2000 m) known as the Western Ghats. The moisture laden SW monsoon winds approach the Ghats from the west and are forced to ascend in the process of which they shed copious amounts of precipitation over the Western Ghats. All this fresh water gets into the coastal Arabian Sea, which reduces the sea surface salinities considerably during the SW monsoon season (Sarkar et al, 2000). Another phenomenon of importance is denitrification that takes place due to the very low concentration of oxygen in the entire Arabian Sea from 250 m to 1250 m water depths (Naqvi, 1987, Wyrki, 1971; Deuser et al, 1978, Olson et al, 1993). This oxygen minimum zone (OMZ) is due to the high oxygen consumption below the thermocline for the oxidation of organic matter supplied by the high overhead surface productivity. Furthermore the sluggish flow of the oxygen poor intermediate water (Olson et al, 1993; You and Tomczak, 1993) along with a strong tropical thermocline (due to relatively high SST that prevents mixing of the oxygen rich surface waters with the deeper waters) maintains the OMZ (Spencer et al, 1982; Qasim, 1982). Although the OMZ and denitrification are not directly affected by the monsoon winds but the ensuing productivity along with other climate controlled factors such as ocean ventilation rate (Reichart et al, 1997, 1998, 2002 a; Schulz et al, 1998; Altabet et al, 2002) affect them.

Such pronounced changes in the seawater characteristics make the Arabian Sea ideal for deciphering the past changes in monsoon intensity. The surface productivity that manifests itself in many forms such as organic, calcareous and siliceous productivity, also affects the carbon isotopic composition of the seawater, which is preserved in the calcitic shells of various foraminifera. Similarly the SST and sea surface salinity alter the oxygen isotopic composition of these shells and they get preserved in the sea sediments. The nitrogen isotopic composition of sedimentary

organic matter can indicate the denitrification intensity relatable to productivity variations. Thus the downcore variations of such proxies could help document the past variations in monsoon intensity and the related climatic changes. The suitability of these proxies for paleoclimatic reconstruction is further discussed in section 2.4.

1.2. A brief review of the earlier work on past monsoon variations:

1.2.1. Western/Northern Arabian Sea:

The western Arabian Sea has received maximum scientific attention for deciphering the past monsoon fluctuations as it experiences the most intense biogeochemical changes during the monsoon season. The earliest and very comprehensive studies were carried out by Prell et al (1980), Prell (1984), Prell and Van Campo (1986) in which they found that SW monsoon was weaker during the glacial periods and stronger during interglacials. They further asserted that much of the 10^3 to 10^5 year variability in the monsoon is due to the changes in solar radiative forcing and the associated feedback effects. Prell and Kutzbach (1987) proposed that glacial boundary conditions such as SST, earth's albedo, sea level, extent and elevation of large ice masses play equally important roles in modifying monsoon patterns. Later Clemens et al (1991), Clemens and Prell (1991) argued that monsoon is mainly governed by the precession induced insolation changes and not by the changing glacial boundary conditions. Several authors such as Gasse et al (1991), Anderson and Prell (1992), Sirocko et al (1993), Van campo and Gasse (1993), Overpeck et al (1996) refuted this hypothesis and maintained that glacial boundary conditions indeed are instrumental in modifying monsoon intensities. Sirocko et al (1993) carried out a high resolution, centennial scale study on a core off the Oman coast and reported that monsoonal climate changed in abrupt steps and not in a gradual manner with increase in its intensity observed at ~15.5 ka BP and a maximum at ~8.5 ka BP, which they attributed to albedo changes during the periods of deglaciation. Sirocko et al (1996) proposed that SW monsoon intensified at 11.4 ka BP that coincides with the climate transition as observed in polar ice cores and hence proposed that monsoon exhibits correlation with the high latitude climatic changes. Naidu and Malmgren (1996) analyzed the cores from the western Arabian Sea

upwelling regions and concluded that SW monsoon was relatively stronger during 22 – 18 ka BP than ~18 – 13.8 ka BP with a major intensification at 13 ka BP and a maximum between 10 and 5 ka BP, after which it declined with the weakest phase at 3.5 ka BP. Naidu and Malmgren (1995) also observed a sub-Milankovitch periodicity of 2,200 years exhibited by the SW monsoon induced upwelling indices from which they inferred that SW monsoon is influenced by oceanic circulation changes that controls the ~2,300 year periodicity, observed in atmospheric ^{14}C . They also extensively measured CaCO_3 and stable isotopes of carbon and oxygen in foraminifera and concluded that lower CaCO_3 in the western Arabian Sea during interglacials along with higher $\delta^{13}\text{C}$ is due to higher non-carbonate productivity and higher dissolution of CaCO_3 due to enhanced Antarctic Bottom Water ventilation in the equatorial Indian Ocean (Naidu et al, 1993; Naidu and Malmgren, 1999). Altabet et al (1995) and Ganeshram et al (2000) have shown that in the western Arabian Sea denitrification intensity is controlled by SW monsoon induced productivity changes, which was weaker during the glacials and stronger during interglacial periods.

Reichart and coworkers have carried out extensive work regarding the monsoon and oxygen minima zone (OMZ) variability for the late Quaternary (covering the past ~225 ka) in the northern Arabian Sea. Reichart et al (1997) studied productivity and dust input records in a core from Murray Ridge (Northern Arabian Sea) and concluded that productivity in this region is mainly controlled by the SW monsoon and the intensity of OMZ is governed by the sea surface productivity, which was lower during the weak SW monsoon that occurred during glacial periods. Reichart et al (1998, 2002 a) showed that OMZ and SW monsoon strength varied in synchronicity with polar ice records. The stadials as deciphered by the polar records are characterized by light colored, bioturbated sediments with low C_{org} implying weak OMZ due to reduced productivity that in turn is because of weaker SW monsoon. Reichart et al (1998, 2002b) showed that during stadials the OMZ was destroyed because of deep convective overturning due to intensified cool and dry winter monsoon winds that led to surface water cooling and enhanced the salinity due to evaporation. Reichart et al (2004) further showed that just after strong stadials at stadial-interstadial boundaries, a brief episode of hyperstratification takes place due to weakened winter monsoon (and hence less cooling due to evaporation) that facilitates

the formation of strong OMZ during interstadials. Schulz et al (1998) and Altabet et al (2002) studied the monsoon induced OMZ variability by analyzing the C_{org} content in cores from the northern Arabian Sea and denitrification intensity in cores from the Oman margin. They showed that monsoon intensity is closely related with the GISP2 ice core record even on short centennial timescales with reduced monsoon during the cooler periods and concluded that high latitude and tropical climates are most probably linked via rapid atmospheric forcing. Leuschner and Sirocko (2000) studied three cores from the northern Arabian Sea analyzing the aeolian dust content that represents humid/arid continental climate and found that it exhibits good correlation with the GISP2 and Vostok ice records with humid periods coinciding with the temperature maxima. Zonneveld et al (1997) obtained a core from the Somalian upwelling region and studied the relative dominance of dinoflagellates cysts of the (SW) monsoon-induced upwelling and non-upwelling species. They found that broadly, monsoon follows the insolation forcing, which is nonlinear due to the effect of snow cover over the central Asia and Tibetan plateau. Other forcing factors, which they identified, are the changing glacial – interglacial boundary conditions (due to varying thermohaline circulation) and tropical land cover forcing (that influences the albedo). Von Rad et al (1999) and Luckge et al (2001) analyzed varve sequences in cores from the northern Arabian Sea raised from OMZ and studied monsoon variations for the past 5000 years. They deduced that precipitation decreased after ~4 ka BP with minima centered at ~2 ka BP and ~500 a BP with higher precipitation during the intervening periods. Burns et al (1998) studied the speleothems from northern Oman covering the past 125 ka and concluded that early Holocene (~10 – 6 ka BP) was a wetter period than the modern times and the last interglacial was even wetter than the early Holocene. They further asserted that precipitation records from the continents do not always match with the sedimentary productivity records, as the latter are essentially wind strength indicators and not precipitation proxies. Neff et al (2001) studied $\delta^{18}O$ in stalagmites from northern Oman and compared with the $\Delta^{14}C$ record from tree rings that reflects changes in solar activity. They found an excellent correlation that led them to conclude that monsoon is controlled by the solar activity on a decadal to centennial scale. Fleitmann et al (2003, 2004) reconstructed the history of SW monsoon from speleothem records from southern Oman for the past

~10 ka and proposed that early monsoon variations are controlled by glacial boundary conditions and monsoon decreased after ~8 ka with the solar induced forcing controlling the decadal to multi-decadal variations. Recently Anderson et al (2002) and Gupta et al (2003) determined the abundance of *G.bulloides* in cores from the Oman upwelling margin and found excellent correlation with the North Atlantic sedimentary records and concluded that SW monsoon exhibits excellent correlation with the high latitude climate on centennial timescales (weak summer monsoon coincides with cold periods). They showed that monsoon broadly follows the insolation curve at 65°N with a monsoon maximum at ~8.5 ka BP and declining since then upto ~1.5 ka BP. They further proposed that monsoon strength has been increasing for the past 400 years due to northern hemisphere warming and will continue to do so as the greenhouse gases concentration increases.

1.2.2. Eastern Arabian Sea:

One of the earliest studies involving the cores from the northern Indian Ocean was carried out by Duplessy (1982) who reconstructed the Holocene and LGM sea surface conditions such as salinity and temperature based on oxygen isotopic analysis of the surface dwelling foraminifera *G.ruber* from the cores spread all over the Bay of Bengal and the Arabian Sea. He concluded that SW monsoon was weaker during the LGM and NE monsoon was stronger than present with more precipitation south of 10°N. Sarkar et al (1990) analyzed a core from the eastern Arabian Sea and proposed that winter monsoon was stronger during LGM as evident by enhanced NE monsoon current during that time. They based their conclusion on the negative excursion shown by oxygen isotope in four different species of foraminifera, which they attributed to influx of enhanced low salinity water via the NE monsoon current and SST increase due to vanishing of SW monsoon induced mixed layer deepening. Sarkar et al (1993) inferred that anoxic conditions prevailed in the deep Arabian Sea during the last glacial period based on enhanced preservation of organic matter and simultaneous removal of uranium in seawater in a core from eastern Arabian Sea. Sarkar et al (2000) carried out oxygen and carbon isotopic analysis on the planktonic foraminifera *G.sacculifer* and *G.menardii* in cores off the west coast of India. They inferred that excess of evaporation over precipitation (E-P) has decreased steadily from the 10 ka BP to ~2 ka BP implying a steady increase in the SW monsoon precipitation during

the Holocene. Thamban et al (2001) measured the oxygen and carbon isotopes in planktonic and benthic foraminifera along with CaCO_3 and C_{org} content from the eastern Arabian Sea near Cochin. They concluded that major increase in SW monsoon precipitation occurred after ~9 ka BP and in contrast to western Arabian Sea records the productivity in this region was lower during 13 - 6 ka BP and was maximum between ~18 – 15 ka BP, which they attributed to increased strength of winter monsoon that led to greater nutrient injection due to enhanced convective mixing. Agnihotri et al (2003 a) studied various sedimentary proxies regarding productivity such as CaCO_3 , C_{org} , nitrogen, Sr and Ba etc. in the cores from eastern Arabian Sea and concluded that surface productivity was lower during the last glacial-interglacial transition and higher during the Holocene. Agnihotri et al (2003 b) found increasing denitrification intensity in a core from the eastern Arabian Sea from ~10 – 2 ka BP that implies an increasing SW monsoon intensity during Holocene. Bhushan et al (2001) calculated the paleoproductivity in the same core mentioned above using the burial flux of CaCO_3 and C_{org} and inferred that SW monsoon intensity increased from ~10 ka to ~2 ka BP. Agnihotri et al (2002) measured the monsoon proxies such as C_{org} , N and Al in a core off the Saurashtra coast for the past millennium and compared with the past variations in the total solar irradiance (TSI) reconstructed from the production rate of cosmogenic ^{14}C and ^{10}Be . They found that SW monsoon exhibits good correlation with the solar activity with reduced monsoon during the periods of solar minima. Yadava and Ramesh (2005) analyzed speleothems samples with very high resolution (~14 years) from Orissa, eastern India, that covers the past ~3500 years and found that SW monsoon was stronger between 3400 and 3000 years with arid periods at ~2000 and 1730 a BP and an enhanced monsoon at ~600 a BP.

1.2.3. Equatorial Arabian Sea:

Studies from the equatorial Arabian Sea are very sparse compared to other parts of the Arabian Sea. A giant piston core MD900963 has been obtained east of the Maldives covering the past 910 ka. Rostek et al (1993) measured the oxygen isotopes in the *G.ruber* in this core and inferred that glacial stages were characterized by increased evaporation and/or decreased precipitation, which they attributed to enhanced dry NE monsoon and/or reduced SW monsoon. Various other studies such as Beaufort et al (1997), Rostek et al (1997), Schulte et al (1999), Paillet et al (2002)

were carried out on the core MD900963. They inferred that primary productivity in this region was enhanced during the glacial periods and was lower during the interglacial periods in contrast to other productivity records from the Arabian Sea. They attributed it to increased convective overturning due to stronger NE monsoon winds that led to nutrient injection in the surface layer and hence increasing the productivity. In all the studies, the productivity proxies exhibit a ~23 kyr precession cyclicity induced by insolation variations. Furthermore they maintain that deep water at this site remained oxygenated for the past 350 ka.

Thus the broad picture regarding the paleomonsoon variation that emerges out of the above discussion is that SW monsoon was stronger during interglacials and weaker during glacial periods with the NE monsoon exhibiting the opposite behaviour. The intensity of monsoon is basically controlled by the sun-earth geometry and the consequent insolation changes. The monsoons are mainly governed by precessional cycle of the earth. It has been verified using the paleoclimate models that the tropical climate is affected more by the precession of the earth's perihelion, while high latitudes are more affected by the changes in earth's obliquity (Kutzbach, 1981; Jagadheesha et al, 1999). A crude understanding is that snow cover increased over the Tibetan plateau/ central Asia during LGM that reduced the land – ocean temperature contrast during summer and enhanced it during winter that led to weakened SW monsoon and strengthened winter monsoon. The monsoon system is further affected by high latitude cooling shown by proxies for North Atlantic Deep Water formation, ice rafting etc. and surface feedbacks such as vegetation (through changes in Albedo, surface friction and evapotranspiration). During the early Holocene, the SW monsoon intensified with a maximum at ~8 – 9 ka BP and declined since then in accordance with the decreasing summer insolation as inferred from the productivity proxies, which are manifestation of SW monsoon wind alone. On the contrary, precipitation proxies indicate that SW monsoon has consistently increased from 10 ka BP to ~2 ka BP. Thus more well dated, high-resolution cores are needed to answer the question that how good is the correlation between the wind and rain proxies from the western and eastern Arabian Sea on different timescales and whether increasing wind intensity in the west (sea) always favours enhanced precipitation in the east (land) or not.

1.3. Aims of the present study:

My study area is the Arabian Sea, which forms a major and distinctive part of the Northern Indian Ocean. The Arabian Sea is most suited for monsoonal studies as it experiences intense biogeochemical changes associated with monsoons (Nair et al, 1989; Overpeck et al, 1996). The Arabian Sea can be divided into three distinct regimes as far as paleomonsoon reconstruction is concerned: (i) Western Arabian Sea, off the Somalian coast (near the mouth of the Gulf of Aden): it experiences intense upwelling during southwest monsoon resulting in increased organic/inorganic productivity (Nair et al, 1989) and negligible fresh water run off due to meager precipitation over adjoining landmass. (ii) Eastern Arabian Sea off the Western Indian coast: it experiences moderate upwelling along the coastal regions of western India and copious fresh water runoff due to intense precipitation (1000-4000 mm/yr) on adjoining land (between Mumbai and Cochin) (Sarkar et al, 2000). And finally (iii) Southern/ equatorial Arabian Sea (east of Maldives), which represents the open ocean regime, which experiences moderate equatorial upwelling/ wind induced mixed layer deepening. In addition part of it receives low salinity water from the Bay of Bengal. Most importantly, the strongest winds are during the intermonsoon period (spring & fall) that are called as Indian Ocean Equatorial Westerlies (Hastenrath et al, 1993; Beaufort et al, 1997).

Most of the previous studies on sea sediments concentrated on millennial scale climate changes using relative dating methods or radiocarbon dates on bulk sedimentary matter that might be relatively inaccurate. Recently with the advent of AMS (Accelerator Mass Spectrometry) we can obtain highly accurate chronologies because, here, instead of dating bulk sediments, planktonic foraminifera are dated (no contamination from detrital carbonate material). As evident from the discussion in the section 1.2, majority of the earlier work was confined to the western Arabian Sea, where the Southwest monsoon signal is the strongest. Any given study focused its attention on only one of the three regions of the Arabian Sea. I have chosen three sediment cores in such a way that they represent each of the three above-mentioned broad regimes and thus record the signatures of climate variations in different parts of the Arabian Sea. Hence I would be able to study various processes that are manifestations of SW monsoon at different locations to delineate local versus regional

responses. The cores were strategically chosen from the locations where sedimentation is fast enough to provide a high time resolution (centennial to sub-centennial). They were radiocarbon dated employing the AMS technique that yield highly accurate ages, which provided better age control. Further, my thesis is a comparative study of past changes in two different aspects of the monsoon: (i) wind induced upwelling, productivity etc. (ii) rainfall and run-off to the ocean, surface salinity etc. It also looks at changes during intermonsoon periods, by the study of the equatorial core.

The specific objectives of this study are:

1. To obtain accurate Radiocarbon chronologies on planktonic foraminiferal separates in sediment cores and to determine the past monsoon variations for the Late Quaternary period (~35,000 a BP to present) on millennial to centennial scales by high-resolution sampling using stable isotopic and chemical tracers.
2. It has been proposed that during the Last Glacial Maximum (LGM), SW Monsoon was weaker & NE Monsoon was stronger resulting in enhanced influx of low salinity water from the Bay of Bengal (Duplessy, 1982; Sarkar et al, 1990). We also aim to verify this and if true, study how this transport varied in the past, in relation to paleoclimate & paleomonsoon variations using the equatorial core.
3. There are significant variations in the paleoclimatic observations from place to place in a single geographical region (e.g. Arabian sea). This is because the rainfall/ wind patterns show strong spatial variability. Therefore one of the aims of the present study is to assess that how different regions/proxies respond to the same climatic forcing on different time scales.
4. SW monsoon has been shown to exhibit correlation with the high latitude climate in the cores from the northern and western Arabian Sea (Reichart et al, 1998, 2002 a; Schulz et al, 1998; Altabet et al, 2002) based on the organic carbon content and denitrification intensity. We plan to verify that whether

such a correlation is exhibited by the SW monsoon precipitation signal as inferred from the oxygen isotopes of planktonic foraminifera.

5. In the equatorial region the winds are strongest during April to November with maximum variability during the intermonsoon periods, which are known as Indian Ocean Equatorial Westerlies (IEW; Schott and McCreary Jr., 2001; Hastenrath et al, 1993). In this region productivity is mostly due to IEW induced mixed layer deepening during the intermonsoon periods (Beaufort et al, 1997). The IEW is positively correlated to Southern Oscillation (SO) index, which in turn is positively correlated to Southwest monsoon and East African rains and negatively to the El Nino frequency (Hastenrath et al, 1993 and references therein). Thus another aim of this study is to document the past variations in SW monsoon, East African rains and El Nino frequency by studying the past productivity variations in this region.
6. Recently there has been a renewed interest in the solar forcing of the climate (Bond et al, 2001; Neff et al, 2001; Agnihotri et al, 2002; Foucal, 2003). This study aims to check that how the SW monsoon is affected by the changes in solar activity on a centennial scale by comparing the high-resolution data from the eastern Arabian Sea core with the reconstructed Total Solar Irradiance (Bard et al, 2000).
7. Lastly, to carry spectral analysis on various SW monsoon proxies to detect the underlying periodicities that might help in detecting the various factors forcing the SW monsoon from centennial to Milankovitch timescales.

1.4. Thesis outline:

In addition to this chapter, this thesis has been divided into five other chapters. **Chapter 2** deals with the materials used, the suitability of various proxies employed in this study and the experimental techniques used. **Chapter 3** deals with the results from the core from the coastal eastern Arabian Sea covering the past ~3 ka and sampled at a sub-centennial scale. **Chapter 4** presents the results of the core from the

southern/equatorial Arabian Sea covering the past ~35 ka BP with a resolution of ~350 years. **Chapter 5** deals with the results from the western Arabian Sea covering the past ~19 ka BP with a resolution of ~300 years. This core records the productivity variations due to the intense SW monsoon winds in that region. **Chapter 6** highlights the conclusions reached in this study and presents the scope for future work.

Chapter 2

**Materials & Experimental
Techniques**

This chapter describes the various materials used and the experimental techniques employed for the present study. The topics covered are:

1. Collection and locations of the sediment cores.
2. A brief introduction to foraminifera and their separation procedure from the sea sediments, for use in AMS Radiocarbon dating as well as stable oxygen and carbon isotopic analyses.
3. Radiocarbon chronologies of the sediment cores.
4. Application and suitability of various isotopic and chemical proxies used in this study.
5. Analytical schemes used to measure various proxies, their precisions and accuracies.

2.1. Collection and locations of the sediment cores:

For the present study three sediment cores were collected viz. SS3827 G, SS4018 G and SK145-9 representing three different regions of the Arabian Sea. The cores SS3827 G and SS4018 G were obtained from the equatorial Indian Ocean and the western Arabian Sea respectively during the Ocean Research Vessel Sagar Sampada cruise no. SS152 and SS164 during 1997 and 1998 respectively. Another sediment core SK145-9 was collected from the eastern continental margin of the Arabian Sea during the ORV Sagar Kanya cruise no. SK145 during the year 1999. The locations of the various cores are shown in Fig.2.1 and other particulars are summarized in Table 2.1.

Table 2.1. Particulars of the sediment cores analyzed in this study.

S. No.	Core Name	Type	Location (Lat., Long.)	Length (cm)	Water depth	Resolution	Age limit (a BP)
1.	SK 145-9	Piston core	12.6 ⁰ N, 74.3 ⁰ E	400 (252)*	400 m	~50 years per cm	13,180
2.	SS 3827 G	Gravity Core	3 ⁰ 42'N, 75 ⁰ 54.5'E	196 (100)*	3118 m	~350 years per cm	34,730
3.	SS 4018 G	Gravity Core	13 ⁰ 21.8'N, 53 ⁰ 15.4'E	130 (130)*	2830 m	~150 years per cm	19,020

- Values in bracket denote the dated length

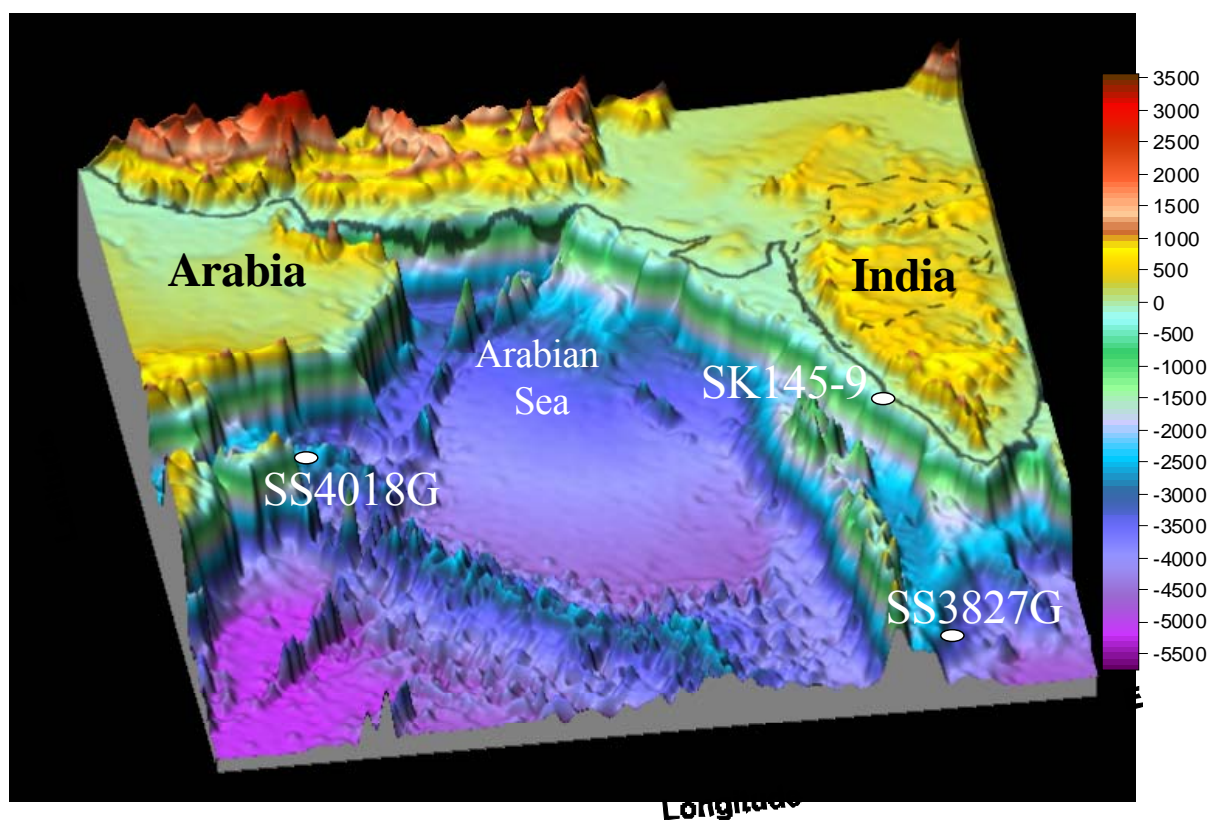


Fig. 2.1. Locations of the sediment cores employed in this study along with the Arabian Sea bottom topography; colour code for altitude and depth in meters, shown on the right.

The cores were sampled onboard with thin perspex sheets and were sealed in the plastic bags, which were then brought back to laboratory for further analysis. The core SK 145-9 was sampled at every cm in the top 50 cm and thereafter the sampling was done at every two cm. In SS 3827 G, sampling was performed at every cm in the top 130 cm and thereafter at every two cm for the remaining length of the core. In SS 4018 G sampling was carried out at every two cm for the entire length of the core.

2.2. Foraminifera and their separation procedure:

Foraminifera are eukaryotic (possessing a distinct nucleus), unicellular (single celled, characterized by the absence of tissue or organs) organisms belonging to the Phylum **Protozoa**. They secrete calcium carbonate shells of incredible beauty and structural complexity, which get preserved in sea sediments as fossils. Their size ranges from 0.01 mm (10 μ) to 10 mm but the average representative size range is 0.1 mm (100 μ) to 1.0 mm. The living organism consists of protoplasm encapsulated in the shell, which is further divided into different chambers. The wall separating one chamber from another is called as **septum**. There is a hole in the septum through which the protoplasm extends throughout the shell. This hole is called **foramen**, from which the name foraminifera (Latin, *foramen* = hole; *ferre* = to bear) is derived. The protoplasm extends outside the test through an opening known as **aperture** and surrounds the shell as a network of branching pseudopodia. The typical life spans of foraminifera are 2-4 weeks. Foraminifera are further divided into “Spinose” and “Non-Spinose” forms. “Spinose” forms are those that bear spines and “Non-Spinose” form lack them. Usually spines get broken and do not get fossilized with the shell.

Nearly all of the foraminifera are marine organisms and are found at all the latitudes. Highest diversity occurs in tropical regions, which decreases with increasing latitude to a single species in the true Antarctic and Arctic waters. They are both **planktonic** and **benthic**. Benthics are the bottom dwelling form and have existed since the Cambrian time (~570 Ma). They may be sessile i.e. constantly attached to the bottom or vagile i.e. free bottom-dwelling organisms. They inhabit all depths ranging from continental shelf to abyssal plain. Planktonic foraminifera float in the water column. They are more recent in origin than benthics and have existed since Jurassic (~200 Ma). Most of the planktonic species inhabit the top 150 m of the water column but their habitat can be upto 1000 m. On the basis of depth habitats,

planktonic foraminifera can be grouped into three categories viz. “Shallow-water”, “Intermediate-water” and “Deep-water” dwelling species. “Shallow-water” species live predominantly in the upper 50 m of the water column. They are mainly spinose forms and include all the species of genus *Globigerinoides* and some species of *Globigerina*. “Intermediate-water” species include both spinose forms and non-spinose forms that inhabit the upper 100 m but predominantly dwell in the 50-100 meters of the water column. “Deep-water” group consist of those species, which live in the euphotic zone as the juveniles, and predominantly below 100 m as adults e.g. all the species of genus *Globorotalia*. Several planktonic foraminifera called as “symbiont bearing” are known to host algae as symbionts within their shells. The species that host dinoflagellates (unicellular, 5-10 μ size, brownish-yellow colour) are *G.ruber*, *G.sacculifer*, *G.conglobatus* and *O.universa*. The species hosting chrysophycophytes (yellow-green eukaryotic algae, 2-3 μ size) are *G.siphonophera* and *G.humilis*. There are some species that are known to sometime possess or lack chrysophycophytes as symbionts. They are called as “symbionts facultative” and include the species *G.inflata*, *G.menardii*, *N.dutertrei*, *P.obliquiloculata* and *G.glutinata*. On the other hand, species like *H.pelagica*, *N.pachyderma*, *G.bulloides*, *G.truncatulinoides* and *G.hirusta* are not known to host symbionts and are called as “symbiont barren” (Hemleben et al, 1988).

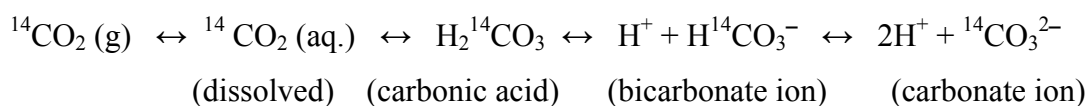
2.2.1. Separation of foraminifera:

About 5-10 g of sediment samples were taken in a 400 ml beaker filled with ~200 ml of distilled water. Around $\frac{1}{2}$ cc of 30% H_2O_2 was added to oxidize any organic matter that might be present in the sediments. Thereafter $\frac{1}{2}$ spoonful of Calgon powder (sodium hexametaphosphate) was added. Calgon acts as a dispersing agent and helps in removing the agglutinated inorganic particles. They were then warmed at 60-80°C for an hour. Care was taken that the mixtures don't get boiled while heating. Thereafter the beakers were kept for 4-5 hours so that total disintegration of the sediments took place. Subsequently wet sieving was carried out using sieves of the sizes 250 μ and 500 μ . The size fraction (500 μ to 250 μ) was transferred to 50ml beakers containing ~25 ml distilled water and were ultrasonically cleaned to remove the remaining inorganic particles sticking to the shells. The excess water was decanted and the shells were dried at 90°C. Thereafter they were kept in a

furnace at 400°C for ~8 hours to remove any volatile organic matter still adhering to the shells. The dry bulk fraction thus obtained is stored in pre-cleaned plastic vials. The planktonic species required are then handpicked under a stereoscopic microscope from the dry bulk fraction. While picking foraminifera care was taken to pick the shells falling approximately in the size range 450 μ to 350 μ and all the chosen shells were more or less in the same size range.

2.3. Radiocarbon chronologies:

The chronologies of the sediments cores studied in this work have been obtained using Radiocarbon dating method (Libby, 1955). The radiocarbon (^{14}C) produced in the atmosphere is oxidized to $^{14}\text{CO}_2$. The chemical cycle of the CO_2 in the ocean is governed by a series of equilibria as shown below:



The bicarbonate ions, which are the dominant species in the oceans at the prevailing pH, are removed by the microorganisms to secrete calcium carbonate shells. These calcitic shells of microorganisms contain the radioactive carbon, and are used for radiocarbon dating. We chose planktonic foraminifera namely *Globigerinoides ruber*, *Globigerinoides sacculifer*, *Orbulina universa* and *Neogloboquadrina dutertrei*. We have selected planktonic foraminifera for our study because they inhabit the surface and near surface oceans (up to ~100 m) and therefore readily incorporate changes occurring in the surface ocean into their calcitic shells. For AMS radiocarbon dating about 10mg of foraminifera are required. This means approximately 200 individuals have to be handpicked for every date. C-14 dating was carried out at 12 depths for SS 3827 G, at 15 depths for SS 4018 G & 11 depths for SK145-9. It was done using the Accelerator Mass Spectrometer at NSF Arizona AMS Facility, University of Arizona, USA in collaboration with A.J.T. Jull and G.S. Burr (Linick et al, 1986; Jull et al, 1989; Somayajulu et al, 1999). The fundamental difference between conventional radiocarbon dating such as Liquid scintillation method and AMS technique is that in the former, decay of the atom is counted whereas in the latter the atoms themselves are counted. This allows us to measure even small samples, which helps in improving the accuracy relative to the bulk

method by the absence of various contaminants that are usually present in the bulk samples. Accelerator mass spectrometry differs from the conventional mass spectrometry in the energies to which the ions are accelerated. In mass spectrometers the energies are in thousands of eV (keV) whereas in the AMS they are in millions of eV (MeV). The practical consequence of having higher energies is that ambiguities in the identification of the atomic and molecular ions with the same mass (isobaric effects) are removed. Thus we can measure isotopic ratio for specific elements to a level of 1 in 10^{15} . The chronologies of the three cores are given in table 2.2 on the next page.

ΔR is the value that has to be added to the global mean reservoir age (400 yrs.) to obtain the age correction needed for the local reservoir effect. The radiocarbon ages have been calibrated to calendar ages using the calibration program “Calib 4.1 (INTCAL 98)” (Stuiver et al, 1998). Radiocarbon ages beyond 24 ka BP were also calculated using the “Glacial polynomial” (Bard, E. 1998) but the age difference came out to be only 2 years so the Calib 4.1 ages have been retained. The errors given are 1 standard deviation.

Table 2.2. Radiocarbon ages

Sample Details	Radiocarbon Age (a BP)	Calibrated Age (a BP)
<u>Core SK 145-9</u>, $\Delta R = 100 \pm 30$		
Depth (0-2) cm	844 \pm 36	410 \pm 80
Depth (23-25) cm	1899 \pm 56	1330 \pm 80
Depth (40-41) cm	2506 \pm 39	2030 \pm 70
Depth (50-52) cm	3210 \pm 41	2860 \pm 70
Depth (78-80) cm	3952 \pm 53	3820 \pm 80
Depth (124-126) cm	6308 \pm 48	6650 \pm 60
Depth (160-162) cm	8124 \pm 66	8450 \pm 90
Depth (174-176) cm	8891 \pm 64	9210 \pm 270
Depth (210-212) cm	9359 \pm 57	9840 \pm 230
Depth (228-230) cm	9922 \pm 58	10430 \pm 380
Depth (250-252) cm	11913 \pm 73	13180 \pm 350
<u>Core SS 3827 G</u>, $\Delta R = 100 \pm 30$		
Depth (4-5) cm	3692 \pm 48	3460 \pm 70
Depth (11-12) cm	5338 \pm 52	5590 \pm 40
Depth (19-20) cm	5788 \pm 52	6100 \pm 90
Depth (39-40) cm	13523 \pm 87	15550 \pm 220
Depth (59-60) cm	17780 \pm 100	20450 \pm 340
Depth (79-80) cm	24040 \pm 180	27680 \pm 210
Depth (99-100) cm	30280 \pm 440	34730 \pm 510
<u>Core SS 4018 G</u>, $\Delta R = 163 \pm 30$		
Depth (2-4) cm	1116 \pm 38	540 \pm 30
Depth (10-12) cm	3097 \pm 58	2720 \pm 30
Depth (20-22) cm	5227 \pm 45	5440 \pm 80
Depth (32-34) cm	7375 \pm 74	7660 \pm 70
Depth (42-44) cm	8734 \pm 49	9000 \pm 160
Depth (50-52) cm	9558 \pm 55	10120 \pm 220
Depth (60-62) cm	10364 \pm 55	11000 \pm 230
Depth (60-62) cm	10543 \pm 60	10930 \pm 380
Depth (72-74) cm	11383 \pm 58	12860 \pm 130
Depth (80-82) cm	12036 \pm 67	13220 \pm 300
Depth (92-94) cm	13170 \pm 91	14720 \pm 570
Depth (102-104) cm	13613 \pm 75	15580 \pm 220
Depth (112-114) cm	14719 \pm 77	16850 \pm 250
Depth (122-124) cm	15098 \pm 83	17290 \pm 260
Depth (128-130) cm	16660 \pm 120	19020 \pm 330

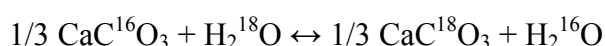
2.4. Isotopic and chemical proxies employed in this study:

Isotopic proxies that have been studied are stable oxygen and carbon isotopes in selected species of planktonic foraminifera and nitrogen isotopes in the sedimentary organic matter. Chemical proxies studied are calcium carbonate (weight %), organic carbon (wt %) and the C/N ratio.

The variations in the physical and chemical properties due to the presence of different isotopes (the so called “isotope effect”) arise due to very small, albeit finite mass differences among them. These differences are most significant for lighter elements such as hydrogen, carbon, nitrogen, oxygen etc. Urey (1947) was the first to explain the variations in physico-chemical properties in isotopic systems on the basis of thermodynamic considerations and proposed that a paleotemperature scale can be constructed based on the fractionation of oxygen isotopes in the calcites.

2.4.1. Oxygen isotopes:

Oxygen has three stable isotopes viz. ^{16}O , ^{17}O and ^{18}O with 99.763%, 0.0375% and 0.1995% abundances respectively. Usually the ratio $^{18}\text{O}/^{16}\text{O}$ is determined as ^{18}O has higher abundance than ^{17}O and greater mass difference with ^{16}O . The fractionation (defined as the relative partitioning of the heavier and lighter isotopes between two co-existing phases) of these isotopes in nature is caused by an equilibrium or kinetic process. Kinetic fractionation is associated with incomplete and unidirectional processes such as evaporation, diffusion, biologically mediated reactions etc. No isotopic equilibrium is attained in this case. Equilibrium fractionation is a special case of chemical equilibrium reaction in which there is no net reaction but an exchange of isotopes takes place. In this case isotopes can move to and fro and equilibrium is attained when there is no more change in the isotopic ratios with time. In the case of foraminifera, calcite is precipitated from water and the following isotopic exchange process takes place:



The equilibrium constant “K” for this reaction can be written as:

$$K = [\text{CaC}^{18}\text{O}_3]^{1/3} [\text{H}_2^{16}\text{O}] / [\text{CaC}^{16}\text{O}_3]^{1/3} [\text{H}_2^{18}\text{O}]$$

or, $K = ([\text{CaC}^{18}\text{O}_3] / [\text{CaC}^{16}\text{O}_3])^{1/3} / ([\text{H}_2^{18}\text{O}] / [\text{H}_2^{16}\text{O}])$

Thus equilibrium constant can be expressed as the ratio of $^{18}\text{O}/^{16}\text{O}$ in the carbonate phase to that in the water. This leads us to the concept of fractionation factor “ α ” that will better represent the partitioning of isotopes between two phases. Fractionation factor is defined as the ratio of isotopes in one phase to the other co-existing phase. In the $\text{CaCO}_3\text{-H}_2\text{O}$ system, the fractionation factor is defined as:

$$\alpha_{\text{CaCO}_3\text{-H}_2\text{O}} = R_{\text{CaCO}_3} / R_{\text{H}_2\text{O}} = 1.031 \text{ at } 25^\circ\text{C}$$

R_{CaCO_3} is $^{18}\text{O}/^{16}\text{O}$ in calcite and $R_{\text{H}_2\text{O}}$ is $^{18}\text{O}/^{16}\text{O}$ in water. The fractionation factor is related to equilibrium constant by:

$$\alpha = K^{1/n}$$

where “n” is the number of atoms exchanged. For the sake of simplicity, isotope exchange reactions can be written in the way that only one atom is exchanged and then fractionation factor “ α ” becomes identical to equilibrium constant “K”. The fractionation factor is temperature dependent in such a way that calcites precipitated from water of constant isotopic composition but at different temperatures will possess different $^{18}\text{O}/^{16}\text{O}$ ratios. This is the basis for the paleotemperature scale, by which various empirical paleotemperature equations are deduced. The overall effect is that approximately 0.25‰ depletion in carbonate $\delta^{18}\text{O}$ occurs for every 1°C temperature increase (Erez and Luz, 1983). The absolute abundances of minor isotopes as well as absolute values of isotope ratios cannot be determined precisely enough for geochemical purposes. Moreover to aid the measurements in mass spectrometers, the isotope abundances are reported in “ δ ” values, which are relative differences of isotopic ratios from an international standard expressed in per mil (‰) units:

$$\delta_A = [(R_A/R_{st}) - 1] \times 10^3 \text{ ‰}$$

Where,

R_A is the ratio of the abundances of the less abundant (heavier e.g. ^{18}O) to more abundant (lighter e.g. ^{16}O) isotope in the sample, and

R_{st} is the ratio of the abundances of less abundant (heavier) to more abundant (lighter) isotope in the standard (e.g. $^{18}\text{O}/^{16}\text{O}$ in the standard)

For oxygen isotopic studies two international standards viz. SMOW and PDB are in the use. SMOW (Standard Mean Ocean Water) is a hypothetical standard with $\delta^{18}\text{O}$ value close to the modern mean seawater value. The value of SMOW was

defined by Craig (1961) with respect to an existing water standard NBS-1 (distilled Potomac river water) with $\delta^{18}\text{O}$ value of -7.94‰ vs. SMOW. As SMOW does not actually exist as a real water sample so it can't be used for calibrating laboratory measurements. Therefore a water sample with values identical to SMOW is distributed by IAEA (International Atomic Energy Agency), Vienna that is called V-SMOW. H.Craig of the University of California prepared it by mixing distilled ocean water (collected from the Pacific Ocean, 0° lat., 180° long, in July, 1967) with small amounts of other waters to adjust the isotopic ratios to the required values (Gonfiantini R, 1981). It has $\delta^{18}\text{O}$ value of 0‰ with respect to SMOW (by definition). This scale has been used for oxygen isotope analyses involving waters, silicates, phosphates, high temperature carbonate etc. The PDB standard is used in the low temperature carbonate studies. It is a carbonate obtained from fossilized rostrum (cigar shaped internal shell) of *Belemnitella americana*, a belemnite (an extinct cephalopod) from the Peedee Formation of Cretaceous Period in South Carolina, USA. It was the laboratory working standard used by Urey's group in the University of Chicago in the 1950s for developing the initial paleotemperature scale (McCrea, 1950). Over the decades, the original PDB standard has been exhausted and is no longer available. To overcome this problem IAEA introduced a hypothetical standard Vienna-PDB (V-PDB) with values nearly identical to PDB and it is defined by its relationship to carbonate reference materials NBS-19 and NBS-20. NBS-19 is calcium carbonate from a marble of geologically unidentified origin with $\delta^{18}\text{O}$ and $\delta^{13}\text{C}$ values of -2.20‰ and $+1.95\text{‰}$ respectively with respect to V-PDB. NBS-20 is a homogenized sample of Solenhofen limestone of Jurassic Period from Southern Germany with $\delta^{18}\text{O}$ and $\delta^{13}\text{C}$ values of -4.14‰ and -1.06‰ with respect to V-PDB (Hoefs, 1997). The conversion equations of $\delta^{18}\text{O}_{(\text{PDB})}$ to $\delta^{18}\text{O}_{(\text{SMOW})}$ and *vice-versa* are (Coplen et al, 1983):

$$\delta^{18}\text{O}_{(\text{SMOW})} = 1.03091 \delta^{18}\text{O}_{(\text{PDB})} + 30.91$$

$$\delta^{18}\text{O}_{(\text{PDB})} = 0.97002 \delta^{18}\text{O}_{(\text{SMOW})} - 29.98$$

Erez and Luz (1983) determined the following empirical temperature equation by comparing isotopic composition of the planktonic foraminifera *Globigerinoides sacculifer* with the actual growth temperature:

$$T^{\circ}\text{C} = 17.0 - 4.52 (\delta^{18}\text{O}_c - \delta^{18}\text{O}_w) + 0.03 (\delta^{18}\text{O}_c + \delta^{18}\text{O}_w)^2$$

T , $\delta^{18}\text{O}_c$, $\delta^{18}\text{O}_w$, are the estimated temperature ($^{\circ}\text{C}$), the isotopic composition of the shell carbonate and the seawater respectively. But there are various complications that inhibit the widespread application of paleotemperature scale. To apply the paleotemperature equation we must know the $\delta^{18}\text{O}$ value of the seawater with which a given specimen of CaCO_3 has equilibrated. This is not easy to establish with certainty because the isotopic composition of seawater as a whole depends on the amount of ice stored on the continents, which gives rise to the so called “ice volume effect”. When water evaporates from the ocean surface, the water vapour gets enriched in the lighter isotopes, as vapour pressure of H_2^{16}O is more than H_2^{18}O . Kinetic effects also take place that further depletes the vapour phase in the heavier isotope. As more and more evaporation takes place and as this isotopically lighter water gets locked in the form of continental ice sheets, the remaining ocean water gets more and more enriched in the heavier isotope. It is believed that during the Last Glacial Maximum the average seawater $\delta^{18}\text{O}$ was 1.2 ‰ heavier than present (Labeyrie et al, 1987, Fairbanks et al, 1989).

The depletion of heavier isotope in freshwater gives rise to the correlation of salinity with $\delta^{18}\text{O}$. As evaporation takes place, the salinity as well as $\delta^{18}\text{O}$ of the seawater increases. In the Arabian Sea it has been found that 1‰ increase in salinity causes a 0.33 ‰ increase in $\delta^{18}\text{O}$ of water (Duplessy et al, 1981, Sarkar et al, 2000). Separately analyzing planktonic and benthic foraminifera from the same site can help to resolve the ice volume effect. The $\delta^{18}\text{O}$ values of the planktonics reflect the changes in both the temperature as well as $\delta^{18}\text{O}$ of water whereas the bottom water is mostly believed to be unaffected by the temperature changes, hence the benthics could record only the change in the isotopic composition of seawater.

There are several effects associated with the biology of foraminifera that cause deviation from the equilibrium. Isotopic disequilibrium effects can be classified as either metabolic or kinetic (McConnaughey, 1989 a, b). Metabolic effects result from the incorporation of ambient dissolved carbon and oxygen (produced due to respiration or photosynthesis) into the shell material. Kinetic effects are due to the preferential uptake of lighter isotopes during the hydration and hydroxylation of CO_2

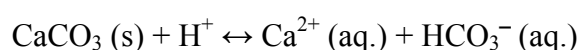
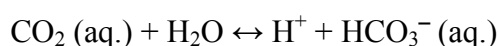
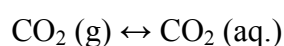
and are generally associated with rapid calcification. These effects, collectively called “vital effects”, include effects due to respiration, ontogeny, secretion of gametogenic calcite etc. The respiration products are depleted in the heavier isotopes (Lane and Doyle, 1956) and their utilization for shell secretion results in depleted $\delta^{18}\text{O}$ values. Progressive $\delta^{18}\text{O}$ enrichment from juvenile to mature chambers has been observed and is assigned to the incorporation of the respired CO_2 during early calcification. The higher metabolic rates in the juvenile specimen would cause the strongest depletions, which then decreases in the adult specimen that has reduced metabolism (Berger et al, 1978; Wefer and Berger, 1991). Furthermore, planktonic foraminifera inhabit different depths at various stages of their ontogeny. In the later part of their lifecycles they tend to secrete shells at deeper and cooler waters resulting in enhanced $\delta^{18}\text{O}$ values (Bouvier-Soumagnac and Duplessy, 1985; Emiliani, 1971). Towards the end of their life cycle foraminifera secrete gametogenic calcite. Before gamete release, foraminifera move to deeper, cooler waters and secrete a layer of calcite that is enriched in $\delta^{18}\text{O}$ over its shell. This calcite layer can comprise 18 to 28% of the shell mass of foraminifera (Be, 1980; Duplessy et al, 1981). Furthermore $\delta^{18}\text{O}$ has been found to vary with varying light intensities (photosynthetic activities in the symbiont carrying foraminifera) and carbonate ion concentrations. The $\delta^{18}\text{O}$ was found to decrease with increasing irradiance that caused enhanced photosynthesis. Enhanced rate of skeletogenesis ensues increased photosynthesis that favours stronger kinetic fractionation resulting in depleted $\delta^{18}\text{O}$ (Spero and Lea, 1993; Wefer and Berger, 1991). $\delta^{18}\text{O}$ in foraminiferal carbonate decreases with increasing carbonate ion concentration that was ascribed to a-biological, kinetic fractionation effect (Spero et al, 1997) as it was also observed in rapidly precipitating inorganic CaCO_3 (McCrea, 1950). The disequilibria due to vital effects can be avoided by choosing the particular species, which are known to precipitate their shells in equilibrium with seawater and by picking mature shells from a particular size range. Also diagenetic alteration after the death of the organism can modify its isotopic composition significantly. The $\delta^{18}\text{O}$ values of planktonic foraminifera from warm subtropical seas are particularly sensitive to alteration as the secondary calcite precipitates in equilibrium with the cold pore fluids at the sediment-water interface (Schrag, 1999). Also shells may get

recrystallized at the micron scale (preserving the shell features and ornamentation) unlike the previous case in which euhedral calcite crystals precipitate on the outer and inner surfaces of the shell (Pearson et al, 2001). This obstacle can be overcome by selected pristine shells, which appear glassy under the microscope and are without any overgrowths.

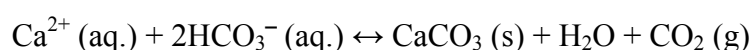
All foraminifera used in this study have been carefully handpicked to as far as possible avoid most of the above complications.

2.4.2. Carbon isotopes:

Carbon has two stable isotopes viz. ^{12}C and ^{13}C with an abundance of 98.89% and 1.11% respectively. The two main carbon reservoirs in the earth are organic matter (2000 Giga Ton) and the sedimentary carbonates (72,000,000 GT) and are characterized by different carbon isotopic signatures because of the two distinct processes controlling them (Craig, 1953). Kinetic isotope effects during photosynthesis cause preferential uptake of ^{12}C in the organic matter. On the other hand, isotope equilibrium exchange reactions within the inorganic carbon system “atmospheric CO_2 – dissolved bicarbonate – solid carbonate” cause enrichment in the heavier isotope (Hoefs, 1997) in the carbonates. The carbonate equilibria in the marine system can be represented by the following equations (Faure, 1986):



These equilibrium reactions govern the carbon and oxygen isotopic variations among various chemical species. Total dissolved inorganic carbon (DIC) comprises of $\text{HCO}_3^- (\text{aq.})$, CO_3^{2-} and $\text{CO}_2 (\text{aq.})$. The net equation for carbonate precipitation comes out to be:



The equilibrium fractionation factors for carbon isotope in this system at 20°C are (Emrich et al, 1970):

$$\alpha_{\text{CaCO}_3 (\text{s}) - \text{HCO}_3^- (\text{aq.})} = 1.00185$$

$$\alpha_{\text{HCO}_3^- (\text{aq.}) - \text{CO}_2 (\text{g})} = 1.00838$$

$$\alpha_{\text{CaCO}_3 (\text{s}) - \text{CO}_2 (\text{g})} = 1.01017$$

At low temperatures the largest fractionation occurs between the dissolved CO₂ and the bicarbonate ion. The bicarbonate ion is the dominant species at the prevailing pH of seawater (7.5 – 8.3) and DIC can be conveniently approximated by HCO₃⁻ (aq.). The isotopic enrichment factor for calcite vs. bicarbonate is (Grossman, 1984):

$$\epsilon_{\text{CaCO}_3\text{-HCO}_3^-} (\text{‰}) = 10.51 - 2980/T, \text{ where } T \text{ is temperature in Kelvin}$$

This relationship gives a temperature dependence of 0.035 ‰ increase in δ¹³C per degree Celsius increase in temperature, which is same as that given by Emrich et al (1970). Thus temperature has a negligible effect on δ¹³C of calcite in comparison to the effect due to the productivity variations. The profile of δ¹³C_{DIC} in the water column is governed by oceanic productivity (Kroopnick, 1974). Phytoplanktons prefer lighter isotope (¹²C) during photosynthesis enriching the ambient surface seawater in the heavier isotope (¹³C). As the organism dies it settles to the deeper water where it gets oxidized releasing CO₂ depleted in ¹³C. Thus the DIC at the surface waters has the highest δ¹³C with a minimum at the base of the thermocline after which it increases a little and thereafter stays more or less uniform. The organisms secreting calcareous shells in equilibrium with the ambient water will record these isotopic signatures. Thus a higher δ¹³C value probably corresponds to an enhanced rate of photosynthesis in the euphotic layer that indicates an increase in productivity.

As δ¹³C has a steep gradient in the water column so the species secreting their shells at different depths in equilibrium with the ambient water during their ontogeny will exhibit deviation from the surface seawater equilibrium values (Kroopnick, 1972). Disequilibria in the δ¹³C values are caused by vital effect as discussed in the case of oxygen isotopes (see Sec. 2.4.1). Respiration products are depleted in heavier isotopes, the incorporation of which causes depletion relative to equilibrium (Weber and Woodhead, 1970; Vinot-Bertouille and Duplessy, 1973; Grossman, 1987). Higher metabolic rates have been found to cause increased depletion in δ¹³C values (Wefer and Berger, 1991, Oritz et al, 1996). Symbionts present in the foraminifera carry out photosynthesis in which they preferentially utilize the lighter isotope. With increased irradiance photosynthesis also increases resulting in enhanced H¹³CO₃⁻ in the ambient microenvironment, resulting in chambers enriched in δ¹³C (Spero and Lea, 1993).

$\delta^{13}\text{C}$ in foraminiferal carbonate decreases with increasing carbonate ion concentration similar to the effect experienced by $\delta^{18}\text{O}$ that was ascribed to be a-biological, kinetic fractionation effect (Spero et al, 1997). Diagenetic alteration at the sediment-water interface or beneath the sediments will shift $\delta^{13}\text{C}$ values toward the lighter side as degradation of organic matter produces ^{12}C depleted CO_2 making the ambient water depleted in the heavier isotope.

To avoid the above-mentioned problems as far as possible, pristine foraminifera from a certain size range have been chosen.

2.4.3. Nitrogen isotopes:

Nitrogen has two isotopes viz. ^{14}N and ^{15}N with abundances of 99.64% and 0.36% respectively. The standard for measuring the nitrogen isotopes is the atmospheric N_2 . Nitrogen gets into the biological system by the process of photosynthesis. Nitrogen fixation involves the reduction of N_2 to ammonia (NH_3), NH_4^+ or any other nitrogen compound by the microorganisms (e.g. *Rhizobium*) under anaerobic conditions. Nitrogen fixing bacteria are called as diazotrophs. “Nitrification” is the conversion of the NH_3 , NH_4^+ to nitrate (NO_3^-) or nitrite (NO_2^-) by the bacteria of *Nitrosomonas* and *Nitrobacter*. If ammonia is directly assimilated then it is called as “ammonia assimilation” but free ammonium ions can’t exist for long in the aerobic soils as they are oxidized to nitrate or nitrite and hence nitrification is the dominant step. Denitrification is the process by which nitrate is reduced to any gaseous nitrogen species, generally N_2 or nitrous oxide (N_2O) under the anaerobic conditions (Deuser et al, 1978; Naqvi and Noronha, 1991).

In the world oceans there are three regions that support perennial anaerobic conditions in the water depths of ~200 m to ~1000 m called as oxygen minima zone (OMZ) with oxygen concentration falling below 0.5 ml/l. This is due to the occurrence of high overhead productivity that consumes the available oxygen during their descent/degradation. These regions are the eastern tropical North Pacific (ETNP), eastern tropical South Pacific and the Arabian Sea (Christensen et al, 1987; Naqvi, 1987, 1994). Due to lack of oxygen in OMZ, the anaerobic bacteria utilize NO_3^- for the decomposition of organic matter. During this process they preferentially consume NO_3^- with lighter isotope (^{14}N), thus enriching the residual nitrate in the heavier isotope, which gets upwelled to the sea surface and is taken by the organisms

as a nutrient. The $\delta^{15}\text{N}$ of the organic matter is governed by the isotopic composition of the source NO_3^- that is upwelled from below and fractionation experienced by NO_3^- during its uptake by the phytoplanktons (Altabet, 1994). In the oxic waters of the euphotic zone the $\delta^{15}\text{N}$ of the nitrate is 5 to 6 ‰ (Liu and Kaplan, 1989) whereas in the regions receiving waters upwelled from the OMZ the $\delta^{15}\text{N}$ is in the excess of 18 ‰ (Cline and Kaplan, 1975) that explains the highly enriched $\delta^{15}\text{N}$ values observed in the particulate organic matter (Kumar et al, 2004). This enriched $\delta^{15}\text{N}$ signature is preserved even when the organic matter settles down and get preserved in sea sediments (Saino and Hattori, 1987). Thus a high $\delta^{15}\text{N}$ can be related to increased denitrification, which in turn is controlled by the climate induced productivity increase (Ganeshram et al, 1995). There are some species of algae that can directly fix atmospheric nitrogen. *Trichodesmium* is a good example. The $\delta^{15}\text{N}$ of organic matter that have contribution from organisms that directly fix N_2 is close to 0 –2 ‰ (Capone et al, 1997).

2.4.4. Biogenic Proxies:

These include CaCO_3 (wt. %), C_{org} (wt. %) and the C/N ratio in the sea sediments. The overhead rain of calcitic shells is a major constituent of the sea sediments. Sediments are composed of minute foraminiferal shells, called as *Globigerina* ooze, and cover most of the open ocean floor. It has been observed that during the monsoon season in the Arabian Sea, 50 – 60 % of the total flux to the bottom is composed of calcitic material (Nair et al, 1989). Thus calcium carbonate percentage in the sea sediments can indicate the overhead productivity provided the core has been raised from depths above the lysocline (~3800 m in the Arabian Sea, Kolla et al, 1976; Peterson and Prell, 1985) and there is no contamination from the terrigenous inputs (Sirocko et al, 1993).

Organic Carbon (C_{org}) preserved in the sea sediments is derived from the particulate organic carbon (POC, the carbon content of particulate organic matter) and is a manifestation of the overhead primary productivity if there are no alterations after the deposition (Muller and Suess, 1979, Calvert and Pederson, 1992; Schulz et al, 1998). Around ~5% of the POC fixed by photosynthesis in the euphotic zone is exported to the deep waters where it undergoes further degradation and only 10%

reaches the ocean bed. Further degradation takes place at the sediment-water interface and just below the sediments (~ 50 cm, the diagenetically active sediment layer) and on an average less than 10% of the POC flux reaching the sediment bed (0.05% - 0.1% of the total surface productivity) gets ultimately preserved (Chester, 2003). The preservation of organic carbon improves drastically in the regions underlying OMZ and in the regions where reducing conditions prevail at the sediment-water interface. It is believed that a high sedimentation rate supports enhanced preservation as it rapidly removes the organic matter from the diagenetically active zone and shields it from oxidizing agents (Heinrichs, 1992).

Organic matter in the sea sediments is derived from the marine as well as terrestrial sources. It is necessary to ascertain the source of the organic carbon before interpreting its downcore variations as due to paleoproductivity. The elemental composition of phytoplanktons and zooplanktons were given by Redfield (1934, 1958) that are called as “Redfield ratios”. The Redfield ratios for marine organic matter are C:N:P = 106:16:1 that yields a C/N value of 6.6. Recently this estimate was revised by Takahasi et al (1985) who gave the ratio as C:N:P = 122 (\pm 18):16:1 that provide a range of 6.5 to 8.7 as the C/N ratio. The C/N ratio of recent sediments comprising marine organic matter has a value of 8 to 10 whereas the ancient sediments have a value of 12-15 (Mackenzie, 1980). Terrestrial sources provide a variety of particulate and dissolved organic matter to the oceans that have some compounds exclusive to terrestrial biota such as lignin, chitin etc. Organic matter derived from land plants has C/N values between 20 and 100 (Premuzic et al, 1982; Meyers, 1994). Diagenetic alteration of organic matter tends to lower the C/N ratio as nitrogenous compounds breakdown to produce ammonia, which is retained by clay minerals (Muller, 1977) whereas CO₂ diffuses out.

2.5. Analytical scheme followed to measure various proxies, their precisions and accuracies:

The following schemes were employed for measuring the various proxies:

2.5.1. $\delta^{18}\text{O}$ and $\delta^{13}\text{C}$ measurements on foraminifera:

For measuring $\delta^{18}\text{O}$ and $\delta^{13}\text{C}$, CO₂ is fed into the mass spectrometer. There are two basic approaches to extract CO₂ from the purified carbonate. The first approach

involves thermal decomposition of carbonate but it is not preferred as the resulting CO₂ exhibits wide isotopic variations.

The other technique involves the acid decomposition of the carbonate with 100% phosphoric acid at different temperatures between 25°C and 150°C (McCrea, 1950; Wachter and Hays, 1985; Rosenbaum and Sheppard 1986; Swart et al, 1991) as shown:



This reaction shows that only two-thirds of the carbonate oxygen is liberated in the product CO₂. The oxygen isotopic fraction factor for CO₂-calcite system during acid decomposition at 25°C is 1.01025 (Rosenbaum and Sheppard 1986). Many precautions have to be taken to follow the acid decomposition technique. The salt produced (Ca₃(PO₄)₂) should be soluble in the solution produced by the interaction of the acid with the carbonate, or else a protective covering will form on the latter that will inhibit further reaction. Also, the acid should not produce radicals in the mass range 44-46, which excludes nitric acid (HNO₃) that decomposes to form nitrous oxide (NO₂). Most importantly, isotopic exchange between water and CO₂ is known to take place that necessitates an acid that has no free water. For these reasons, orthophosphoric acid is chosen as it has an extremely low vapour pressure and also the concentration of water is very low in comparison to other acids. The acid was prepared following Coplen et al (1983).

The mass spectrometer used in this study is the Europa–Scientific GEO 20 –20 stable isotope ratio mass spectrometer with an attached Carbonate Preparation System (CAPS). The schematic diagram of CO₂ preparation using the CAPS (from the CAPS manual) and that of mass spectrometer inlet system (from the GEO 20-20 manual) are shown in Fig. 2.2. CAPS system had a factory fitted aluminum carousel that can hold upto 24 sample vials and is supposed to measure them automatically. But it never worked as intended due to some inherent mechanical defect. Therefore all the measurements were made manually. The total CO₂ production assembly was maintained at 80°C for rapid acid digestion of the carbonates. At first, air was put into the acid reservoir by opening the valves V1 and V2. Thereafter sample vial is connected to the acid dosing assembly. Then the valves V4 and V3 were opened to evacuate the vial to medium vacuum of 10⁻³ torr using a rotary pump. In the meantime

rest of the preparation line was pumped to high vacuum (of the order of $\sim 10^{-8}$ torr) by keeping V6 closed and opening other valves that connect the lines to turbo pumps. When the total line was under vacuum and the temperature is 80°C , then acid was dropped for 0.175 second (~ 0.5 ml) on the sample. V6 was closed as soon as the reaction was over, which took around 1-2 minutes. The evolved gases were immediately removed from the reaction vial and are passed through the water trap between V6 and V7 that is kept at -100°C . Here H_2O molecules were frozen out and the remaining, moisture free CO_2 was frozen at the cold fingers (CF) using the liquid nitrogen (-196°C) trap. If the gas amount was very low, then the CF near V9 was used or else CF near V10 was used. After that any residual gases that may be present above the frozen CO_2 (at V9 or V10) were pumped out. This cryogenically cleaned CO_2 was then fed into the mass spectrometer inlet system.

The mass spectrometer sample inlet line was first brought to medium vacuum and then to high vacuum by opening V21 (connects to rotary pump) and V20 (connects to turbo pump) respectively. The V22 was closed and the sample gas was put into the variable sample reservoir by opening V11, V12 and V13. There the gas was left for 2 minutes for equilibration. Thereafter the V12 was closed and the gas was introduced into the mass spectrometer via a changeover valve by opening V14. The reference reservoir stores the reference gas, which is called CD Standard. It is a CO_2 gas prepared by reacting around 50g of mixed foraminiferal assemblage from a sediment core (raised from the Arabian Sea during a cruise of RV Charles Darwin in January, 1997) with orthophosphoric acid at 25°C (Ghosh, 2000). Its $\delta^{18}\text{O}$ and $\delta^{13}\text{C}$ values with respect to PDB are 1.07‰ and 1.7‰ respectively. The changeover valve acts as dual inlet in the way that it allows the sample gas and reference gas to alternately enter the mass spectrometer at preset intervals and when one is connected to the mass spectrometer the other is connected to waste line so that both the reference and the sample gas face the same amount of depletion. The variable volume reservoirs were adjusted to give a current of around 10 nanoampere for the major beam (mass 44) and the current was kept the same for both the sample and the reference gas.

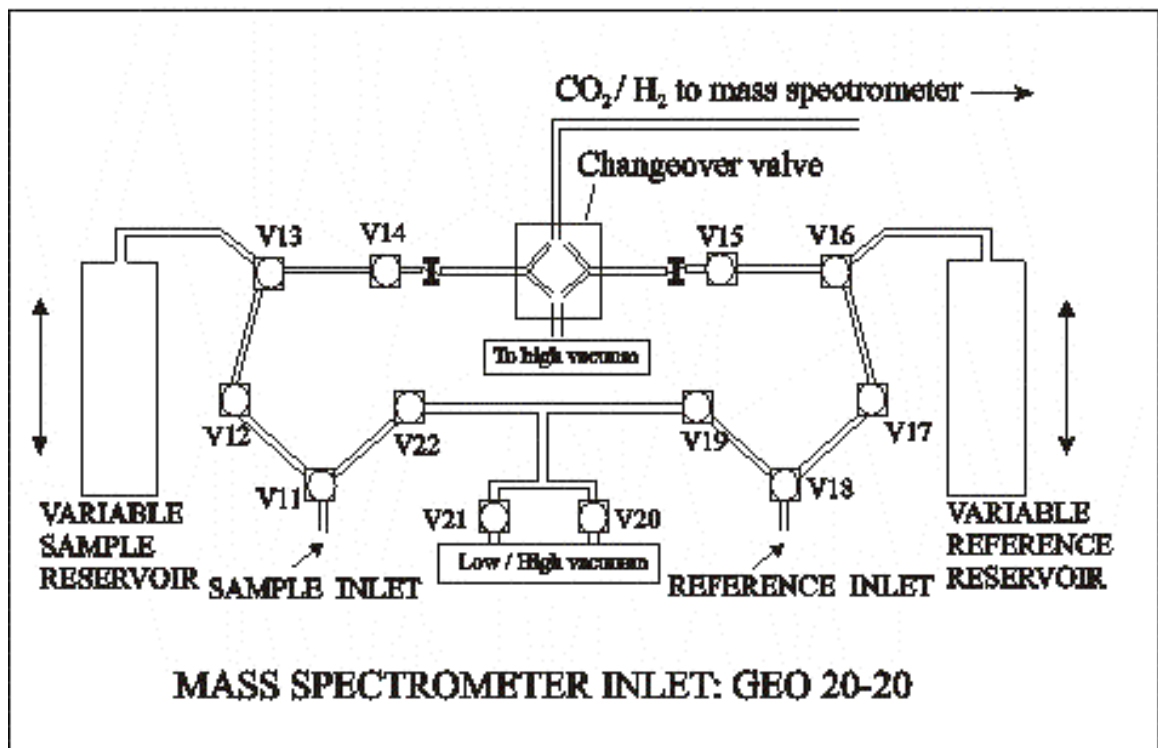
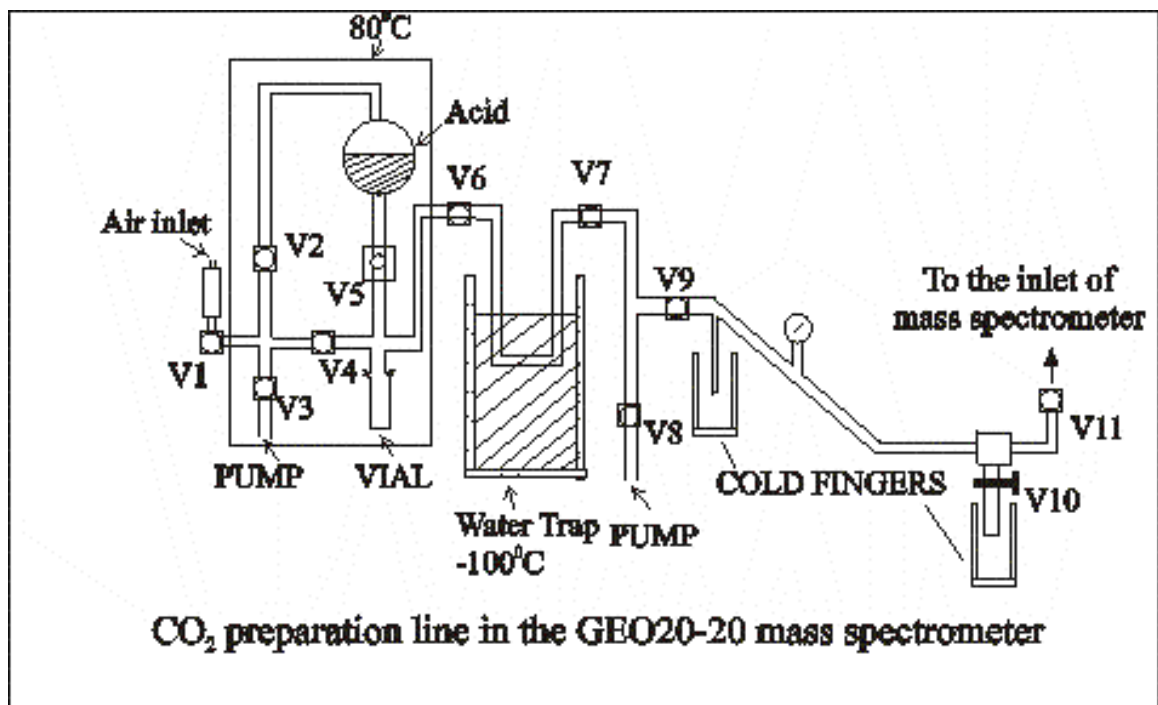


Fig 2.2. Schematic diagram of CO₂ preparation using CAPS and the Mass Spectrometer inlet system.

The predominant species of CO₂ belongs to the mass 44 viz. ¹²C¹⁶O₂(100%) followed by mass 45 viz. ¹³C¹⁶O₂ (93.67%), ¹²C¹⁶O¹⁷O (6.33%) and mass 46 viz. ¹²C¹⁶O¹⁸O (99.79), ¹³C¹⁶O¹⁷O (0.205), ¹²C¹⁷O₂ (0.003%) (Craig, 1957). Given in the parentheses is the relative abundance of that particular isotopic species with respect to other isotopic species with the same mass. The masses 47, 48 and 49 constitute only 0.0052% of natural CO₂ and are usually neglected. It is evident that ¹³C dominates in the mass 45 and ¹⁸O in the mass 46. GEO 20-20 mass spectrometer is a triple collector system having three faraday cups for collecting ions corresponding to three beams of masses 44, 45, and 46. Thus both δ¹⁸O and δ¹³C can be measured simultaneously under the same focusing conditions. The ion beams falling at the three collectors are converted to current using the appropriate electronic circuits and the ratio of currents are related to δ values as:

$\delta_{45} = [(I_{45}/I_{44})_{\text{sam}} / (I_{45}/I_{44})_{\text{std}} - 1] 10^3$ and $\delta_{46} = [(I_{46}/I_{44})_{\text{sam}} / (I_{46}/I_{44})_{\text{std}} - 1] 10^3$ where I_{44} , I_{45} and I_{46} are the currents generated due the beams of masses 44, 45 and 46 respectively. These current ratios are converted to δ¹³C and δ¹⁸O using the Craig correction (Craig, 1957):

$$\delta^{13}\text{C} = 1.06754400 \delta_{45} - 0.03600782 \delta^{18}\text{O}$$

$$\delta^{18}\text{O} = 1.00096600 \delta_{46} - 0.00206322 \delta^{13}\text{C}$$

In order to check the precision, a lab standard called as Z-Carrara (ZC-2002) was run at least three times daily viz. at the start of the measurement, in the middle and at the end of the day's measurement. It is a homogenized, fine carbonate powder (<63μ) from an Italian marble kindly provided by Prof. N.J. Shackleton. The δ¹³C and δ¹⁸O values of the Z-Carrara have been determined by repeated measurements and are 2.11‰ and -2.11‰ respectively. All the sample values have been corrected with respect to Z-Carrara on a daily basis to account for the variation in the machine and carbonate preparation line conditions. We measure sample (sam) as well as Z- Carrara (ZC) with respect to reference gas (rg) i.e. $rg\delta^{\text{sam}}$ and $rg\delta^{\text{ZC}}$. δ value for reference gas with respect to Z-Carrara can be calculated as follows:

$${}_{ZC}\delta^{rg} = \{(1/1 + {}_{rg}\delta^{ZC} 10^{-3}) - 1\} 10^3$$

Now, sample δ values with respect to Z-Carrara can be calculated using the formula:

$${}_{ZC}\delta^{sam} = {}_{rg}\delta^{sam} + {}_{ZC}\delta^{rg} + {}_{rg}\delta^{sam} {}_{ZC}\delta^{rg} 10^{-3}$$

Z-Carrara values with respect to PDB (${}_{PDB}\delta^{ZC}$) are known hence sample δ values with respect to PDB can be calculated as:

$${}_{PDB}\delta^{sam} = {}_{ZC}\delta^{sam} + {}_{PDB}\delta^{ZC} + {}_{ZC}\delta^{sam} {}_{PDB}\delta^{ZC} 10^{-3}$$

Table 2.3 gives the Z-Carrara $\delta^{13}\text{C}$ and $\delta^{18}\text{O}$ values measured from 19th June, 2003 to 4th April, 2004.

The precision on $\delta^{13}\text{C}$ measurement is $\pm 0.1\text{‰}$ while for $\delta^{18}\text{O}$ it is $\pm 0.2\text{‰}$. Uncertainties given are one standard deviation. Another standard that was run occasionally to check the stability of the machine is the Check Standard with $\delta^{13}\text{C}$ and $\delta^{18}\text{O}$ values of 0.33‰ and 2.33‰ with respect to PDB.

Table 2.3. Z-Carrara $\delta^{13}\text{C}$ and $\delta^{18}\text{O}$ values with respect to PDB in per mil, measured from 19.7.03 to 4.4.04:

$\delta^{13}\text{C}$	$\delta^{18}\text{O}$	$\delta^{13}\text{C}$	$\delta^{18}\text{O}$	$\delta^{13}\text{C}$	$\delta^{18}\text{O}$	$\delta^{13}\text{C}$	$\delta^{18}\text{O}$
1.98	-2.26	2.05	-2.07	1.94	-2.12	1.99	-2.11
2.04	-2.21	2.06	-2.03	1.92	-2.30	1.98	-2.14
1.99	-2.35	2.05	-2.02	2.10	-1.78	1.96	-2.17
1.90	-2.45	2.01	-2.21	1.98	-1.89	1.87	-2.17
1.92	-2.63	1.93	-2.44	1.97	-2.03	1.87	-2.25
1.84	-2.32	2.01	-2.14	2.02	-2.08	2.09	-1.79
1.95	-2.35	2.04	-2.00	1.96	-2.05	1.90	-2.15
1.96	-2.47	1.92	-2.32	1.96	-2.06	1.92	-1.87
1.92	-2.49	1.97	-2.29	2.03	-1.92	1.97	-2.25
1.99	-2.36	2.08	-1.98	2.22	-2.17	2.03	-1.97
1.92	-2.30	2.03	-1.96	2.18	-2.07	1.92	-2.16
2.03	-2.08	1.90	-2.24	2.25	-1.96	1.94	-2.11
2.10	-1.77	1.81	-2.51	2.07	-2.13	1.97	-2.00
2.03	-2.12	1.89	-2.26	1.94	-2.09	1.85	-2.19
2.06	-1.89	1.89	-2.32	2.04	-2.22	1.95	-2.17
1.99	-2.00	1.82	-2.34	1.99	-2.31	2.02	-2.00
2.11	-1.85	1.98	-2.22	2.12	-2.14	1.88	-2.22
1.98	-2.12	2.09	-1.73	2.06	-2.35	1.94	-2.09
1.99	-2.09	2.04	-1.90	2.02	-2.43		
1.99	-1.93	2.04	-2.11	2.02	-2.21		
2.00	-1.86	2.00	-2.03	2.00	-2.25		
2.05	-2.05	1.81	-1.94	2.08	-1.96		
2.08	-1.92	2.06	-1.89	2.03	-2.08		
1.90	-2.32	2.03	-2.01	1.98	-2.15		
1.90	-2.35	2.02	-1.95	1.84	-2.36		
2.07	-1.76	1.99	-2.06	1.98	-2.12		
2.08	-1.95	1.96	-2.08	2.02	-2.22		
2.10	-1.82	2.03	-2.00	1.95	-2.24		
2.10	-1.88	2.00	-1.97	1.97	-2.19		
2.06	-2.09	2.09	-1.94	1.95	-2.31		
2.06	-1.88	1.93	-2.13	2.04	-1.87		
2.03	-1.94	1.99	-1.91	2.03	-2.01		
2.10	-1.70	2.01	-1.91	2.17	-1.96		
2.07	-1.86	2.01	-2.03	1.98	-2.12		
2.06	-1.81	1.99	-2.20	1.97	-2.15		
2.06	-1.75	2.06	-1.90	2.08	-1.76		
2.07	-1.87	2.00	-1.88	1.92	-2.08		
2.06	-1.82	1.93	-2.25	1.98	-1.94		
2.07	-1.83	1.79	-1.89	1.89	-2.28		

Mean $\delta^{13}\text{C}$ = 2.00 ± 0.08 ; Mean $\delta^{18}\text{O}$ = -2.09 ± 0.19 , total no. of measurements=135

2.5.2. Calcium Carbonate and Organic Carbon measurements:

Calcium carbonate in the sea sediments from the cores SS 3827 G and SS 4018 G were measured using the *UIC* Coulometer, Model 5012 (*UIC* Inc., IL, USA). CO_2 is evolved from the sediments by reacting the carbonate present in them with 40% orthophosphoric acid at 70°C . It is purified and analyzed following the standard procedure (Bhushan et al, 2001). The standard used is the Na_2CO_3 . Calcium carbonate in the core SK 145-9 was estimated using the EDTA titration method (Vogel, 2002). Around 0.1g sediment sample was taken to which was added 10 ml of 2% acetic acid. The leachate obtained was titrated with 0.01M EDTA solution using the 0.4% Eriochrome Black-T indicator. The CaCO_3 concentration obtained is divided by the weight of the sediment to obtain the value in weight %.

Total carbon and total nitrogen were measured using a *Fisons* NA 1500 NC Elemental Analyzer (*Fisons* Inc., Italy). Around 10-15 mg of sediment sample is packed in a tin foil, which is released into a combustion chamber at 1020°C . The evolved CO_2 and nitrogen oxides are then passed through a reduction chamber maintained at 650°C that contains metallic copper. After further purification the gases are passed through a gas chromatograph that release them sequentially. The gases enter a thermal conductivity detector, which generate electric signals proportional to the concentrations of the gases present. A calibration curve is prepared using Deer River Black Shale as a standard, having 2.53% carbon and 0.12% nitrogen (Bhushan et al, 2001). Again the values are expressed in weight % by dividing by the weight of the sediment taken. Organic Carbon was calculated by subtracting inorganic carbon values (obtained from coulometer and EDTA titration) from the total carbon values i.e.,

$$C_{\text{org}} = C_{\text{total}} - C_{\text{inorg}}$$

The precision in measuring CaCO_3 , Total Carbon and Nitrogen are 3%, 4% and 6%. The precision calculated for C_{org} is 5%. All the uncertainties quoted are 1σ .

2.5.3. Nitrogen isotope measurements:

For this study, an Elemental Analyzer (Flash EA 1112 Series, *CE* Instruments, Italy) interfaced with *Finnigan* Delta Plus continuous flow mass spectrometer (*Thermo Quest* *Finnigan*, Germany) via *Conflo* III was used. For isotopic analysis,

adequate amount of the sediment sample (5 to 50 mg, depending on the nitrogen concentration) was wrapped in a silver foil and dropped into the combustion furnace of the elemental analyzer. There flash combustion takes place in the presence of 5-grade oxygen (99.999%). The evolved gases pass through reduction chamber containing metallic copper that reduces the oxides of nitrogen to N₂. Thereafter the gases pass through a water adsorbant and a gas chromatograph that introduces pure N₂ in the mass spectrometer where ¹⁵N abundance was determined. Dry helium (99.999%) acted as a carrier gas. The δ¹⁵N values have a systematic offset of approximately -3.5‰ as evident by comparison with other studies in the same region (e.g. Altabet et al, 2002; Altabet et al, 1995; Ganeshram et al, 2000), probably due to the low nitrogen content of the sediment samples. But this offset is not going to affect the interpretations as we are looking at trends exhibited by relative variations in these values and not the absolute values. The precision of isotopic measurement is 0.38 ‰ with a standard error of 0.08 ‰ obtained by making multiple measurements of ammonium sulphate standard, IAEA-N-2 [(NH₄)₂SO₄, No. 342] as shown in the Table 2.4. The error reported is 1σ.

Table 2.4. Ammonium sulphate standard δ¹⁵N values in per mil with respect to air.

δ ¹⁵ N	δ ¹⁵ N
19.96	19.74
19.75	20.82
19.80	19.80
20.43	19.95
20.72	19.74
20.03	20.07
19.78	20.44
20.67	19.85
20.60	19.71
20.05	

Mean δ¹⁵N = 20.10 ± 0.38, total no. of measurements = 19

Standard error = 0.08 ‰, 1 standard deviation

Chapter 3

**Eastern Arabian Sea: High Resolution
Monsoon Reconstruction for the
Past ~2800 years**

3.1. Introduction:

Most of the earlier studies on paleomonsoon variations have concentrated on the western Arabian Sea, as it undergoes intense biogeochemical changes during the SW Monsoon (Nair et al, 1989) that are easily detectable. But most of these studies have focused on the effect of SW Monsoon winds on various processes such as wind induced upwelling, dust transport etc (e.g. Clemens et al, 1991; Anderson and Prell, 1993; Sirocko et al, 1993; Naidu et al, 1993, Reichart et al (2002 a), Gupta et al, 2003 and references therein) and not on the precipitation signal. Stronger SW Monsoon winds do not necessarily mean higher monsoon precipitation as, the latter depends on various other parameters such as the moisture content of the air-masses, which is probably influenced by the SST of southern Indian Ocean (Clemens et al, 1996), air parcel convergence and convection etc. (Gadgil, 2003). So it becomes very important to test how the wind speed correlates with the precipitation and how this relationship varied in the past. The eastern Arabian Sea receives abundant fresh water as either direct overhead precipitation or surface runoff from the adjacent hills, present along the western Indian coast (Western Ghats), which induce intense orographic precipitation during the SW monsoon (June – September). The influx of copious amounts of fresh water into the coastal eastern Arabian Sea reduces the sea surface salinity (SSS) that is reflected in the various proxies that ultimately get preserved in the sea sediments. A sediment core *viz.* SK145-9 has been strategically chosen from the eastern Arabian Sea, where sedimentation is fast enough to provide a high time resolution comparable to studies from the western Arabian Sea. This can help in the comparative study of past changes on two different aspects of the monsoon: (i) wind induced upwelling and productivity (ii) rainfall and runoff to the ocean and its effect on surface salinity. Furthermore, because of the high-resolution sampling, it can delineate centennial and sub-centennial scale variations in the monsoon rainfall during the past ~2800 years, corresponding to the studied length of the core SK145-9.

3.2. Core location:

Core SK 145-9 has been raised from the eastern continental margin of the Arabian Sea from a water depth of 400m off the Mangalore coast. It is from a depth that falls well within the oxygen minimum zone (OMZ), which is 250 – 1250 m in the present day Arabian Sea (Wyrki, 1971; Deuser et al, 1978; Naqvi, 1987; Olson et al, 1993). For further details regarding the core location, please refer to Table 2.1. The core location is shown in Fig.3.1 with the locations of other cores from the Arabian Sea with which results are compared.

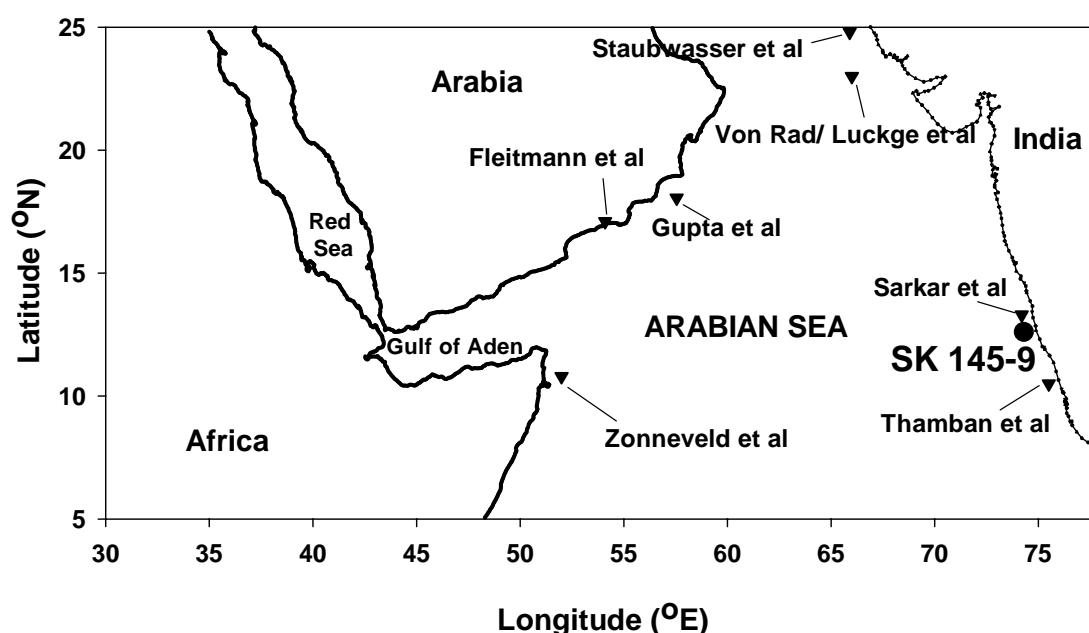


Fig.3.1. Locations of the core SK145-9 (this study, shown by circle) and other cores with which it has been compared.

3.3. Oceanographic conditions at the core site:

During the SW monsoon abundant orographic precipitation takes place over the Western Ghats (upto 4000 mm yr⁻¹, Sarkar et al, 2000) that lie parallel to western Indian coast from ~20°N to ~10°N latitudes. This freshwater ultimately gets into the coastal Arabian Sea as surface runoff and reduces the sea surface salinity considerably. This reduction in the surface salinity is evident in the Fig.3.2, during September. The salinity contours were taken from the website www7320.nrlssc.navy.mil/global_ncom/ara.html maintained by the Naval Research

Laboratory, United States Navy. Along the southwestern Indian coast, the salinity contours become north-south with low salinities of upto 34.5 PSU pointing towards the fresh water influx and away from the coast, salinities rapidly increase.

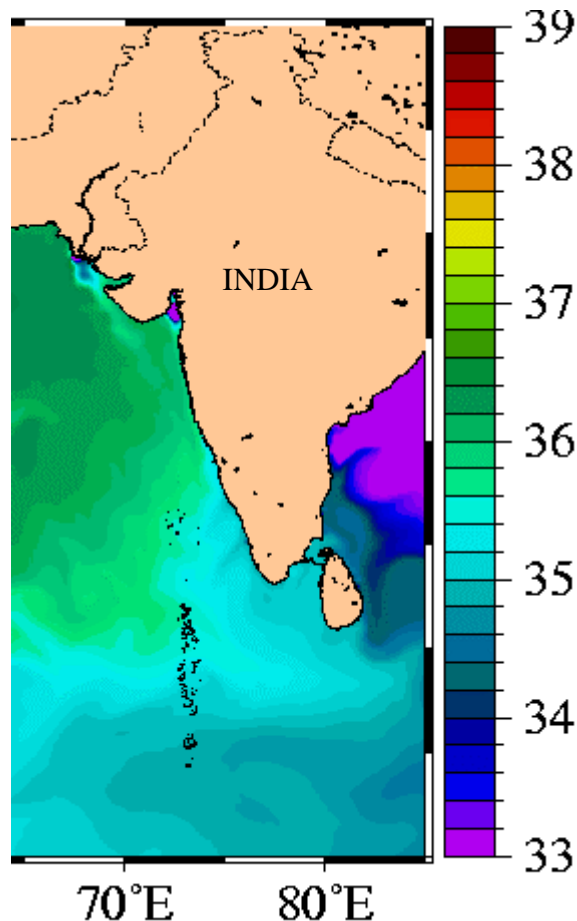


Fig. 3.2. September Salinity contours in the eastern Arabian Sea. Salinity units are in PSU.

The surface circulation in the eastern Arabian Sea is characterized by seasonally reversing West Indian Coastal Current (WICC). Please refer to the Fig.1.1 and 1.2 for schematic diagrams of the Indian Ocean circulation during the summer and winter monsoons respectively. During the summer monsoon (SW monsoon), WICC flows southward along the western Indian coast involving the Laccadive Low (LL) and meets the Southwest Monsoon Current (SMC) that flows eastward (Cutler and Swallow, 1984; Shetye and Shenoy, 1988). There is a weak northward flowing undercurrent carrying the low salinity waters at 150-200 m (Antony, 1990; Shetye et al, 1990). During the winter monsoon (NE monsoon), the westward flowing Northeast Monsoon Current (NMC) supplies water to the WICC that now flows northward. This northward flowing WICC is associated with a southward flowing undercurrent

(Shetye et al, 1991) at a depth of 150-200 m. During this season an anticyclonic gyre develops just north of the Laccadive Islands at the southern end of WICC, which is known as Laccadive High (LH) as sea surface height increases by ~12 cm during that time (Bruce et al, 1994).

3.4. Age-Depth Model:

The core SK145-9 has eleven dates covering ~13,000 calendar years (spanning 252 cm length) providing an average sedimentation rate of 19 cm/10³ years. This core has an average resolution of ~50 year per cm. The top 50 cm have been sampled at every cm and below 50 cm the sampling was done at every 2 cm. Thus it offers a high-resolution and therefore will aid in understanding sub-centennial scale variability. The top 50cm of this core (sampled closely), covering a time span of approximately 2800 years, has been taken for further studies. The top of the core (*viz.* 0-2 cm) has a calibrated age of 410 ± 80 yr. For dates in the tabular form and other related information please refer to Table 2.2.

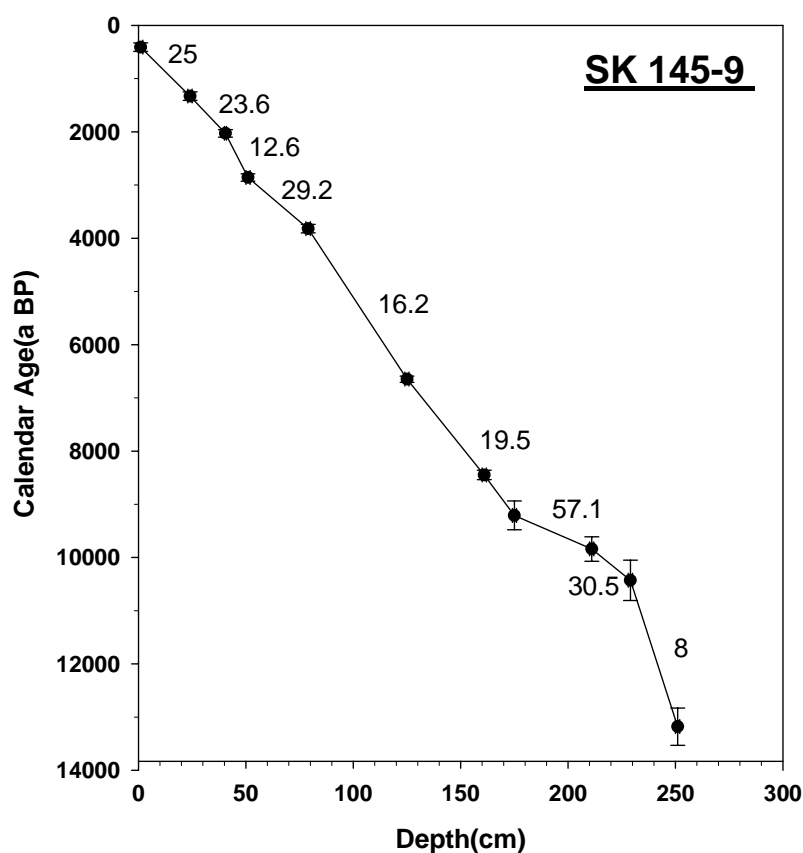


Fig. 3.3. Calibrated radiocarbon ages and sedimentation rates (cm/ka) for various intervals in the core SK145-9.

The radiocarbon dates in this core have been converted to calendar ages using the calibration program “Calib 4.1 (INTCAL 98)” (Stuiver et al, 1998) with a reservoir age correction of 500 ± 30 years (deviation from the assumed value of 400 years i.e. $\Delta R = 100 \pm 30$ yr, Dutta et al, 2001). Dutta et al (2001) measured gastropod and bivalve shells from western Indian off the Dwarka (in Saurashtra) coast and southern India off Rameshwaram. They reported a ΔR value of 163 ± 30 yrs for Saurashtra coast and 32 ± 20 yrs for southern Indian coast. So an approximate value falling midway between these two values was taken as the ΔR value for the core location. Later Southon et al (2002) have reported a ΔR value of 126 ± 64 yr for a location very close to the core site, which is similar to that of Dutta et al (2001).

3.5. Precipitation Signals as Manifested by Oxygen Isotopes:

Oxygen isotopic analyses have been carried out on three different species of foraminifera viz. *Globigerinoides ruber*, *Globigerinoides sacculifer*, *Globorotalia menardii* as shown in the Fig.3.4. *G.ruber* and *G.sacculifer* are surface dwelling species predominantly inhabiting top 25 m and 50 m respectively whereas *G.menardii* is a deeper dwelling species predominantly inhabiting 100-150 m (Be, 1977, Fairbanks et al, 1980; Fairbanks et al, 1982). Thus an oxygen isotope signal arising due to any surface processes (e.g. salinity change) will be most pronounced in the surface dwelling species viz. *G.ruber* and *G.sacculifer* and will be subdued in the deeper dwelling species i.e. *G.menardii*. As evident from Fig. 3.4, all the three species show similar signals that are somewhat restrained in the deeper dwelling one. Furthermore comparative analysis with *G.bulloides* data from the ODP Site 723A and a box core RC2730 from the adjacent Oman margin, western Arabian Sea (Gupta et al, 2003) has been carried out to check whether high/low SW monsoon wind intensity results in higher/lower precipitation. *G.bulloides* is a temperate water species and can occur in tropics where cooler water is present due to upwelling. Thus their abundance as expressed as percentage of total planktonic foraminifera is an excellent indicator of upwelling, which in turn is controlled by the wind strength (Anderson et al, 2002).

The factors controlling the oxygen isotopes in foraminiferal shells are the sea surface salinity (SSS) and sea surface temperature (Shackleton, 1967, Niitsuma et al, 1991). For the past ~3 ka there has been no salinity fluctuations due to the global ice-volume effect as there were no significant global ice-melting episodes affecting sea

level (Fairbanks, 1989). Moreover the SST variations in the tropics for the past 10 ka are very small ($\sim 0.5^{\circ}\text{C}$, Rostek et al, 1993). The studied species are known to grow predominantly during the SW monsoon months and hence are likely to record the signals arising mainly due to SW monsoon fluctuation (Guptha et al, 1997). In the eastern Arabian Sea, SSS variation is mainly controlled by the variation in the supply of fresh water as surface runoff from the adjacent Western Ghats during the southwest monsoon. Furthermore, a weak upwelling system occurs in the eastern Arabian Sea along the western Indian coast prior to the SW summer monsoon that gets established from February onwards (Shetye, 1984). This upwelling is controlled by factors other than the SW monsoon winds. Studies by Shankar and Shetye (1997) and McCreary et al (1993) have shown that the early upwelling is a result of the remote forcing by winds in the Bay of Bengal and southwest coast of India that generate the northward propagating Kelvin and westward propagating Rossby waves. It is further confirmed by the study carried out by Thamban et al (2001) on a sediment core near the Cochin coast (southwest continental margin of India). They suggest that the remote forcing on upwelling could have been more active during the past. With the onset of SW monsoon winds, the upwelling intensifies and the SST drops by upto 3°C (Levitus and Boyer, 1994). But as the upwelling is affected by basin-wide remote processes in Arabian Sea and Bay of Bengal (McCreary et al, 1993), the variation in the local upwelling intensity will only affect the interannual SST changes in a small way (Thamban et al, 2001). We therefore assume that the dominant factor controlling the $\delta^{18}\text{O}$ signals in the eastern Arabian Sea is the SSS changes induced by the variation in the SW monsoon precipitation. A reduction in SSS occurs due to the influx of large amount of fresh water, depleted in ^{18}O , as surface runoff into the coastal eastern Arabian Sea during intense SW monsoon precipitation events. In the eastern Arabian Sea, for every per mil decline in salinity, the $\delta^{18}\text{O}$ value decreases by 0.33 ‰ (Duplessy et al, 1981; Sarkar et al, 2000). Thus a depleted $\delta^{18}\text{O}$ signal indicates enhanced southwest monsoon precipitation whereas an enriched $\delta^{18}\text{O}$ signal points towards reduced precipitation due to weaker southwest monsoon (indicated by arrows in the Fig. 3.4).

In order to have a quantitative estimate of the rainfall variation over the southeastern coastal Arabian Sea, a parameter P-E i.e. excess of precipitation over

evaporation has been approximately estimated. Ramesh Kumar and Prasad (1995) calculated P-E values for this region during the monsoon season (the primary data being temperature, salinity and wind stress). The core top $\delta^{18}\text{O}$ values of *G.sacculifer* (predominantly inhabits top ~50 m and major growing season is during SW monsoon) have been calibrated with the P-E data and an approximate transfer function has been obtained (Ramesh, 2001) for the eastern Arabian Sea, which is as follows:

$$(P-E) \text{ mm} \sim -800 \delta^{18}\text{O} - 1400$$

The P-E values are depicted at the top of the second panel of the Fig.3.4, as shown below:

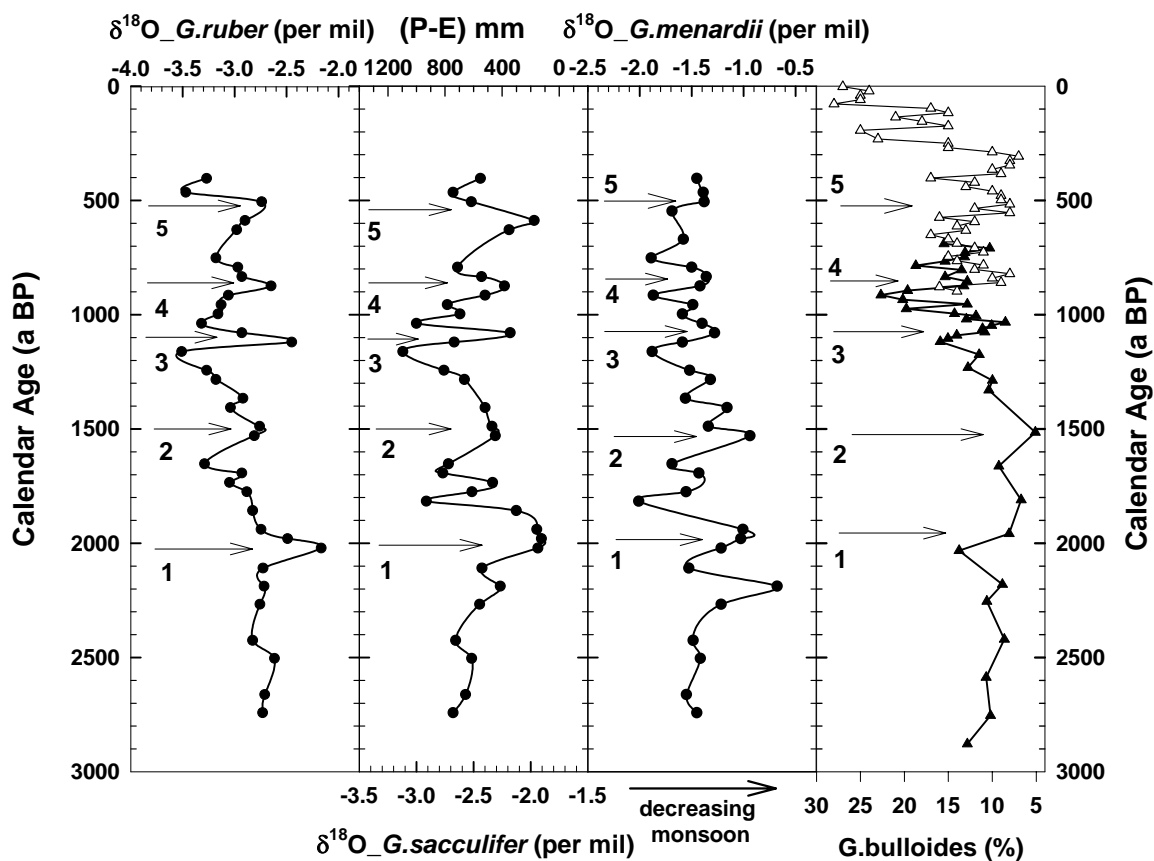


Fig.3.4. Downcore variations of $\delta^{18}\text{O}$ of three species of foraminifera in the core SK 145-9 (shown by closed circles, this study), % *G.bulloides* data from the ODP Site 723A (closed triangles) and the Oman margin box core RC2730 indicated by open triangles (Gupta et al, 2003), P-E values shown at the top of the 2nd panel.

The first enriched $\delta^{18}\text{O}$ signal observed at 2000 a BP (indicated by arrow-1 in Fig.3.4) points towards an increase in SSS and hence a reduction in the monsoon intensity at that time. This arid event is reflected not only in both the surface dwelling species i.e. *G.ruber* and *G.sacculifer* (which will be more affected by the increase in SSS) but also in the deeper dwelling species *G.menardii* in which it is quite pronounced. This points towards the severity of the 2000 a BP arid event. This arid event centered at 2000 a BP has been widely seen in many terrestrial and marine records. Yadava and Ramesh (2005) noted a prominent arid event (enriched ^{18}O) in the speleothem deposits in a cave from Orissa, eastern India. Similarly Von Rad et al (1999) and Luckge et al (2001) analyzed a core from the northern Arabian Sea off the Karachi coast covering the past 5000 years, which is influenced by the river runoff from Pakistan. They have reported low precipitation at 2000 a BP based on the Ti/Al and varve thickness data. Our observation above, the low SW monsoon precipitation at 2000 a BP, is based on an entirely different proxy from a different location in the Arabian Sea. The 2000 a BP arid event is also observed in the % *G.bulloides* (Gupta et al, 2003) record that shows a decrease at that time indicated by the arrow-1 pointing towards reducing wind intensity. A reduction in monsoon is also indicated by a hiatus in the growth of speleothem in Oman from 2500 a BP to 1500 a BP (Fleitmann et al, 2003). Staubwasser et al (2003) found reduced precipitation on the basis of increasing $\delta^{18}\text{O}$ in *G.ruber* from a core off the Pakistan coast. Zonneveld et al (1997) obtained a core from the Somalian coast, western Arabian Sea and found a decline in the upwelling intensity ~2000 a BP on the basis of dinoflagellates cysts and inferred that SW monsoon strength declined during that time. Similarly, Sarkar et al (2000) and Thamban et al (2001) have taken sediment cores from the eastern Arabian Sea near to the Manglore coast and Cochin coast respectively and measured $\delta^{18}\text{O}$ values in planktonic foraminifera. Although their cores have coarser resolution, still they exhibit reduction in SW monsoon precipitation during ~2 ka BP. Thus it is clear that this 2000 a BP arid event was recorded in diverse proxies not only in the Arabian Sea but also on the Indian Subcontinent. Thereafter the monsoon tends to strengthen upto 1600 a BP as exhibited by the decreasing $\delta^{18}\text{O}$ signal and P-E values that increased from 100 mm to 1000 mm (Fig. 3.4).

An earlier, short aridity signal in the form of enhanced $\delta^{18}\text{O}$ value at 2200 a BP is seen only in the deeper dwelling species i.e. *G.menardii* (~150-200 m water depth). One possible explanation could be the following. During SW monsoon, southward flowing West Indian Coastal Current (WICC) is accompanied by a northward flowing undercurrent carrying low salinity waters at a depth of 150-200 m (Antony, 1990; Shetye et al, 1990). If SW monsoon strength reduced, then it would weaken the WICC as well as the undercurrent and the $\delta^{18}\text{O}$ values of only the deeper dwelling species would increase as the inflow of low salinity water reduced.

Another arid event of a smaller magnitude is observed at 1500 a BP (shown by arrow-2), shown by all the three species of foraminifera. At that time % *G.bulloides* exhibits minimum abundance (~5 %) in the western Arabian Sea (Gupta et al, 2003) pointing towards an extreme reduction in upwelling and hence the wind strength. But this minimum wind strength does not correspond to minimum precipitation, which happens at ~2000 a BP as evident by the maximum $\delta^{18}\text{O}$ values during that time. This indicates that variation in the monsoon wind strength is not linearly related to the variation in monsoon precipitation.

Thereafter, precipitation intensity strengthens upto ~1200 a BP after which it shows a sudden decline centered at ~1100 a BP (shown by arrow-3) and then monsoon intensified as rapidly. This sudden reduction and subsequent enhancement in monsoon intensity is also observed in the wind intensity record of the western Arabian Sea as shown by sharp decline in % *G.bulloides* during the above period. It is also observed in the speleothem records (Yadava and Ramesh, 2005), varve record (Von Rad et al, 1999; Luckge et al, 2001), sediment record (Staubwasser et al, 2003) and the Oman stalagmites (Fleitmann et al, 2003).

Another episode of precipitation reduction is observed at the ~800 a BP to ~900 a BP that is reflected all the three species of the foraminifera (arrow-4). This reduction is accompanied by a corresponding reduction in the SW monsoon wind intensity (Gupta et al, 2003). This event is seen by Von Rad et al (1999) in varve thickness records and by Staubwasser et al (2003), who find a prominent $\delta^{18}\text{O}$ enhancement at that time. Fleitmann et al (2004) also observed this event in the stalagmites from the southern Oman.

The next arid event as evident by the $\delta^{18}\text{O}$ record of the core SK145-9 occurs at ~500 a BP (indicated by arrow-5) that is shown by all the three species. The % *G.bulloides* also exhibits a decrease at that time implying reduced wind strength. This event is also observed in the varve thickness record (Von Rad et al, 1999) and sediment record (Staubwasser et al, 2003). Luckge et al (2001) measured Ti/Al ratio in the varve sediments (Von Rad et al, 1999) indicating fluvial input. They found reduced fluvial input during that time indicating reduced monsoon precipitation. Furthermore, Fleitmann et al (2004) observed a reduction in precipitation at ~500 a BP in stalagmite deposits from southern Oman.

Thus the above discussion proves that the periods of aridity observed in the eastern Arabian Sea were widespread and were reflected in diverse proxies from different regions around it. Also, wind speed indicators from the western Arabian Sea exhibit a good correlation with the precipitation signals from the eastern Arabian Sea at least during the last 2800 years. Reduced precipitation was accompanied with weakened winds and vice-versa. But the relationship appears to be non-linear as precipitation minimum occurred at ~2000 a BP while the wind minimum occurred at ~1500 a BP.

3.6. Temporal variation in productivity:

Various productivity indicators such as CaCO_3 %, organic carbon content and $\delta^{13}\text{C}$ of the three different species of foraminifera along with $\delta^{15}\text{N}$ in the sedimentary organic matter were also measured in the same core.

3.6.1. Productivity as manifested by CaCO_3 and C_{org} content:

During the SW monsoon months, strong winds might cause mixed layer deepening, which injects nutrient rich waters into the surface layer enhancing surface productivity. Another possibility is increased productivity due to nutrients derived from land in the form of surface runoff. Thus, higher productivity may result either from increased runoff or increased winds. Data from the JGOFS-India program during the 1994-1995 shows that the primary productivity reaches ~0.6 $\text{gC/m}^2/\text{d}$ during the SW monsoon whereas it is only ~0.3 $\text{gC/m}^2/\text{d}$ and ~0.2 $\text{gC/m}^2/\text{d}$ during the NE monsoon and intermonsoon respectively (Bhattathiri et al, 1996). The present core has been raised from a water depth of 400 m that lies well within the OMZ (150 m – 1250

m) in the Arabian Sea. In the oxygen depleted waters of OMZ, organic carbon is better preserved for which various reasons have been given, which include (1) the need to establish complex microbial communities for the stepwise degradation of organic substrates, (2) the buildup of toxic waste products such as H_2S , (3) due to unavailability of oxygen, benthic organisms do not inhabit the sediments overlain by OMZ waters hence lack of bioturbation, (4) the presence of compounds that resist anoxic degradation but are easily degraded aerobically via O_2 -requiring oxidative enzymes (Hedges and Kiel, 1995; Emerson and Hedges, 1988; Lee, 1992, Aller, 1994). It also escapes the diagenetically active layer rapidly due to the high sedimentation rate (average ~ 19 cm/ka) and thus gets shielded from other oxidizing agents such as nitrate, sulphate etc. (Heinrichs, 1992).

The following figure shows the downcore variations in the calcareous and organic productivity, along with the C/N ratio.

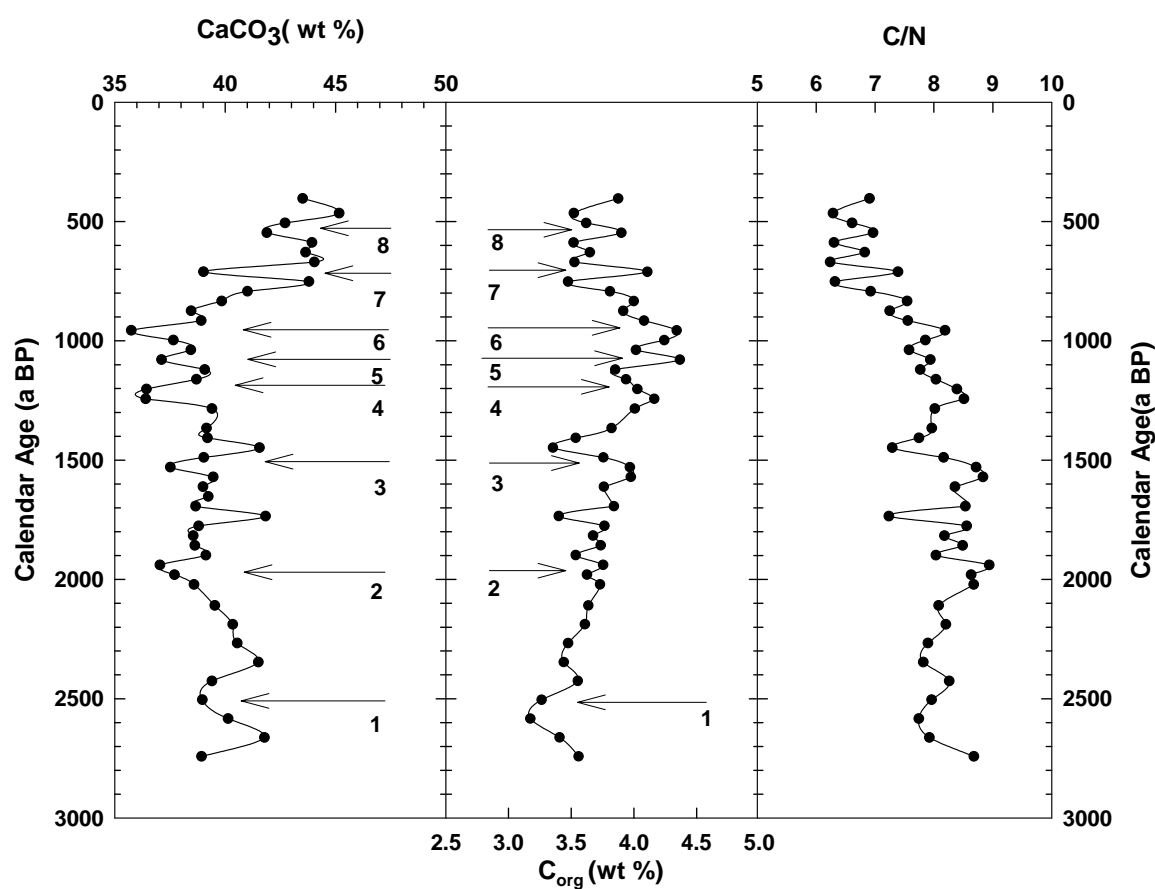


Fig 3.5. Downcore variation of $CaCO_3$, C_{org} and C/N ratio in the core SK145-9 covering the last ~ 2800 years.

C/N ratio has been a traditional proxy to determine the origin of organic matter. Recent marine organic matter has a typical C/N ratio of $\sim 8 \pm 2$ (Mackenzie, 1980) whereas the terrestrial organic matter has a C/N ratio of ~ 20 to ~ 100 (Premuzic et al, 1982; Meyers, 1994). As evident from the last panel in the Fig3.5, it is clear that the organic matter is mainly of the marine origin as all the values fall well within the marine C/N range. It indicates that although the core is from coastal region and probably influenced by terrestrial inflow, mostly the marine surface productivity governs the downcore variation of the various productivity indices.

Centered at ~ 2500 a BP there is a decline exhibited by the calcareous productivity, which is also reflected in the organic productivity (arrow-1, Fig.3.5). A slight decrease in monsoon intensity is observed at that time as evident from the increasing $\delta^{18}\text{O}$ values in all the three species of foraminifera (Fig.3.4). Subsequently calcareous and organic productivity show a very interesting trend. During the periods of reduced monsoon, calcareous productivity decreases whereas organic productivity increases. At 2000 a BP, which is the time of widespread aridity (seen in $\delta^{18}\text{O}$), we observe a decline in CaCO_3 (%) while C_{org} (%) follows an increasing trend (arrow-2, Fig.3.5). During the next major arid episode, centered at ~ 1500 a BP, we again find a decrease in calcareous productivity whereas organic productivity shows enhancement (arrow-3). Similarly during the next arid event as deciphered from the oxygen isotopes at 1100 a BP, the calcareous and organic productivity exhibit reduction and enhancement respectively (arrow-5). Thereafter calcareous productivity exhibits an increasing trend with decline observed at the major arid events such as at ~ 900 a BP (arrow-6) and ~ 500 a BP (arrow-8). In contrast the organic productivity stays more or less uniform or displays a slightly decreasing trend.

A possible reason for the opposite behaviour of organic and inorganic (calcareous) productivity could be: while winds mix up the ocean, providing nutrients from below and enhancing productivity, fresh water runoff from the land forms a lid and suppresses mixing; however runoff might carry nutrients from lands such as silicate and phosphate to enhance diatom and organic productivity. During the periods of reduced SW monsoon, upwelling intensity decreases considerably resulting in reduced supply of nutrients from below but surface runoff (although relatively lower)

will bring a little amount of nutrients that will result in organic productivity. Calcareous organisms are not the primary producers in the oceans; instead they are the secondary consumers i.e. consume the primary producers (main contributor to organic productivity). The relatively lower organic productivity will affect calcareous organisms more as they are higher on the food web and are more sensitive to the changes in food supply. Hence a reduction in nutrient supply could result in reduced calcareous productivity but could support the organic productivity. Such a contrasting behaviour with calcareous productivity is also exhibited by $\delta^{13}\text{C}$ in the planktonic foraminifera that is further discussed in the next section (section 3.5.2) along with another probable reason *viz.* onset of *Trichodesmium* (a blue-green algae) blooms.

There are several signals of reduced calcareous productivity such as at 1200 a BP and 700 a BP (shown by arrows- 4 & 7), which are the periods of enhanced precipitation, as inferred from oxygen isotopes. A possible cause can be that productivity in the eastern Arabian Sea is an interplay of at least two factors i.e. wind induced surface layer mixing (or upwelling) and fresh water runoff from the land as discussed earlier. Thus productivity is not controlled solely by SW monsoon wind strength but depends on which factor dominates during that particular period. During reduced SW monsoon, wind intensity weakens that in turn reduces the upwelling because of which calcareous productivity reduces as is the case for 2500 a BP, 2000 a BP, 1500 a BP signals. But, during enhanced monsoonal precipitation large amount of fresh water get into the coastal Arabian Sea, which forms a low salinity lid over the seawater that inhibits upwelling (Thamban et al, 2001) and reduces calcareous productivity. But this terrestrial inflow also brings nutrients that enhance the organic productivity. When the primary productivity is relatively lower due to the reduced upwelling and is sustained by terrestrial nutrient supply only, it will affect secondary consumers more as they are more sensitive to the changes in food supply. Thus even relatively higher monsoon intensity e.g. at 1200 a BP and 700 a BP could result in reduced calcareous productivity.

3.6.2. Productivity as manifested by $\delta^{13}\text{C}$:

The $\delta^{13}\text{C}$ in foraminifera are controlled by the carbon isotopic composition of seawater, which in turn is governed by the organic productivity as discussed in the section 2.4.2. The following figure shows the temporal variations in $\delta^{13}\text{C}$ in three species of foraminifera viz. *G. ruber*, *G. sacculifer* and *G. menardii*.

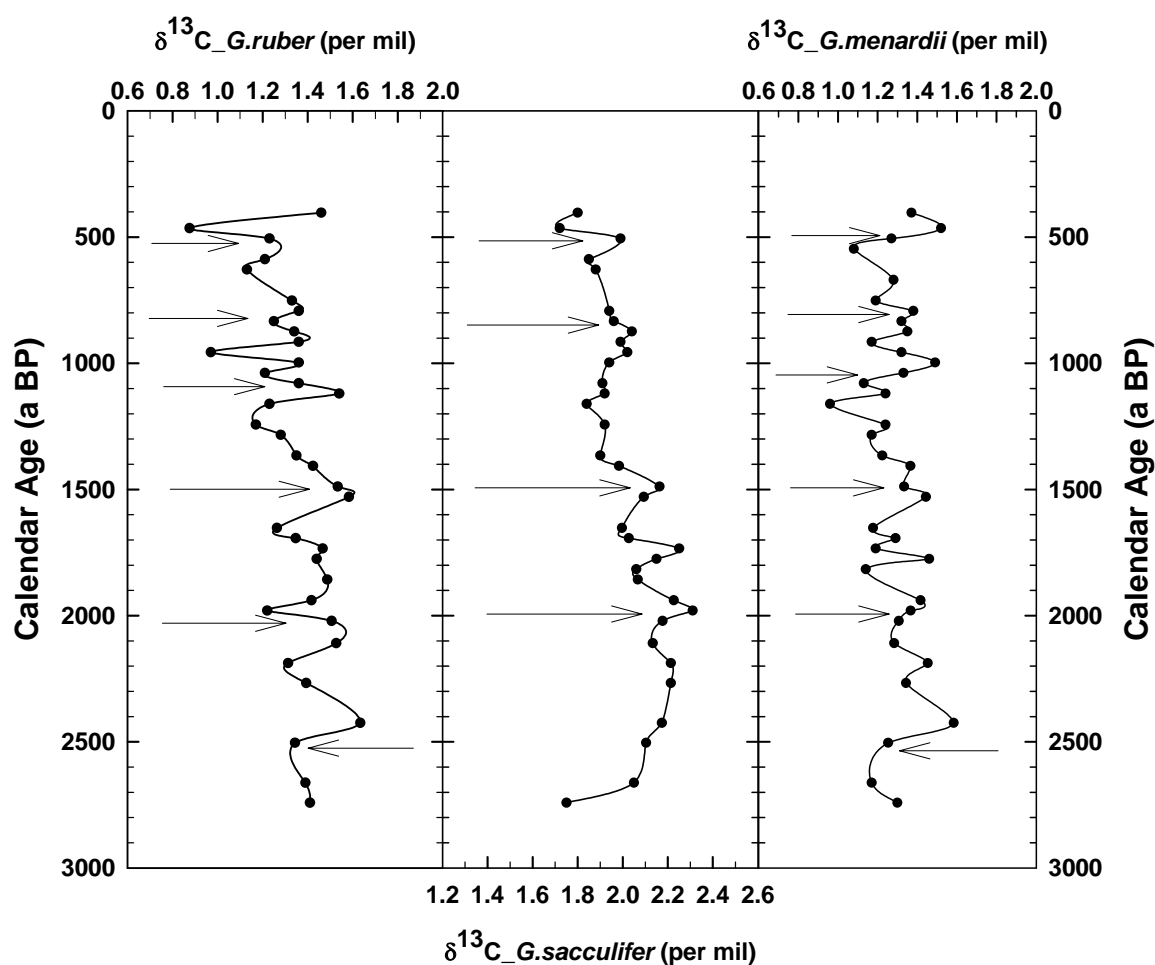


Fig 3.6. Downcore variation of $\delta^{13}\text{C}$ of three species of foraminifera in the core SK 145-9.

At 2500 a BP, we find a decrease in $\delta^{13}\text{C}$ that is conspicuously seen in the two species viz. *G. sacculifer* and *G. menardii*. Such a decrease is observed in both calcareous and organic productivity indicators along with a precipitation decline as inferred from slightly increasing $\delta^{18}\text{O}$ at that time. It implies that SW monsoon

precipitation reduced at that time, which is reflected in various productivity indicators.

At 2000 a BP we find an increase in $\delta^{13}\text{C}$ values, which is the time of widespread aridity. This observation is in contrast to calcareous productivity that shows a decrease; but $\delta^{13}\text{C}$ is akin to C_{org} , which increases during that time. Thus $\delta^{13}\text{C}$ variations in foraminifera indeed reflect organic rather than inorganic productivity. A similar contrast between the calcareous productivity and the $\delta^{13}\text{C}$ in all the three species is also observed during other periods of reduced SW monsoon viz. at ~1500 a BP, ~1100 a BP, ~850 a BP and ~500 a BP. During these periods C_{org} (%), which is an indicator for organic productivity exhibits an enhancement. These observations points towards a very interesting fact that the organic productivity increases during the periods of reduced calcareous productivity, possibly due to runoff supplying nutrients as explained in the previous section.

Another explanation is possible if we take the growth of *Trichodesmium* into account in the surface waters of the eastern Arabian Sea. Genus *Trichodesmium* (Greek; *tricho* = hair, *desmos* = chain) comprises marine, planktonic, blue-green algae that form filamentous colonies. They occur dominantly in the oligotrophic (nutrient poor) tropical and subtropical waters (Carpenter, 1983). They can survive in the nutrient poor water, as they are diazotrophic i.e. directly fix dissolved N_2 rather than NH_3 or NH_4^+ , which is the more preferred pathway. *Trichodesmium* possess gas vesicles that help them float on the sea surface. When the wind stress is low for an extended period of time then extensive blooms could develop, which are called as “Red Tides”. In fact Red Sea derived its name from the coloration imparted by *T.erythraeum* blooms. Some species of *Trichodesmium* are toxic and prevent consumption by organisms higher in the food chain (Hawser et al, 1992; Capone et al, 1997). During reduced monsoon conditions when oligotrophic conditions develop due to reduction in vertical mixing and runoff, extensive *Trichodesmium* blooms can occur in the eastern Arabian Sea. *Trichodesmium* blooms have been reported from the eastern Arabian Sea, along the western Indian coast (Devassy et al, 1978; Sarangi et al, 2004). If toxic species of *Trichodesmium* prevails then it could reduce the production of other carbonate and siliceous shell secreting organisms but

Trichodesmium biomass will contribute to organic productivity. This could explain the contrasting behavior exhibited by the organic and calcareous productivity.

This is further supported by the depleted $\delta^{15}\text{N}$ observed in the sedimentary organic matter as discussed below.

3.7. Temporal variation in the stable isotopes of nitrogen:

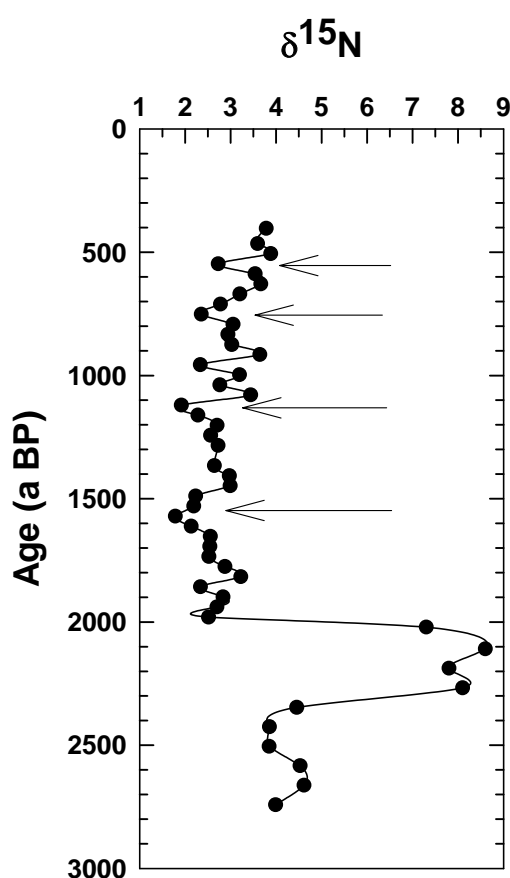


Fig.3.7. Downcore variation of $\delta^{15}\text{N}$ of the sedimentary organic matter in the core SK145-9.

$\delta^{15}\text{N}$ of the organic matter is controlled by the isotopic composition of the source nitrogen species and the fractionation occurring during the uptake of the nitrogen by the organisms. The organisms such as *Trichodesmium* that directly utilize N_2 dissolved in the seawater ($\delta^{15}\text{N}$ near to 0 ‰) will have very depleted $\delta^{15}\text{N}$ signature compared to organisms utilizing NO_3^- or NH_4^+ ($\delta^{15}\text{N}$ is 5 to 6 ‰, Liu, 1989; Kumar et al, 2004). The sedimentary organic matter, which has contributions from organisms directly fixing the atmospheric nitrogen, possesses a typical $\delta^{15}\text{N}$ value of 0-2 ‰

(Capone et al, 1997). Thus sediments constituting *Trichodesmium* will have lower $\delta^{15}\text{N}$ values.

The onset of *Trichodesmium* bloom took place near ~2000 a BP in the eastern Arabian Sea as evident from the sudden decrease observed in $\delta^{15}\text{N}$ values at that time. This period is the major arid event (as seen in $\delta^{18}\text{O}$), which would have led to the development of oligotrophic conditions with very low wind stress that would have facilitated the growth of *Trichodesmium*. Thereafter these blooms seem to persist for the remaining time period covered by the core.

Furthermore, several millennial scale variations are observed during ~1500 a BP, ~1100 a BP, ~800 a BP and ~500 a BP (shown by arrows) that are periods of reduced monsoon. During such periods $\delta^{15}\text{N}$ of the sedimentary organic matter exhibits depleted values that indicates that contribution of the isotopically lighter *Trichodesmium* increases.

Nitrogen percentage is sufficient in this core (typically a value of 0.7 % whereas in the other two cores that are from the open ocean location, it varies from 0.1 % to 0.05 %) and isotope measurements have been rechecked, and confirmed.

However the unusual nature of variation (a sudden jump) needs to be verified by analyzing more cores from the same location. Therefore the above interpretation is only tentative.

3.8. The Solar connection:

It has been proposed that earth's climate is sensitive to very mild changes in solar output, not only at decadal time scales but also at centennial to millennial scales (Bond et al, 2001). Currently there has been a renewed interest in climate forcing by Total Solar Irradiance (TSI), observed to show a remarkable agreement with the smoothed global temperature in the 20th century (Foucal, 2003). Precise measurement of TSI has been made using space borne radiometers, which show that it varies with an rms amplitude of about 0.1% in response to the changing area covered by sunspots. But this variation seems to be too low to cause widespread climatic changes. It is suggested that there is a large amplitude, slowly varying component of TSI that has been overlooked by the radiometric measurements. It is believed that TSI might have been lower by as much as 0.25% during the Maunder Minimum than at present (Lean et al, 1995) and even a minor variation in TSI (0.1 -

0.3%) can bring about major changes in monsoonal precipitation via various positive feedback processes such as moisture availability and changes in atmospheric circulations (Mehta and Lau, 1997; Neff et al, 2001; Bond et al, 2001). Neff et al (2001) studied speleothem samples from Oman for the period 9 ka to 6 ka and compared them with $\Delta^{14}\text{C}$ record from tree rings, which is dependent on cosmic ray fluxes modulated by solar activity. They found an excellent correlation between the monsoon and solar proxies and concluded that variation in solar radiation exhibits a prominent control over the monsoon system on centennial to decadal timescales. Similarly, Fleitmann et al (2003) analyzed Holocene speleothems from Oman and compared the $\delta^{18}\text{O}$ data with GRIP $\delta^{18}\text{O}$ and $\Delta^{14}\text{C}$ record from tree rings. They proposed that early Holocene monsoon circulation was controlled by glacial boundary conditions such as North Atlantic northward heat transport and the thermohaline circulation. After 8 ka BP, as the thermohaline circulation stabilized, the monsoon circulation responded more directly to solar forcing. Agnihotri et al (2002) obtained a core from the eastern Arabian Sea off the Gujarat coast and analyzed it for various paleoclimatic proxies for the past 1200 years and compared with TSI data. They found nearly similar trends for all these proxies and TSI variation within the radiocarbon dating errors; lower TSI is accompanied by lower productivity and reduced runoff denoting weakened monsoon precipitation. Spectral analyses of the TSI, paleoclimatic proxies and the Indian summer monsoon rainfall yielded similar periodicities, which led them to propose that solar forcing controls the monsoonal precipitation.

Bard et al (2000) reconstructed TSI data for the past 1200 years, which has been taken for the present study. They based the TSI estimation on the common fluctuations of the ^{14}C and ^{10}Be production rates obtained from tree rings and polar ice. The TSI curve used in this study assumes a 0.25% reduction in TSI during Maunder Minimum as proposed by Lean et al (1995). The TSI data is unequally spaced at 8 to 10 years interval, which is first splined for every 10-year and then a 10 point running average is taken so that resolution of the TSI data becomes comparable to the resolution for the core SK 145-9. The TSI data are compared with the $\delta^{18}\text{O}$ in all the three foraminiferal species, which is a more robust proxy for the SW monsoon intensity as discussed in the section 3.4. The productivity proxies can't be used as

they are affected not only by SW monsoon wind induced surface mixing but also by surface runoff that complicate their relationship with monsoon. The figure 3.8 compares the temporal variation in TSI and paleoclimatic proxies.

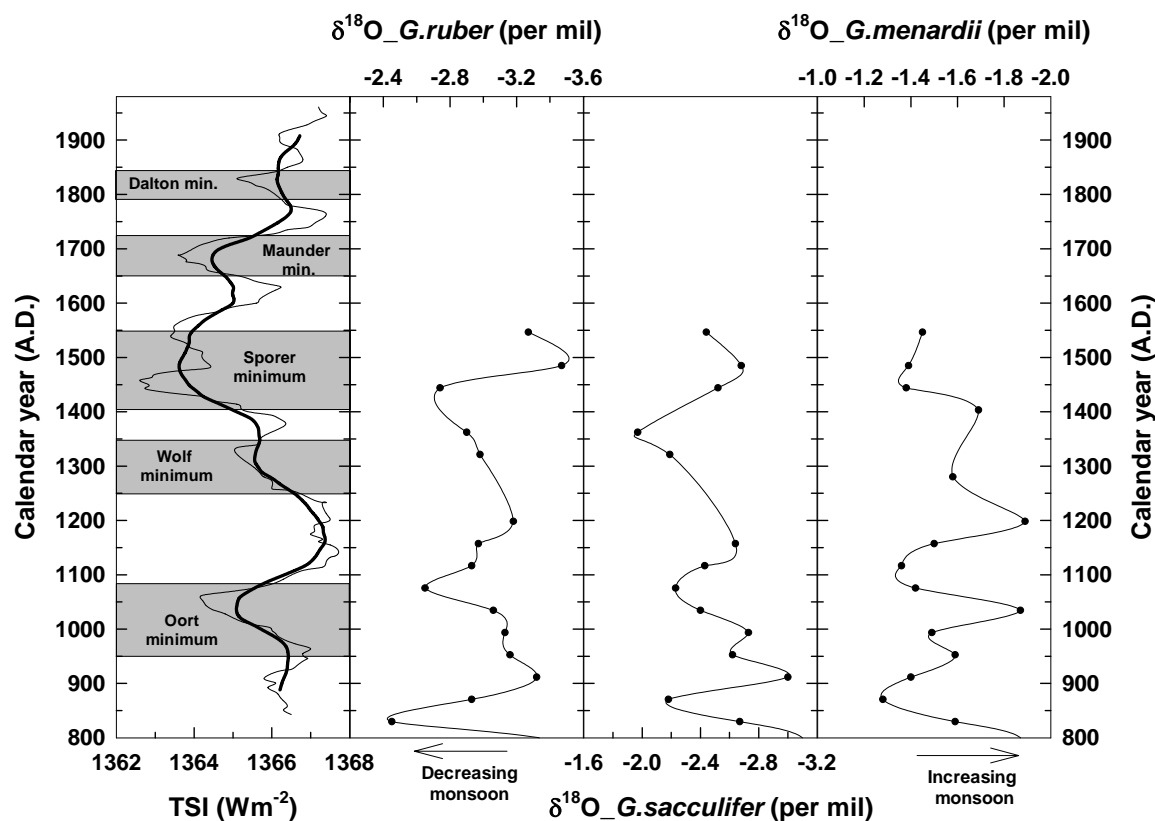


Fig. 3.8. Comparison of the TSI data and precipitation proxies ($\delta^{18}\text{O}$ in the three species of the foraminifera viz. *G. ruber*, *G. sacculifer* and *G. menardii*) for the past 1200 years. The thick line in the first panel depicts the 10-year running average of the splined data showing centennial scale variations.

The core SK 145-9 does not extend above 1550 A.D., hence comparison for the last four centuries can't be made. As evident from the above figure, the precipitation signal from all the three species matches reasonably well with the TSI fluctuations within the radiocarbon age uncertainties (~ 80 years). In general, during periods of lower TSI values, we get lower precipitation implying a solar forcing on the SW monsoon precipitation on a centennial timescale. Thus our study appears to confirm earlier findings of Agnihotri et al (2002) from this region.

3.9. Spectral analysis:

Spectral analysis can possibly help in delineating the factors forcing the monsoon. Spectral analysis has been carried out in the oxygen isotope timeseries of all the three species of foraminifera using the REDFIT 3.6 program (Schulz and Mudelsee, 2002). The spectral analysis is performed only on oxygen isotope data because they are directly governed by the SW monsoon strength whereas other productivity proxies are manifestation of at least two competing processes (wind strength and surface runoff) that tend to confuse their correlation with monsoon intensity.

The $\delta^{18}\text{O}$ in *G. menardii* exhibits a significant periodicity of ~ 215 yr and in *G. ruber* it shows a periodicity of ~ 230 yr that is just below the 95% significance level. This points towards the fact that SW monsoon follows a dominant quasi periodicity of ~ 200 yr as evident from the oxygen isotope time series. In the case of *G. sacculifer*, all the frequencies are suppressed and well below the 95% significance level.

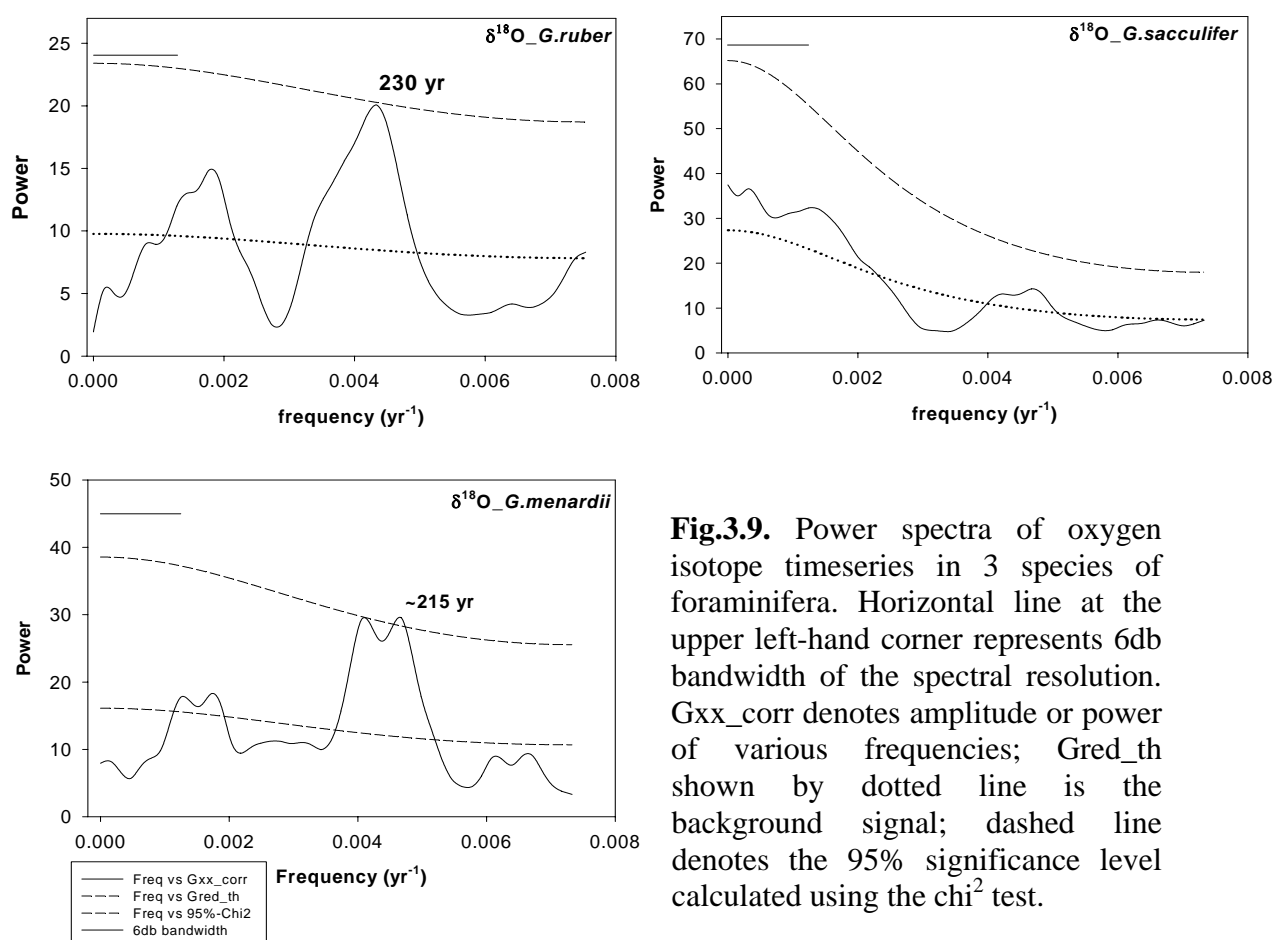


Fig.3.9. Power spectra of oxygen isotope timeseries in 3 species of foraminifera. Horizontal line at the upper left-hand corner represents 6db bandwidth of the spectral resolution. Gxx_corr denotes amplitude or power of various frequencies; Gred_th shown by dotted line is the background signal; dashed line denotes the 95% significance level calculated using the χ^2 test.

Earlier, ~200 yr, 113 yr, ~77 and ~53 yr periodicities have been observed by Agnihotri et al (2002) in the TSI (Total Solar Irradiance) data obtained from sunspot numbers (Lean et al, 1995) and ^{10}Be (Bard et al, 2000). Furthermore, power spectra of various proxies controlled by monsoon strength in a core raised from the northeastern Arabian Sea by Agnihotri et al (2002) show significant periodicities of ~200, ~110 and 56 years. Lower frequencies are not observed in this core due to the average sample resolution, which is ~65 years. This along with the periodicities observed in this study probably indicates that SW monsoon intensity on a centennial scale is governed by the variation in TSI. The exact linking mechanism is not yet clear. It is also unclear why *G.sacculifer* responds differently.

3.10. Inferences:

Based on a high-resolution geochemical data from the eastern Arabian Sea, the following inferences have been drawn:

- i. A widespread arid period is observed at ~2000 a BP. Thereafter several arid periods are observed at ~1500 a BP, ~1100 a BP, ~850 a BP and ~500 a BP. These arid events are also seen in other proxy records such as varved sediments and speleothems.
- ii. The precipitation – evaporation (P-E) values ranged from ~100 mm for arid episodes e.g. ~ 2000 a BP and ~500 a BP to ~1000 mm for high monsoon events such as at ~1800 a BP and ~1150 a BP.
- iii. Comparison with a study from the western Arabian Sea indicates that SW monsoon wind intensity exhibits excellent correlation with the SW monsoon precipitation over southwestern coastal India on centennial timescales. But the relationship appears to be non-linear as precipitation minimum occurred at ~2000 a BP while the wind minimum occurred at ~1500 a BP.
- iv. Productivity in the eastern Arabian Sea is not only a manifestation of SW monsoon wind intensity but also governed by various other

processes such as fresh water inflow, and probably *Trichodesmium* blooms etc.

- v. Spectral analysis and visual matching with TSI reconstruction point towards a possible solar control over the SW monsoon on centennial timescales.

Chapter 4

**Equatorial Arabian Sea: SW Monsoon,
NE Monsoon and Intermonsoon
Variations during the Past 35,000 years**

4.1. Introduction:

The equatorial/southern Arabian Sea is the least studied region of the Arabian Sea as most of the studies have focused on either the western/northern Arabian Sea (Prell et al, 1980; Prell and Kutzbach, 1987; Clemens et al, 1991; Anderson and Prell, 1993; Sirocko et al, 1993; Naidu et al, 1993; Naidu and Malmgren, 1995; Reichart et al, 1997, 1998, 2004; Schulz et al, 1998; Burns et al, 1998; Von Rad et al, 1999; Neff et al, 2001; Gupta et al, 2003; Fleitmann et al, 2003) or the eastern Arabian Sea (Sarkar et al, 2000; Thamban et al, 2001; Agnihotri et al, 2003a, 2003b). Nevertheless, the equatorial Arabian Sea is very important to paleoclimatic studies as it experiences the effect of Southwest monsoon as well as Northeast monsoon (Duplessy, 1982; Sarkar et al, 1990) unlike the above-mentioned other two regions, which are affected mostly by the SW monsoon. It has been proposed that during LGM, the SW monsoon was weaker (Prell et al, 1980; Van Campo et al, 1982) with a feeble indication of stronger NE monsoon than at present (Duplessy, 1982) with associated stronger oceanic currents (Sarkar et al, 1990). Furthermore, the South Asian monsoon periods have received much attention as they represent the extremes of planetary scale atmospheric and hydrospheric cycles. In comparison, the monsoon transition periods *viz.* April-June and September-November have not been looked into in detail in spite of the fact that they are the main rainy season for the eastern Africa and feature a short lived but intense upper oceanic jet in the equatorial Indian Ocean (Wrytki, 1973; Hastenrath et al, 1993; O'Brien and Hulburt, 1974). The strongest winds in the equatorial Indian Ocean are during the intermonsoon period (spring & fall) that are called as Indian Ocean Equatorial Westerlies or IEW (Beaufort et al, 1997) in comparison to rest of the Indian Ocean where winds reach their maximum intensity during the SW or NE monsoon. These IEW are result of the Walker circulation and have been found to exhibit positive correlation with Southern Oscillation index, which is supposed to be a measure of the intensity of the Walker circulation/ El Nino events (Hastenrath et al, 1993; Bjerkness, 1969). The Indian summer monsoon is known to be stronger during the periods of high Southern Oscillation phase (Hastenrath et al, 1993; Pant and Parthasarathy, 1981; Rasmusson and Carpenter; 1983; Ropelewski and Halpert, 1987). To study such an important phenomenon, a core namely SS 3827 G has been raised from the equatorial Indian

Ocean that can help in deciphering the past variations in the intensities of the two monsoon periods and oceanic and atmospheric conditions during the intermonsoon periods.

4.2. Core Location:

Core SS 3827 G is a gravity core with a total length of 196 cm. It was recovered during Sagar Sampada cruise number SS152 during 1997 from a water depth of 3118 m and thus represents an open ocean regime. The location is east of Maldives Islands at latitude $3^{\circ}42'N$ and $75^{\circ}54.5'E$ longitude. For further details refer to Table 2.1. The following figure shows its location along with other cores with which it has been compared.

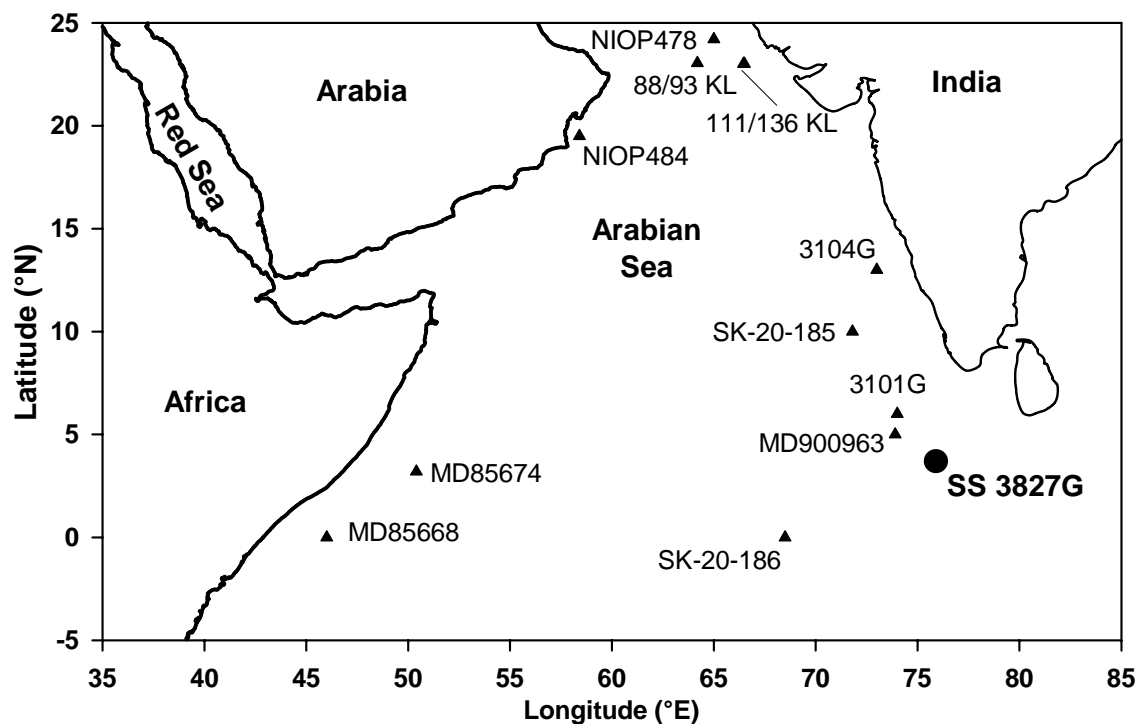


Fig. 4.1. Locations of the core SS3827 G and other cores (depicted by triangles) with which it has been compared.

4.3. Oceanographic and Climatologic conditions at the core site:

A unique wind-forcing pattern occurs over the equatorial Indian Ocean in the form of strong eastward winds during the intermonsoon periods i.e. April to June and October to November (Hastenrath et al, 1993; Schott and McCreary Jr., 2001). These strong Westerlies are called as Indian Ocean Equatorial Westerlies or IEW (Beaufort et al, 1997) that drive short-lived but intense eastward equatorial jets (EEJ), also known as Wyrki jets, in the upper oceanic layers (Wyrki, 1973). Because of EEJ, the mixed layer deepens from ~ 38 m in the west (60°E) to ~60 m in the east (~90°E). The currents due to EEJ reach a maximum intensity in the central basin (70°E – 75°E), which induces upper oceanic divergence and upwelling in the west and convergence and downwelling in the east with a subsequent gradient in the SST from 26°C in the west to 29°C in the east (Hastenrath et al, 1993). On reaching the eastern end of the basin, the EEJ get reflected in the form of the Rossby waves as well as northward propagating eastern boundary waves. Along the way, the eastern boundary waves generate slowly propagating mid latitude Rossby waves that radiate into Bay of Bengal and the eastern Arabian Sea (Perigaud and Delecluse, 1992; Basu et al, 2000).

During the two different monsoon periods, the core location is dominated by two different currents namely Southwest Monsoon Current (SMC) and the Northeast Monsoon Current (NMC). Please refer to the Fig.1.1 and 1.2 for a schematic diagram of the Indian Ocean circulation during the summer and winter monsoon respectively. During the summer monsoon, one branch of the Somali Current (SC) turns off shore at around 4°N and supplies the eastward flowing SMC. SC supplies most of the water of the SMC but part of its water is contributed by southward flowing West Indian Coast Current (WICC) after circulating around Laccadive Low (LL). After passing Sri Lanka most of the SMC turns northward into the Bay of Bengal, flowing around cyclonic Sri Lanka Dome, which is generated due to local wind stress. In the Bay of Bengal SMC supplies water to the northeastward flowing East Indian Coast Current (EICC). It is unclear whether a second SMC branch radiates further eastward and eventually bends southward to cross the equator. The chances are bleak as the 6°N transport is almost same as carried past Sri Lanka (Schott and McCreary Jr., 2001).

During the winter monsoon the westward flowing Northeast Monsoon Current (NMC) dominates the currents at the core site. In the Bay of Bengal, EICC reverses

direction twice a year *viz.* northeastward from February to September with strongest flow during March-April. During the boreal winter (October to January) EICC flows southwestward with its peak in November. Thus during the NE monsoon period EICC contributes low salinity water to the NMC (as shown in Fig.4.2), which in turn supplies water to the then northward flowing WICC after circulating around the Laccadive high (Bruce et al, 1994).

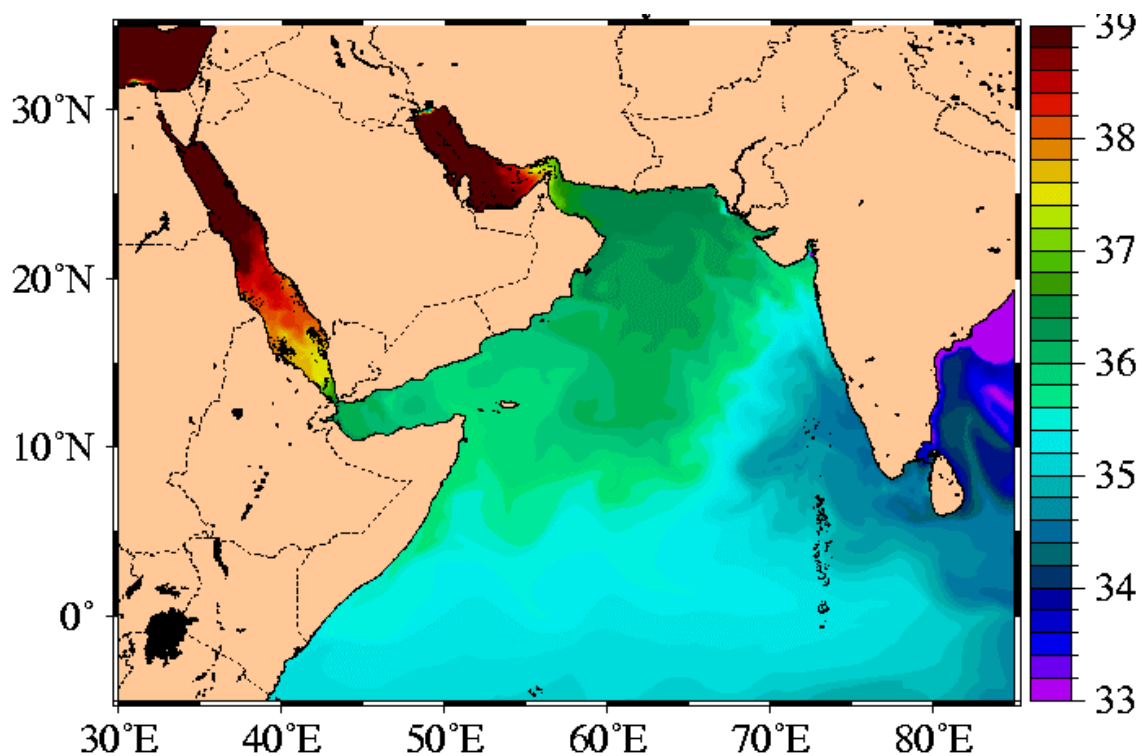


Fig.4.2. The inflow of low salinity water from the Bay of Bengal into the Arabian Sea along the NMC in the month of December. The salinity contours (unit is in PSU) were taken from the website www7320.nrlssc.navy.mil/global_ncom/ara.html.

Another branch of NMC flows westward and meets the southward flowing Somali Current (SC) at around 5°N . SC in turn meets the East African Coast current (EACC) at $\sim 2^{\circ}\text{S}$, which then supplies water to the eastward flowing South equatorial countercurrent (SECC) (Schott and McCreary Jr., 2001).

4.4. Age-Depth Model:

In this core seven AMS dates on planktonic foraminiferal separates, going up to 34,730 calendar years covering the LGM (Last Glacial Maximum; ~21,000 calendar years BP) are available. The total length of the dated core is 100cm. Thus the average sedimentation rate is $\sim 3 \text{ cm}/10^3 \text{ years}$, which is typical of open ocean locations. After 100cm, reversal of the dates was found which is possible if there was a double bounce during coring. The time resolution is approximately 350 years per cm. For dates in tabular form and other related information please refer to Table 2.2.

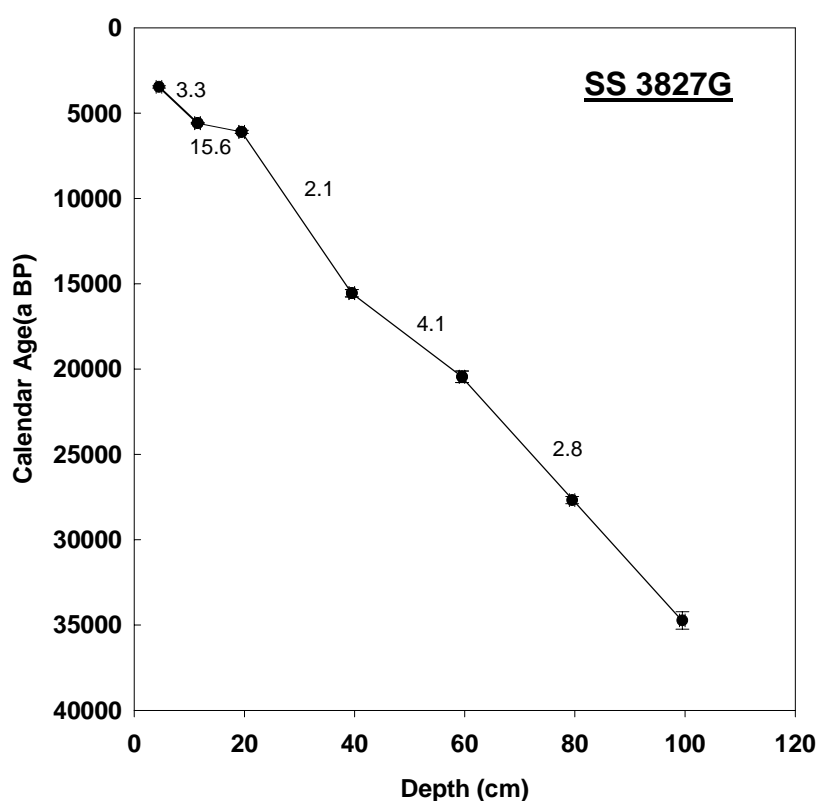


Fig. 4.3. Calibrated Radiocarbon ages and sedimentation rates (cm/ky) for the core SS 3827G.

The radiocarbon dates in this core have been calibrated to calendar ages using the calibration program “Calib 4.1 (INTCAL 98)” (Stuiver et al, 1998) with a reservoir age correction of $500 \pm 30 \text{ years}$ ($\Delta R = 100 \pm 30 \text{ yr}$, Dutta et al, 2001; see pp 49 for details regarding correction). Southon et al (2002) have reported a ΔR value of $122 \pm 25 \text{ yr}$ (weighted mean of the four values) from a location south of Sri Lanka, which is similar to that of Dutta et al (2001).

4.5. Oxygen isotope Analysis:

4.5.1. SW Monsoon vs. NE Monsoon:

Duplessy (1982) studied $\delta^{18}\text{O}$ signatures in the foraminifera *G.ruber* (a surface dwelling species) in 41 piston cores and 36 core top samples from the Arabian Sea, the Bay of Bengal and the Andaman Sea for the Holocene and LGM (Last Glacial Maximum). He found a marked difference in the $\delta^{18}\text{O}$ values for the above two periods that indicated that salinity changed considerably at LGM, which he attributed to reduced river inflow into the Bay of Bengal and increased evaporation in the northern Arabian Sea due to strengthened dry northeastern winds that blew from continents to the ocean. Furthermore, during LGM, the low salinity, low $\delta^{18}\text{O}$ area along the southwestern coast of India (signifying SW monsoon precipitation) and cool, high $\delta^{18}\text{O}$ region along the Arabian coast (signifying upwelling and hence SW monsoon wind strength) also disappeared. Based on these, he concluded that during the LGM southwest monsoon was weaker than today and northeastern monsoon was relatively stronger.

Sarkar et al (1990) obtained a core SK-20-185 from the eastern Arabian Sea (10°N , $71^{\circ}51'\text{E}$; for core location refer to Fig.4.1) and measured oxygen isotopes in planktonic foraminiferal species viz. *G.sacculifer*, *O.universa*, *G.ruber* and *G.menardii*. The chronology of the core was obtained by radiocarbon dating on the bulk sediments. They found that all the species exhibited an excursion towards lighter $\delta^{18}\text{O}$ values (by $\sim 1\%$) for around 4 kyr centered on LGM. They argued that such a negative excursion can be explained if we consider that during LGM vertical mixing due to SW monsoon reduced considerably resulting in a relative warming by $1\text{-}2^{\circ}\text{C}$ and causing $\delta^{18}\text{O}$ values to become lighter by $\sim 0.3\%$. More importantly, they proposed that during LGM, NE monsoon winds were stronger that would result in enhanced precipitation (cyclones) over the southeastern India resulting in increased fresh water influx and lower salinities in the southwestern Bay of Bengal. They further argued that Northeast Monsoon Current (NMC) also intensified due to enhanced northeast winds, which brought the low salinity water from the southwestern Bay of Bengal to the core location resulting in reduction of $\delta^{18}\text{O}$ values by 0.6% making the total offset to $\sim 1\%$. They measured $\delta^{18}\text{O}$ in *G.sacculifer* in

another core from the equatorial Indian Ocean (0.2°S, 68°30'E) namely SK-20-186 (for location, refer to Fig.4.1) but did not find any negative excursion during LGM. They explained this observation by maintaining that probably NMC did not reach the core site during LGM (similar to present time oceanographic condition), hence the low salinity waters did not affect this core.

Oxygen isotope analysis was carried out in the core SS 3827G to check the hypothesis of the enhanced inflow of low salinity water into the eastern Arabian Sea along the Northeast Monsoon Current (NMC) during LGM. It should be noted that our chronological control is better than that of Sarkar et al (1990). The core SS 3827G has been strategically chosen from a location that falls well in the way of NMC and is closer to the southwestern Bay of Bengal (see Fig.4.1). If there was indeed a flow of low salinity water along the NMC during LGM, then its signature should be more pronounced in the core SS 3827G. The $\delta^{18}\text{O}$ measurements were carried out in the three species of planktonic foraminifera viz. *Globigerinoides ruber*, *Globigerinoides sacculifer*, *Globorotalia menardii* as shown in the Fig.4.3. *G.ruber* and *G.sacculifer* are surface dwelling species predominantly inhabiting top 25 m and 50 m respectively whereas *G.menardii* is a deeper dwelling species predominantly inhabiting 100-150 m (Be, 1977, Fairbanks et al, 1980; Fairbanks et al, 1982). It is remarkable that all the three species exhibit similar variations inspite of the fact that they dwell at different depths. It indicates that the signals recorded by them are genuine and are corroborated by each other. As evident from the figure 4.3, during LGM (~21,000 a BP, calendar age) the $\delta^{18}\text{O}$ values in all the three species of foraminifera exhibit a shift towards heavier values indicating that at the core site there is no influence of low salinity, isotopically lighter water. In fact, during LGM the oxygen isotopes in planktonic foraminifera exhibit most positive values indicating that the temperature was at its lowest with the maximum salinity (due to global ice-volume effect) and least precipitation at the equatorial region. Had there been an enhanced inflow of low salinity water along the strengthened NMC, then it should have been reflected in the oxygen isotopic composition of the planktonic foraminifera, which is not the case. All these evidences point towards the fact that during LGM Northeast Monsoon Current did not probably strengthen and hence the transport of low salinity water did not probably intensify during that time.

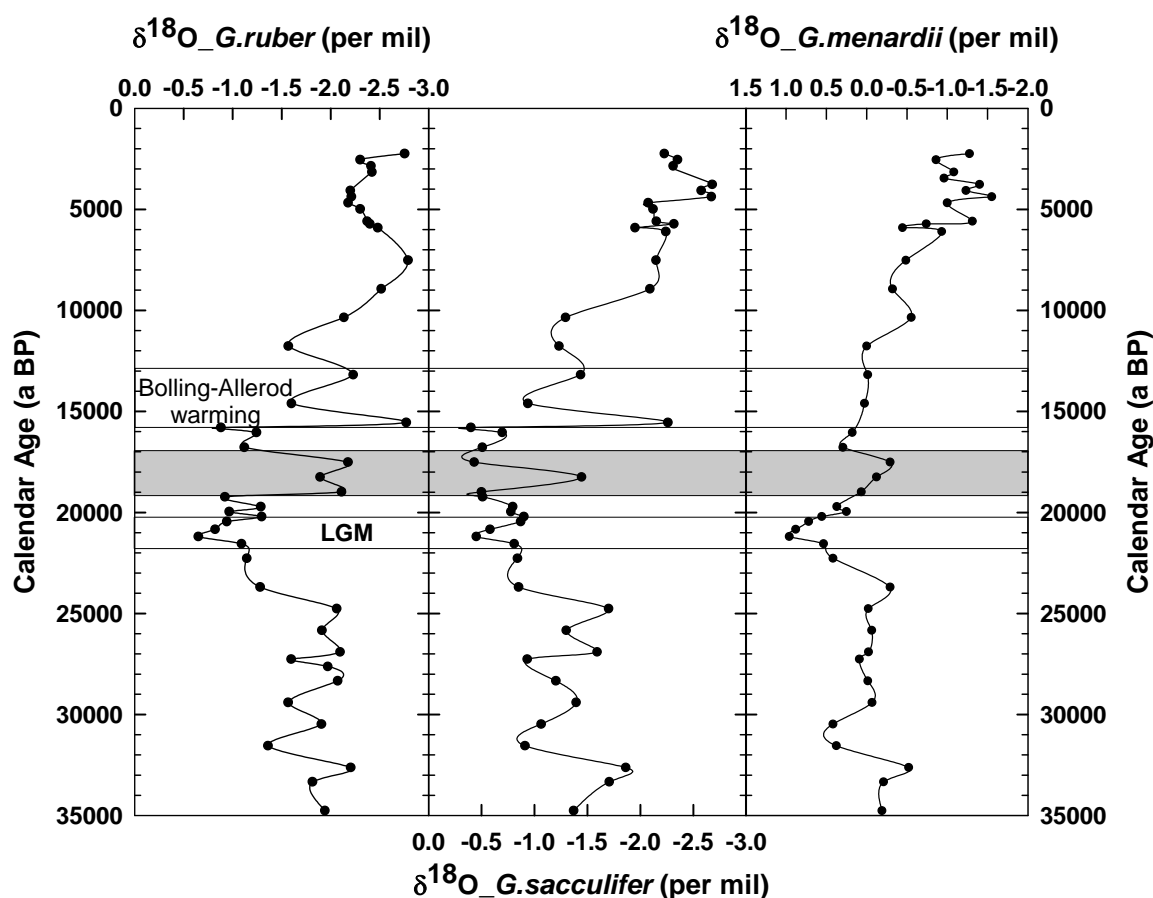


Fig. 4.4. Temporal variations in the oxygen isotope ratios ($\delta^{18}\text{O}$) of three species of foraminifera viz. *Globigerinoides ruber*, *Globigerinoides sacculifer*, *Globorotalia menardii* in the core SS3827 G; negative excursion during early deglacial is shown by shaded region

But then, the question arises as to the signal reported by Sarkar et al (1990). The problem seems to lie in the bulk-dating scheme adopted by them. It has been observed that bulk dating usually yields older ages by a few thousand years because of the contribution by dead carbon due to contamination from detrital carbonate. For example, two cores from adjacent regions namely SS 3268G5 (Sarkar et al, 2000) and SK 145-9 (this study) have been obtained off the coastal southwestern India. In the core SS 3268G5 bulk sediment dating was carried out whereas in the core SK 145-9, AMS dates have been obtained on the selected species of planktonic foraminifera (see section 3.3). The difference between the bulk dates and AMS dates on planktonic

separates might vary depending upon the contribution of the detrital carbonate. So, the signal observed by Sarkar et al (1990) during LGM and lasting for ~ 3000 to 4000 years seems to be the negative excursion in $\delta^{18}\text{O}$ values observed at ~18 ka BP (calendar ages) with a total duration of approximately 3 ka. Thus our study clarifies that the signal seen by the Sarkar et al (1990) is true but the timing of intensification of the NMC is not during LGM but 19ka BP to 17 ka BP (early deglacial period). The core employed in this study is nearer to the southwestern Bay of Bengal (that mainly contributes the low salinity water to the NMC) and possesses better chronological constraints as well as better confidence on results. During that time $\delta^{18}\text{O}$ values decreased by about 1‰ in the surface dwelling *G.ruber* and *G.sacculifer* and by ~0.6‰ in the deeper dwelling *G.menardii* as evident from the Fig.4.3. The $\delta^{18}\text{O}$ decrease due to global ice – volume effect at that time was negligible (0.1‰; Fairbanks, 1989). It has been observed that during SW monsoon the SST in the equatorial region decreased by ~2°C (Wyrтки, 1971) probably due to wind-induced mixed-layer deepening. During the early deglacial SW monsoon was weaker as exhibited by the calcareous and organic productivity indicators and oxygen isotope analysis as discussed in the next chapter (refer sections 5.4.1 and 5.5). Due to reduced mixing the SST would rise by ~2°C that would account for around 0.5 ‰ reduction in $\delta^{18}\text{O}$ values. Moreover, enhanced precipitation would take place over the southeastern India if the NE monsoon was stronger than present. It would result in increased river run off from peninsular India and the SSS (sea surface salinity) in the southwestern Bay of Bengal would reduce further. The remaining ~0.5 to 0.6‰ reduction in the surface dwelling *G.ruber* and *G.sacculifer* can be explained by the enhanced inflow of low salinity water along the enhanced Northeast Monsoon Current (due to enhanced NE monsoon wind strength). If the salinity reduced by ~2‰ it would account for the ~0.6‰ decrease in the $\delta^{18}\text{O}$ values (as in this region for every per mil decrease in salinity $\delta^{18}\text{O}$ values decreases by 0.33‰; Duplessy et al, 1981; Sarkar et al, 2000). Since *G.menardii* is deeper dwelling (~150m; Be, 1977) so it is not affected by the NMC, which is a surface current. The NMC is known to exist upto a depth of ~120m (Schott and McCreary Jr., 2001). Thus the signal exhibited by *G.menardii* only reflects the relative warming of the sea surface due to slackening of the SW monsoon winds. Many studies based on various paleoclimatic proxies have shown that SW

monsoon was relatively weaker than present during the LGM (Prell et al, 1980; Van Campo et al, 1982; Duplessy, 1982; Prell and Van Campo, 1986). It has been further suggested that there are weak oceanic indications of concurrently stronger NE monsoon (Duplessy, 1982). The reason proposed for this observation is that during glacial times Tibetan plateau was covered with glaciers (Singh and Agrawal, 1976). Hence during summer, enough heat was not taken up by Tibetan landmass resulting in a lower land – sea pressure difference because of which SW monsoon winds were weaker. They further proposed that during winter months the land was cooler than present (due to permanent ice cover) in the vicinity of a warm ocean resulting in the relatively stronger NE monsoon. But our study points towards a slightly revised picture. During the LGM, no doubt, the SW monsoon slackened because of permanent ice cover. But the SSTs also fell by 2-3⁰C in the tropical regions (Kienast et al, 2001; Rosenthal et al, 2003; Lea et al, 2003). The outcome was that NE monsoon also weakened along with the SW monsoon. But during early deglacial period the SW monsoon was still in a weakened mode due to presence of considerable ice cover that disappeared only during the Termination IA (T IA). During the early deglacial period there were not much ice melting episodes as evident from the sea level rise of only 15m in ~5000 years (LGM to T IA) whereas in the next 5000 years starting from T IA, the sea level rose by ~75m (Fairbanks, 1989). In contrast the SSTs in the equatorial Indian Ocean and southern tropical Indian Ocean rose during early deglacial period (by ~1⁰C (Bard et al, 1997) that accounts for about 33% of the total LGM to Holocene temperature amplitude) resulting in the enhancement of the NE monsoon. This period of relatively stronger NE monsoon lasted for about ~2000 years starting from ~19 ka BP, which is clearly reflected in the oxygen isotope record.

4.5.2. Correlation with the high latitude temperature record:

The oxygen isotopic values for the equatorial core SS3827 G exhibit a good resemblance with the GISP2 $\delta^{18}\text{O}$ record (Grootes et al, 1993; Stuiver et al, 1995; Grootes and Stuiver, 1997; Meese et al, 1994 a, b) as depicted in Fig.4.5.

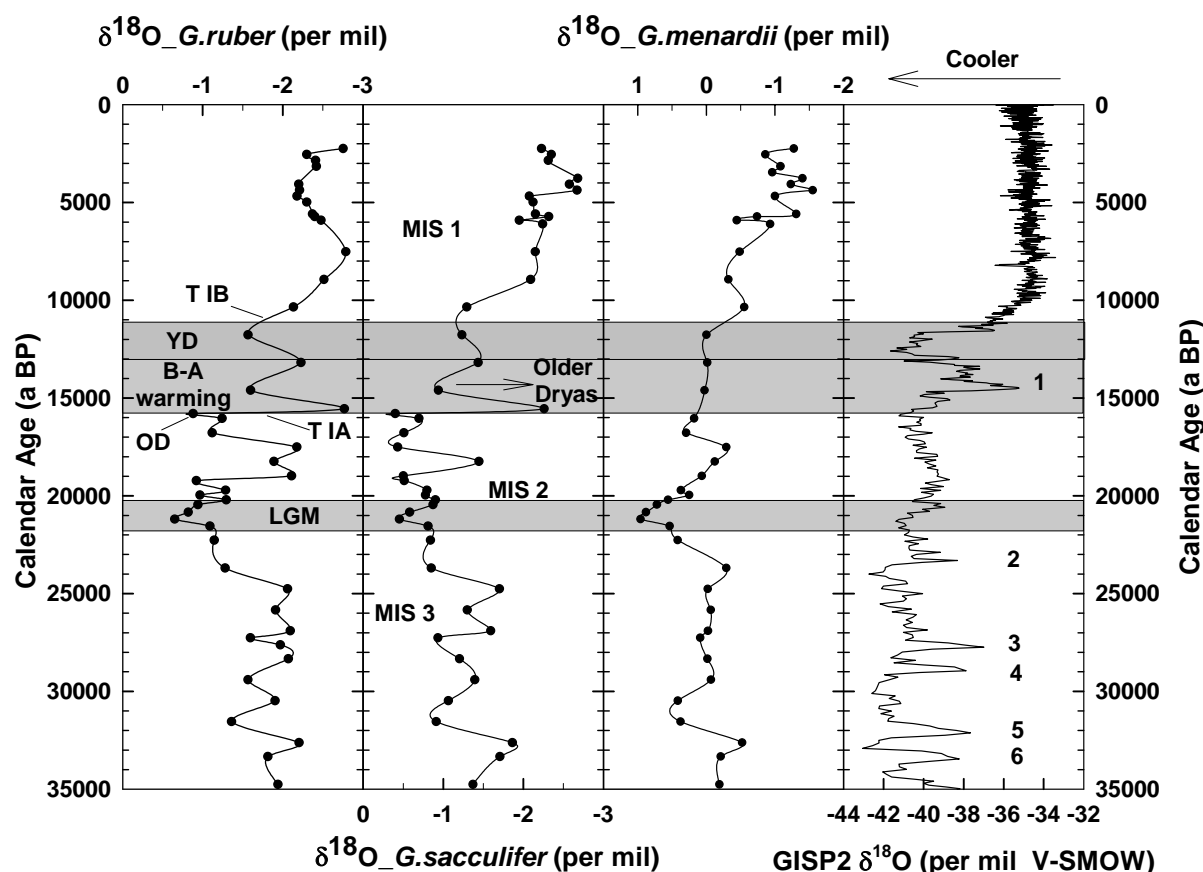


Fig.4.5. Comparison of the $\delta^{18}\text{O}$ record of the core SS3827 G with the GISP2 $\delta^{18}\text{O}$ record; OD, T IA, B-A warming, YD and T IB shown in the first panel refers to Oldest Dryas, Termination IA, Bolling-Allerod warming, Younger Dryas and Termination I B respectively (Stuiver et al, 1995); MIS 1, MIS 2, MIS 3 in the second panel refer to standard SPECMAP (Martinson et al, 1987) Marine Isotope Stages 1, 2 and 3; Arabic numerals in the last panel (1 to 6) indicate Dansgaard/Oeschger Interstadials.

Foraminiferal $\delta^{18}\text{O}$ values respond to sea surface temperature (SST), global change in seawater $\delta^{18}\text{O}$ due to the ice volume effect (sea level change) and local

salinity changes due to evaporation – precipitation (E-P) budget. Low sedimentation and bioturbation limit the temporal resolution of sedimentary cores. Furthermore equatorial and tropical regions, by virtue of their distance, are not directly affected by ice sheet behaviour. That is why there are very few studies [e.g. Kienast et al (2001) in the South China Sea; Lea et al (2003) from the Cariaco Basin, northern Venezuelan shelf; Rosenthal et al (2003) from the Pacific] comparing the oxygen isotope analysis of equatorial/tropical sediment cores with ice cores. Bard et al (1997) carried out oxygen isotope and alkenone measurement from two cores *viz.* MD85674 and MD85668 (see Fig. 4.1) for the past 150 ka BP in the northwest equatorial Indian Ocean. They reported that 70% – 80% of the total ^{18}O signal is due to global ice-volume effect and the LGM to Holocene temperature change is of the order of $\sim 2^{\circ}\text{C}$, which is in marked contrast to $5\text{-}6^{\circ}\text{C}$ deglacial warming inferred from the Sr/Ca ratio in tropical corals (Guilderson et al, 1994). Schulz et al (1998) measured total organic carbon in cores from the northern Arabian Sea namely SO 90-88KL, SO 90-93KL, SO 90-111KL and SO 90-136KL as shown in the Fig.4.1. They found that strong SW monsoon as manifested by organic carbon rich bands corresponded to mild interstadials of the North Atlantic (D/O events) and periods of weak SW monsoon correlated with high-latitude atmospheric cooling and injection of melt water into the North Atlantic basin (Heinrich events). They concluded that such events (D/O and Heinrich) are an important component of low-latitude climate that points towards a large scale element of the ocean-atmosphere system interacting rapidly with the high and low latitudes. They further maintained that interstadials recorded in the ice core records represented periods of global warmth associated with high levels of greenhouse gases as suggested by Mayewski et al (1994) and Brook et al (1994). Reichert et al (1998, 2002 a) measured the C_{org} content in the cores NIOP478 and NIOP484 from the northern and western Arabian Sea (see Fig. 4.1). They found excellent correlation between the low C_{org} values (denoting reduced summer monsoon) during the stadials. Altabet et al (2002) studied the denitrification records from the western Arabian Sea and found that denitrification intensified (denoting more productivity and hence enhanced SW monsoon winds) during periods of polar warmth as suggested by the $\delta^{18}\text{O}$ data from the GISP2. Rostek et al (1993) estimated the SST for the past 170,000 years in the core MD900963 (location shown in the Fig.4.1)

using the alkenone unsaturation ratio. They found that for the past 35,000 years (the studied length of the present core SS3827 G), the SST variation at the core site was within 2.5°C with a minimum at LGM (25.5°C) and a present SST maximum (28°C). In spite of the comparatively poorer resolution [the $\delta^{18}\text{O}$ measurements have been carried out usually at alternate depths or after every 3 cm, (except for some periods such as LGM that were sampled at every cms) that provides a resolution ranging from 700 yrs to 1000 yrs] than the ice core record, we find very good correlation to the extent that even some rapid events like Dansgaard/Oeschger (D/O) Interstadials appear to be reflected in the sediment core oxygen isotope record. Because of the resolution problem many of the peaks observed in the ice core record are merged into one in the sedimentary record. For example the D/O event 5 and 6 are represented by a peak at 32.5 ka BP in all the three species of foraminifera; D/O events 3 and 4 are shown by a peak at 28.5 ka BP (again in all the three species). Similarly the D/O event 2 is represented by peaks at 24 ka BP and a peak at 15 ka BP corresponds to D/O event 1 in all the three species of planktonic foraminifera.

During the MIS (Marine Isotope Stage) 3 (upto 25 ka BP) various millennial scale fluctuations are found in the sedimentary record that correspond quite well with those of the ice record as outlined above. These negative excursions (upto 0.5 ‰) are observed at 32.5 ka BP and 28.5 ka BP corresponding to the D/O events 5,6 and 3,4 respectively (Fig.4.4). The equatorial Indian Ocean SSTs increased by $\sim 1^{\circ}\text{C}$ from 35 ka BP to 25 ka BP (Rostek et al, 1993) before plunging back to LGM levels and global seawater $\delta^{18}\text{O}$ first decreased and then increased by 0.2‰ in the 10 ka (Labeyrie et al, 1987). But these long-term changes will not have much bearing on the short term, high frequency fluctuations. Thus these millennial scale fluctuations can be only be explained by changes in the evaporation – precipitation (E-P) balance. Enhanced precipitation can shift the $\delta^{18}\text{O}$ values towards the negative side. Since precipitation over Indian Ocean is related to the strength of the SW monsoon (Cadet and Reverdin, 1981; Rostek et al, 1993), it can be deciphered that negative excursions coinciding with the North Atlantic interstadials reflect an increase in the precipitation over equatorial Indian Ocean.

From 25 ka BP to LGM the oxygen isotope values show an increase of about 1.5‰ in all the three foraminiferal species. During that period the temperature

plummeted by 1.5°C (Rostek et al, 1993) that would account for the $\sim 0.3\text{‰}$ to $\sim 0.4\text{‰}$ (considering a slope of 0.25‰ rise in foraminiferal $\delta^{18}\text{O}$ for every $^{\circ}\text{C}$ fall in temperature; Erez and Luz, 1983) enhancement in foraminiferal $\delta^{18}\text{O}$ and global seawater $\delta^{18}\text{O}$ increased by 0.6‰ . These two effects will account for the $\sim 1\text{‰}$ increase in the $\delta^{18}\text{O}$ values. The remaining $\sim 0.5\text{‰}$ increase is due to the reduced precipitation, which points towards the fact that during LGM the precipitation at the equatorial Indian Ocean reduced considerably corroborating many of the earlier studies that were carried out in the western Arabian Sea (Prell et al, 1980; Van Campo et al, 1982; Duplessy, 1982; Prell and Van Campo, 1986). The maximum $\delta^{18}\text{O}$ signal is obtained for the LGM signifying that during that time precipitation was at its minimum corresponding exactly with the maximum global glaciation.

After LGM, during early deglaciation we find a negative excursion by $\sim 1\text{‰}$, which is due to the effect of relatively enhanced NE monsoon as discussed in the previous section (Sec.4.5.1). The transition from glacial to Holocene is punctuated with numerous fluctuations in the foraminiferal $\delta^{18}\text{O}$ record that are synchronous with those occurring in the GISP2 record within the dating errors and the core resolution. At around 15.7 ka BP an increase by 0.5‰ in the $\delta^{18}\text{O}$ values is found for the sea surface dwelling species (*viz.* *G.ruber* and *G.sacculifer*) that probably corresponds to the cold “Oldest Dryas” observed in the GISP2 record (Stuiver et al, 1995) indicating that precipitation reduced during that time. This signal was not observed for the *G.menardii*, which is the deeper dwelling species (~ 150 m water depth). It is interesting that $\delta^{18}\text{O}$ values in *G.menardii* do not show rapid fluctuation as in the case of other two species during the late deglaciation period (16 ka BP – 11 ka BP). In the case of *G.menardii*, the $\delta^{18}\text{O}$ values just exhibit an uniform increase by $\sim 0.7\text{‰}$, which is the global ice-volume effect during the late deglaciation. This clearly indicates that during this time the precipitation variation was not as strong as glacial times when it affected the depths at which *G.menardii* dwells. At 15.5 ka BP we observe a rapid decline in the $\delta^{18}\text{O}$ values by $\sim 1.7\text{‰}$ in surface dwelling species which corresponds to the Termination IA (T IA), and the GISP2 $\delta^{18}\text{O}$ record. During this event the equatorial SST increased by roughly 1°C (Rostek et al, 1993) and the global seawater $\delta^{18}\text{O}$ decreased by $\sim 0.35\text{‰}$ that would account for nearly 0.6‰ reduction in $\delta^{18}\text{O}$.

The remaining 1‰ depletion has to be explained by some other process. Out of that around 0.4‰ can be attributed to precipitation increase due to SW monsoon enhancement. But it can't be more than 0.4‰ because the precipitation fluctuations are weaker than what was during glacial times as reasoned above. The remaining 0.6‰ decrease can be explained if we take into account the fact that during TIA, surface temperature increased that would cause the Himalayan glaciers to melt. This along with the enhanced SW monsoon precipitation would result in greater fresh water runoff as rivers in to the Bay of Bengal. The influx of water with salinity lower by upto 2‰ at the core site via the Northeast Monsoon current would result in the reduction of foraminiferal $\delta^{18}\text{O}$ by upto 0.6‰ (as in the eastern Arabian Sea, foraminiferal $\delta^{18}\text{O}$ values are assumed to decrease by 0.33‰ for every ‰ decrease in salinity, Sarkar et al, 2000). But this influx of low salinity water was not as strong as that during the early deglacial period because deeper dwelling *G.menardii* was not affected.

The Bolling-Allerod (B-A) warming is manifested by depleted $\delta^{18}\text{O}$ values from 15.5 ka BP to 13 ka BP. These values shows that precipitation increased during the warm periods observed in ice core records. Centered at 14 ka BP between the B-A interstadial is the “Older Dryas”, a cold period that represents a rapid deterioration in the north Atlantic climate. It is recorded in the foraminiferal $\delta^{18}\text{O}$ values in the form of a sudden increase by ~1‰. This sudden enrichment in the oxygen isotopic values reflects the reduction in SW monsoon precipitation that would account for about 0.4‰. This would reduce the river runoff to the Bay of Bengal with consequent increase in the salinity, which might affect the core site accounting for the remaining 0.6‰ enhancement.

The “Younger Dryas” in the sedimentary oxygen isotope record is represented by an enhancement in $\delta^{18}\text{O}$ values by ~0.4‰ in the *G.ruber* and *G.sacculifer* from 13 ka BP to 11 ka BP. During that period the SST reduction in the equatorial region was negligible (~0.2°C; Rostek et al, 1993; Bard et al, 1997) and the global seawater $\delta^{18}\text{O}$ decrease was by ~0.15‰ (Fairbanks, 1989). Thus the total enhancement in the $\delta^{18}\text{O}$ values would have been by approximately 0.5‰ that could be explained by a reduction in the SW monsoon. Thus we find that the one of the major North Atlantic

cold period, the signature of which have been recorded all over the globe, is conspicuously reflected in the SW monsoon as well.

At the end of YD we find a rapid decrease in the $\delta^{18}\text{O}$ values by $\sim 0.5\text{‰}$ representing the Termination IB (T IB). During that time SST increased by 0.8°C in the equatorial Indian Ocean (Rostek et al, 1993; Bard et al, 1997) that would account for $\sim 0.2\text{‰}$ enhancement in $\delta^{18}\text{O}$ values. During the same time global seawater $\delta^{18}\text{O}$ value reduced by 0.2‰ (Fairbanks, 1989). These two processes would account for most of the signal with the remaining decrease being explained by increasing precipitation.

During the Holocene, which is a period of uninterrupted warmth, the $\delta^{18}\text{O}$ values exhibit a decreasing trend upto the core top ($\sim 2,200$ years) in the *G.sacculifer* and *G.menardii*. The total decrease is about 1‰ out of which around 0.4‰ is accounted by the global seawater $\delta^{18}\text{O}$ decrease and 0.1‰ is due to $\sim 0.5^{\circ}\text{C}$ rise in equatorial SST (Rostek et al, 1993). The remaining $\sim 0.5\text{‰}$ can be explained by an increasing SW monsoon precipitation. *G.ruber* exhibits a decreasing trend upto ~ 7 ka BP after which it shows increase in $\delta^{18}\text{O}$ values for the next 3 ka and then it shows decreasing trend upto core top (2.2 ka). In the Late Holocene (after 5 ka), there are many fluctuations in sedimentary record that seem to have a local origin such as centennial scale variations in precipitation. But they are not found in the polar record. Similarly, the prominent 8,200 a BP cold event in the GISP2 record does not seem to have a counterpart in the present sedimentary record.

Notwithstanding resolution problems, it appears that SW monsoon correlates very well to the North Atlantic climate, represented by the GISP2 $\delta^{18}\text{O}$ record. The nearly similar variations observed in three different species of foraminifera gives confidence to this. Even the rapid events like D/O events, T IA, T IB, Oldest, Older and Younger Dryas are well recorded in the sedimentary record within the restraints put by the dating errors and the sampling resolution. Such a good correspondence with the North Atlantic climate necessitates for a mechanism that would control both the high latitude and low latitude climate on timescales much shorter than a millennium. It appears that synchronous changes in the equatorial and North Atlantic climate indicate that low latitude played an important role in modifying the high latitude climate via atmospheric forcing. It is possible that tropical/equatorial regions

were instrumental in putting high amount of tropospheric moisture and greenhouse gases such as methane during the interstadials, which acted as a positive feedback mechanism (e.g. Schulz et al, 1998; Altabet et al, 2002; Mayewski et al, 1994).

4.6. Temporal Variations in Productivity:

Various proxies were measured to decipher the past variation in the productivity at the core site, which includes calcium carbonate content, organic carbon percentage, stable isotope of nitrogen ($\delta^{15}\text{N}$) in the sedimentary organic matter along with $\delta^{13}\text{C}$ in the three different species of planktonic foraminifera.

4.6.1. Productivity as Exhibited by Calcium Carbonate Content:

Calcareous productivity was estimated by determining the total carbonate content in a given weight of sediment expressed in percent as shown in the Fig.4.6. Since the core location is well away from land i.e. in the open ocean, terrestrial input is negligible and calcareous productivity observed at the core site is likely to be of marine origin.

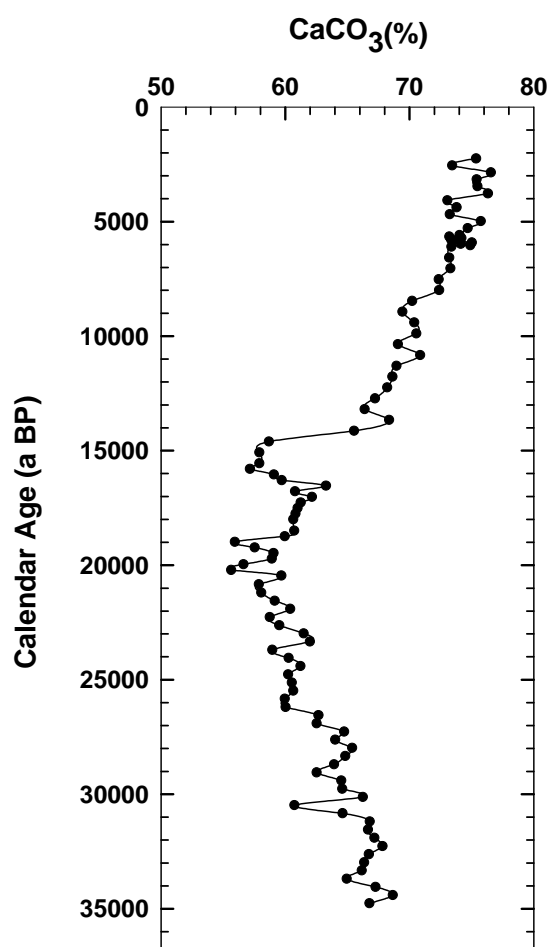


Fig.4.6. Downcore variation of CaCO_3 (%) in the core SS3827 G for the past 35 ka.

In this core calcium carbonate percentage varies from 55% to 75% with a minimum during LGM and a present maximum value. The productivity in the open equatorial Indian Ocean at the core site is due to the wind stress (Beaufort et al, 1997). The wind induced mixed layer deepening would cause the deeper nutrient rich water to surface that would cause the productivity to increase. In this region winds are strongest during April to November with maximum variability during the monsoon transition periods *viz.* April to June and October to November that are called as Indian Ocean Equatorial Westerlies or IEW as discussed in the section 4.3 that cause short-lived but intense eastward upper ocean water currents called Eastward Equatorial Jets (EEJ) (Wrytki, 1973; Schott and McCreary Jr., 2001; Hastenrath et al, 1993; Beaufort et al, 1997). The strong variability during the monsoon transition period is the result of strong wind bursts capable of causing deeper mixing of the surface water to the effect that maximum productivity in this region occurs during the intermonsoon periods (McIntyre and Molino, 1996; Beaufort et al, 1997). Thus the productivity variation at the core site is a proxy for the strength of IEW. The IEW in turn is positively correlated to Southern Oscillation (SO) index (Hastenrath et al, 1993) and the Walker Circulation with implications to ENSO (El Nino–Southern Oscillation) variability (El Nino tends to occur in the low SO phase e.g. Reverdin et al, 1986; Hastenrath et al, 1993). If so, the equatorial Indian Ocean productivity records should exhibit a correlation with the eastern equatorial Pacific productivity records. In fact Beaufort et al (1997) have shown that the Maldives primary productivity-insolation phase is similar to that of the Pacific primary productivity records in the precession band indicating the influence of SO on both regions on a millennial timescale. Eastern Africa possesses two rainy seasons. The first, which is more abundant in terms of rainfall, occurs during the March to June with its core around April-May (called as “long rains” in Kenya and “Gu” rains in Somalia). The second occurs from September to November, which exhibits more interannual variability in the precipitation, with its core around October-November (called as “short rains” in Kenya and “Der” rains in Somalia). High correlation of these rainfalls with the SO phase have been reported by various authors. During high SO phase enhanced “long rains” have been found by authors like Hastenrath et al (1987); Bhatt (1989); Beltrando and Camberlin (1993); Ogallo et al (1998) and strengthened “short rains” have been found by Van Heerden et

al (1988); Martarira (1990) and Walker (1990). El Nino affects the Indian monsoon in the way that the rising limb of the Walker circulation and the tropical convection, which is usually located in the western Pacific shifts towards the central and eastern Pacific. It would result in subsidence over the western Pacific and the Indian subcontinent, which suppresses convection and precipitation over the Indian landmass (Pant and Parthasarthy, 1981; Rasmusson and Carpenter; 1983; Ropelewski and Halpert, 1987). The high SO phase is related to a low El Nino activity and hence strengthened Indian SW monsoon (Hastenrath et al, 1993). Thus past variation in the intensity of IEW can illuminate the past fluctuations in the El Nino/Southern Oscillation index, Indian summer monsoon and east African rainy seasons.

The calcareous productivity at the core site exhibits a decreasing trend upto LGM (~21 ka BP; calibrated age) as shown in the Fig.4.5, which points towards the uniformly decreasing strength of the IEW. At LGM we find the minimum calcareous productivity signifying the minimum IEW strength. It implies that at LGM the Southern Oscillation index was at its minimum, which indicates that at that time Walker circulation weakened considerably. The low SO index further indicates that SW monsoon as well as the east African rains weakened gradually upto LGM with their minimum values at LGM.

Thereafter the calcareous productivity shows a slight increase from LGM to 16.5 ka BP, which coincides with the early deglacial period. After that it suffered a decline for the next 1000 years falling back to LGM values indicating that IEW strength reduced considerably during that time which implies a lower SO phase i.e. reduced SW monsoon and east African rains at that time. Thereafter a sharp increase in the calcareous productivity was found at ~14.5 ka BP, which coincides with the Termination IA, as also recorded in the Greenland ice cores. This points towards enhancement of SW monsoon and east African rains during that time along with a decrease in the El Nino events. A similar trend in the calcareous productivity with a decline during the late deglacial period and a sudden increase at ~15 ka BP was also observed in the core from the western Arabian Sea (SS 4018 G; this study, Chapter-5), which indicates SW monsoon intensification at that time. Till then to the core top (2.2 ka BP) the productivity shows a steadily increasing trend implying a

strengthening Walker Circulation, which means strengthening SW monsoon, east African rains and lower El Nino frequency during the Holocene.

4.6.2. Regional climatic evolution: comparison with eastern Arabian Sea:

The calcareous productivity record of the SS 3827G was compared with other calcareous productivity records to further explore the regional climatic conditions in the eastern and southern Arabian Sea. Agnihotri et al (2003 a) analyzed two cores from the eastern Arabian Sea viz. SS3104 G and SS 3101 G (location shown in the Fig.4.1) from the water depths of 1680 m and 2680 m. The chronologies of the cores were obtained by AMS radiocarbon dating on the selected planktonic foraminifera species. They attributed the productivity variation to the variation in the SW monsoon wind strength. The following figure compares the productivity variations in the three cores for the past 35 ka.

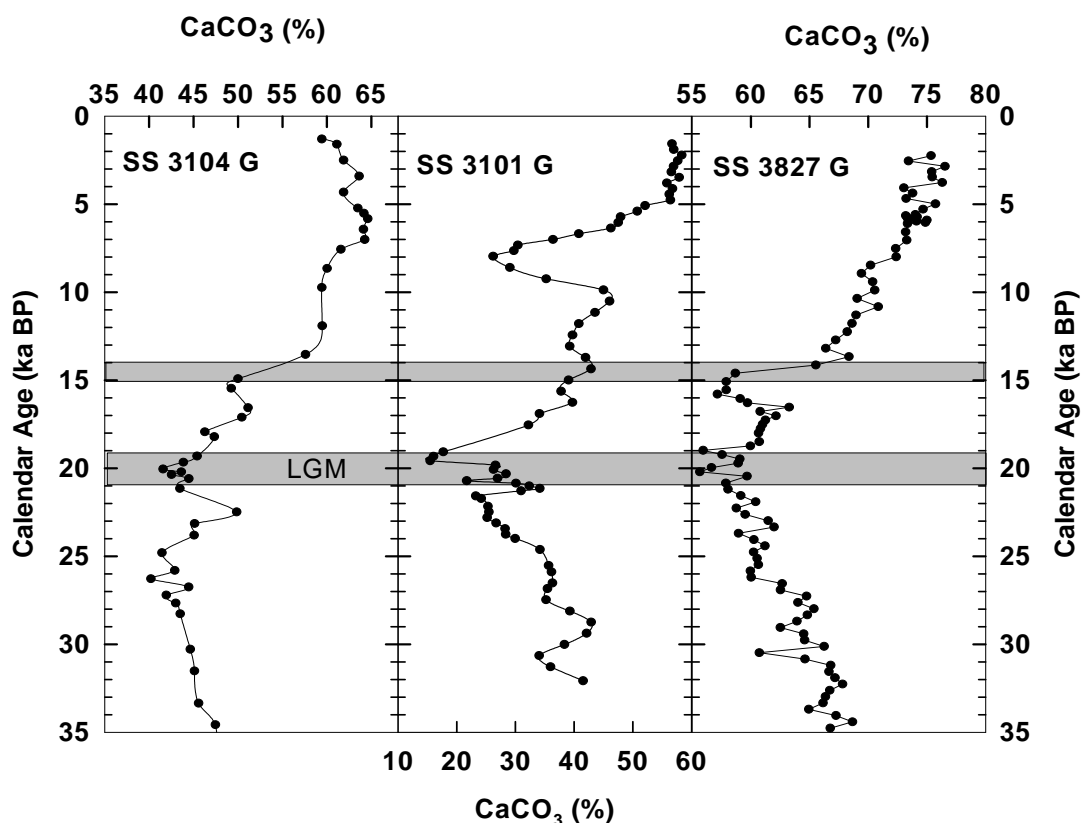


Fig. 4.7. Comparative study of the core SS3827 G (last panel; this study) with other cores from eastern Arabian Sea viz. SS3104G and SS3101G (Agnihotri et al, 2003 a).

All the three cores exhibit more or less similar downcore variations in calcareous productivity, which shows a decreasing trend upto LGM (shown by the

shaded region) from 35 ka BP. It implies that both the SW monsoon winds as well as the Indian Ocean Equatorial Westerlies (IEW) declined in tandem upto LGM pointing towards the fact that the same forcing factor (insolation) is governing both of them. Thereafter around 14.5 ka BP another episode of SW monsoon winds and IEW strengthening are observed as indicated by sharp increase in the calcareous productivity at that time. During the Holocene all the cores show more or less increasing trend in the calcareous productivity except for the core SS3101 G that suffers an abrupt decline during 7-9 ka BP. This abrupt decline is quite intriguing, as it is not observed in the cores north and south of it. It clearly points towards some local effect that dominates the productivity signal. Agnihotri et al (2003 a) explained that timing of this decline coincides with the Holocene humid interval, which is a period of intensified SW monsoon in the Arabian Sea (Sirocko et al, 2000). They speculated that this sharp decline could be due to the build up of low salinity cover due to influx of fresh water from the coastal regions that would inhibit upwelling and hence reduce the productivity (Thamban et al, 2001).

Thus based on the comparative analysis of these three cores we can infer that the productivity trends in the eastern and southern Arabian Sea were similar (apart from some local effects), which points towards the fact that IEW as well as SW monsoon winds strengthened and weakened in synchronicity, implying a common forcing factor.

4.6.3. Productivity as exhibited by Sedimentary Organic Matter:

The core SS3827 G is from an open ocean location from a water depth of 3118 m. Schulte et al (1999) have shown that the equatorial Indian Ocean near the core site of SS3827 G has remained under oxic conditions for the past 330 ka. The C_{org} (%) is a traditional proxy for the organic productivity (Muller and Suess, 1979; Rixen et al, 2000; Ganeshram et al, 1999) but because of the prevailing oxic conditions the preservation of organic carbon in the present core is very poor as shown by the very low values of C_{org} with most of the values being less than 0.5% and in many cases even less than 0.1%. The organic carbon content (C_{org} %) has been obtained by subtracting the inorganic carbon values estimated from the $CaCO_3$ (%) from the total carbon values as discussed in the section 2.5.2. When the organic carbon content is

very low then the total carbon is essentially reflected by the inorganic carbon content of the CaCO_3 . Subtracting the inorganic carbon from the total carbon content to obtain the organic carbon will yield an C_{org} variation that exhibits an exact anticorrelation with the CaCO_3 variation as shown in Fig.4.7.

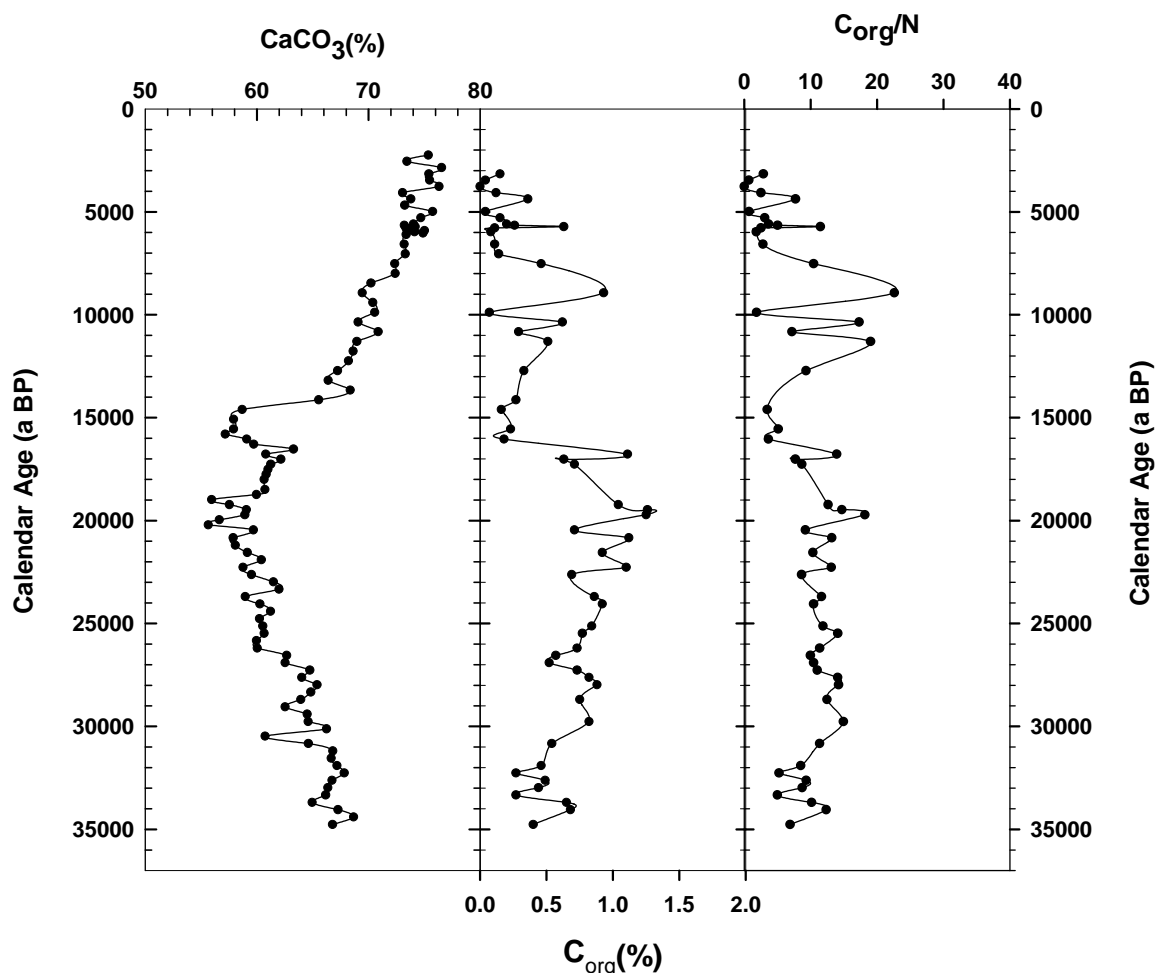


Fig.4.8. Downcore variations in C_{org} plotted along with CaCO_3 (%) and C/N ratio

C/N ratio is obtained by dividing the organic carbon content (C_{org}) with nitrogen content of the sedimentary organic matter that is again very low with a typical value of $\sim 0.04\%$ and has stayed more or less same throughout the core. Therefore the C/N ratio also exhibits a fluctuation similar to the C_{org} variations. Thus this method of determining C_{org} can't be used in the regions with such a low organic carbon content, which may be either due to poor preservation or due to low overhead productivity. In such cases C_{org} cannot be used reliably as a productivity indicator.

4.6.4. Productivity as exhibited by $\delta^{15}\text{N}$:

Denitrification is known to occur in the oxygen deficient waters and is ultimately controlled by the overhead productivity (Deuser et al, 1978; Naqvi, 1991). The $\delta^{15}\text{N}$ of the sedimentary organic matter has been used as a proxy for the water column denitrification (Altabet et al, 1995, 1999; Ganeshram et al, 1995; Agnihotri et al, 2003 b). Near the core site, oxygen deficient conditions are known to exist between 100 to 200 m and then between 500 to 1000 m with the O_2 levels falling to ~ 1 ml/l (Schulte et al, 1999). $\delta^{15}\text{N}$ of the sedimentary organic matter has been measured in the core SS3827 G to explore the possibility of productivity induced denitrification in the water column. The $\delta^{15}\text{N}$ values exhibit very wide fluctuations without any trend as shown in Fig.4.8.

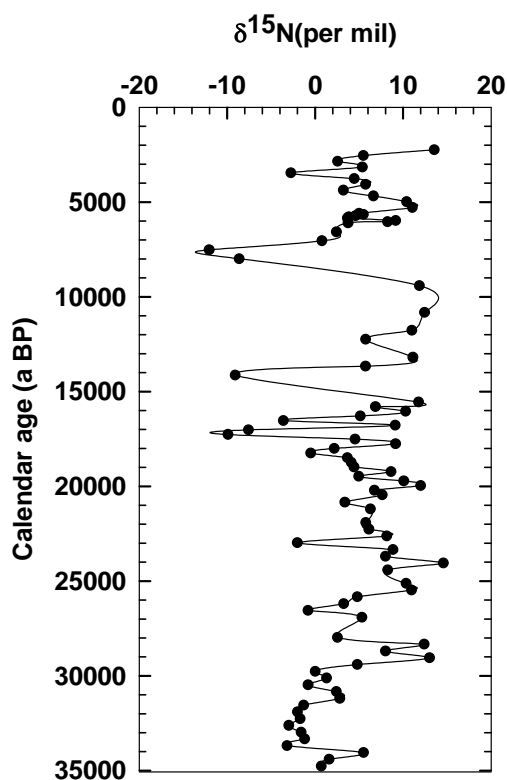


Fig.4.9. Downcore variation of $\delta^{15}\text{N}$ in the core SS3827 G for the past 35 ka.

The reason for such a behaviour by $\delta^{15}\text{N}$ in this core is the low amount of sedimentary nitrogen present. As discussed above in the section 4.6.2, the percentage of sedimentary organic matter is very low. Because of low organic matter and hence low nitrogen percentage the measurement of $\delta^{15}\text{N}$ could not be performed satisfactorily as nitrogen content was less than the range for which the mass spectrometer behaviour is linear. To test this, the $\delta^{15}\text{N}$ values for all the three cores

analyzed in this study were plotted with respect to the respective nitrogen content as shown below in the figure 4.10.

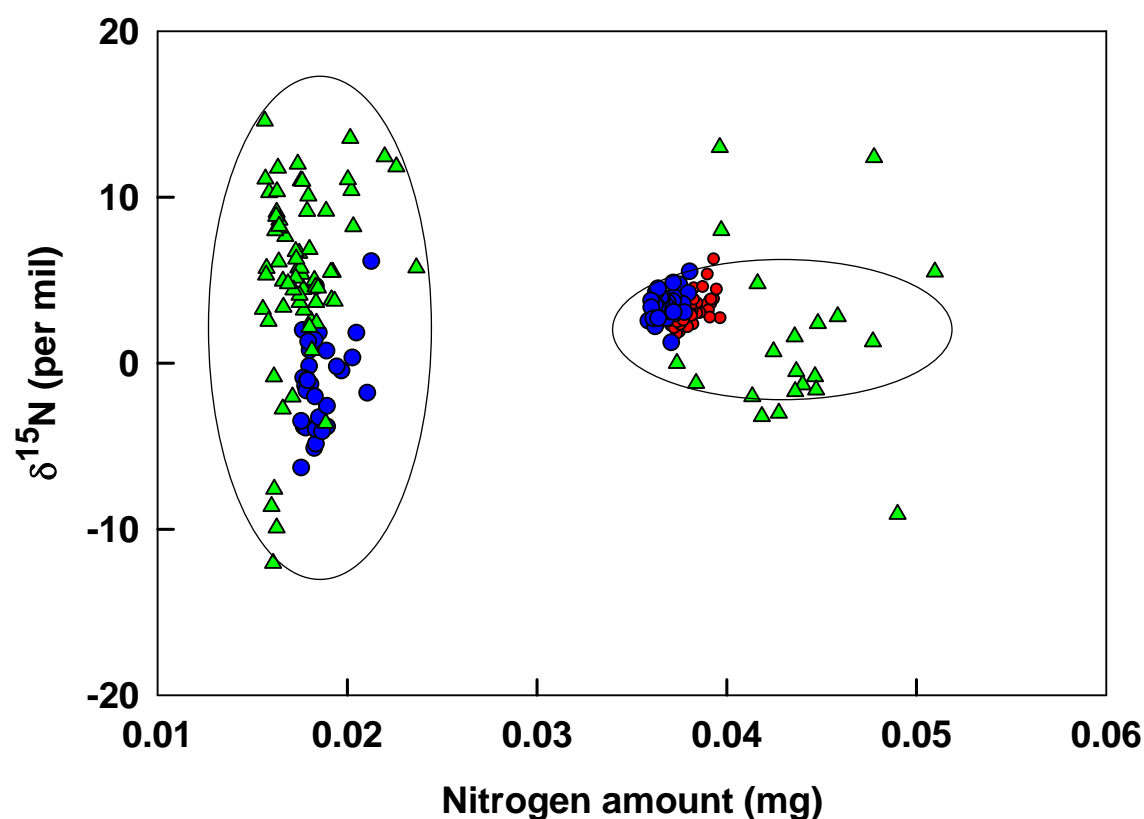


Fig.4.10. $\delta^{15}\text{N}$ vs. Nitrogen content (in mg) for all the three cores viz. SS3827 G (green triangle), SS4018 G (blue circle) and SK 145-9 (red circle) analyzed in this study.

There are clearly two clusters of the data points corresponding to different amount of nitrogen content. As evident, when the nitrogen content of the sedimentary sample is sufficient (>3.5 mg) then the $\delta^{15}\text{N}$ values vary between very small range and fall well within the linear range of the mass spectrometer. On the other hand, when the nitrogen content is less (<2 mg, approximately) then the $\delta^{15}\text{N}$ values fluctuate widely, clearly getting out of the range along which mass spectrometer exhibits linear behaviour. Most of the data points in the cluster showing wide variation in the isotopic values belong to the core SS3827 G. We conclude that $\delta^{15}\text{N}$

values are not useful as a productivity indicator in this case because of the very low amount of sedimentary organic matter/ nitrogen content present.

4.6.5. Productivity as exhibited by carbon isotopes:

The carbon isotopic values ($\delta^{13}\text{C}$) of planktonic foraminifera are known to be controlled by the $\delta^{13}\text{C}$ of the bicarbonate ions present in the seawater as discussed in the section 2.4.2. The $\delta^{13}\text{C}$ of the bicarbonate ions in turn is controlled by the organic productivity and the $\delta^{13}\text{C}$ of the water coming from below e.g. due to wind induced mixed layer deepening or upwelling. The $\delta^{13}\text{C}$ was measured in the three different species of foraminifera viz. *Globigerinoides ruber*, *Globigerinoides sacculifer*, *Globorotalia menardii*, as shown below in fig. 4.11.

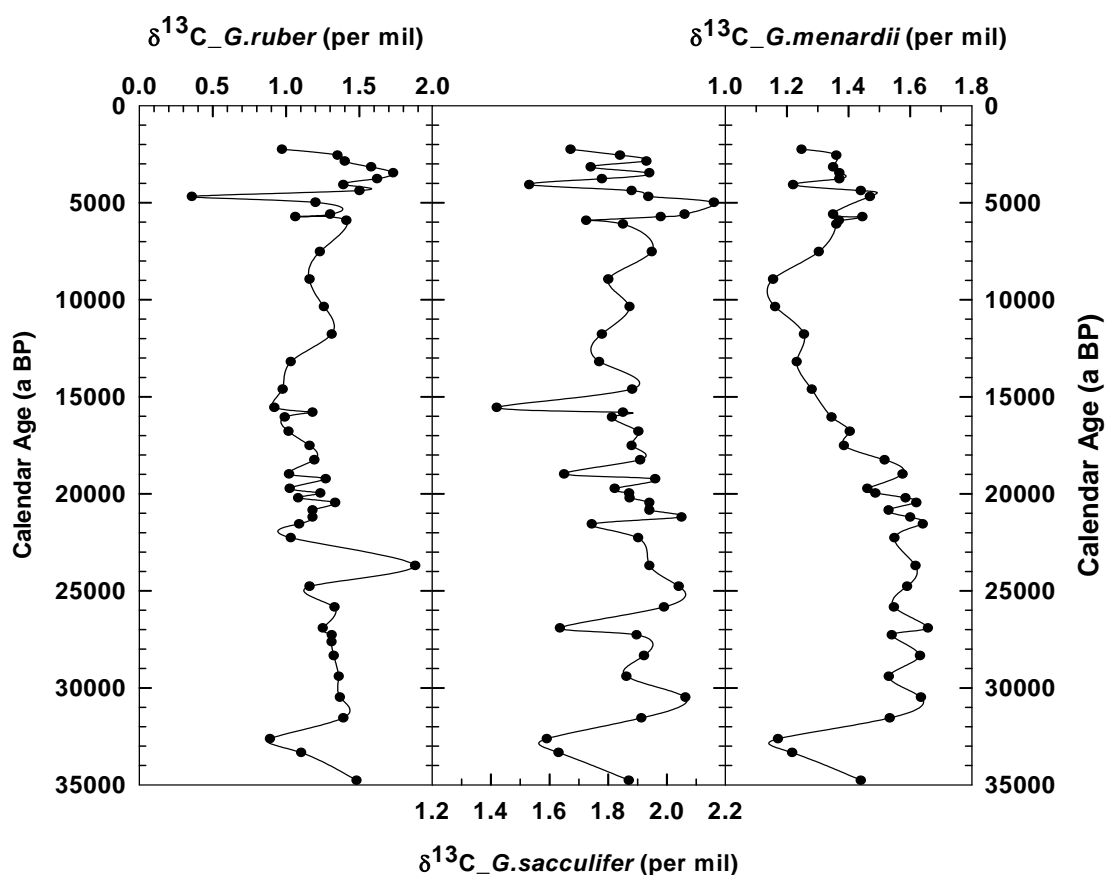


Fig. 4.11. Downcore variation of $\delta^{13}\text{C}$ values of the three species of planktonic foraminifera in the core SS3827 G.

As evident from the above figure the $\delta^{13}\text{C}$ values of any of the three species do not exhibit any trend shown by calcareous productivity such as minimum productivity

at LGM with a sharp increase at ~15 ka BP. One possible reason for such a behaviour by $\delta^{13}\text{C}$ is that it is governed by two competing processes i.e. productivity and upwelling. During enhanced winds, productivity increases due to the influx nutrients from below resulting in the consumption of more of the ^{12}C by the phytoplanktons thus increasing the $\delta^{13}\text{C}$ of the seawater. But the enhanced winds also enhance upwelling and bring the water from the deeper level, which is depleted in $\delta^{13}\text{C}$ (e.g. typically water from a depth of 100 m are depleted by 0.5‰ with respect to surface values, increases to 1‰ by ~600m; Kroopnick, 1985). This upwelled water depleted in $\delta^{13}\text{C}$ essentially negates the enrichment due to productivity and thus reduces the signal. The core site falls in the equatorial upwelling zone and is also influenced by the wind induced mixed layer deepening. When due to stronger winds productivity is higher then surface layer mixing and upwelling are also higher resulting in a mixed signal as discussed above. The $\delta^{13}\text{C}$ can be used as a productivity signal in those regions only where the productivity signal is so strong that it masks the upwelling effect e.g. in the western Arabian Sea.

4.7. Spectral Analysis:

Spectral analysis has been carried out on the time-series data of various proxies to detect the underlying inherent periodicities that might point towards the various forcing factors governing the climatic condition at the core site. The proxies that were analyzed included $\delta^{18}\text{O}$ in all the three species of foraminifera viz. *G.ruber*, *G.sacculifer* and *G.menardii* along with the $\text{CaCO}_3\%$ using the REDFIT 3.6 program (Schulz and Mudelsee, 2002). Proxies such as C_{org} content and $\delta^{15}\text{N}$ in the sedimentary organic matter were excluded from this exercise as their variations do not truly represent the changes in overhead productivity because of their low content as discussed in the section 4.6.2 and 4.6.3. Similarly $\delta^{13}\text{C}$ in foraminiferal species were not analyzed, as their variations are the mixed outcome of two processes i.e. productivity and upwelling, which tends to confuse the signal. The various spectra that were obtained are shown in Fig.4.11.

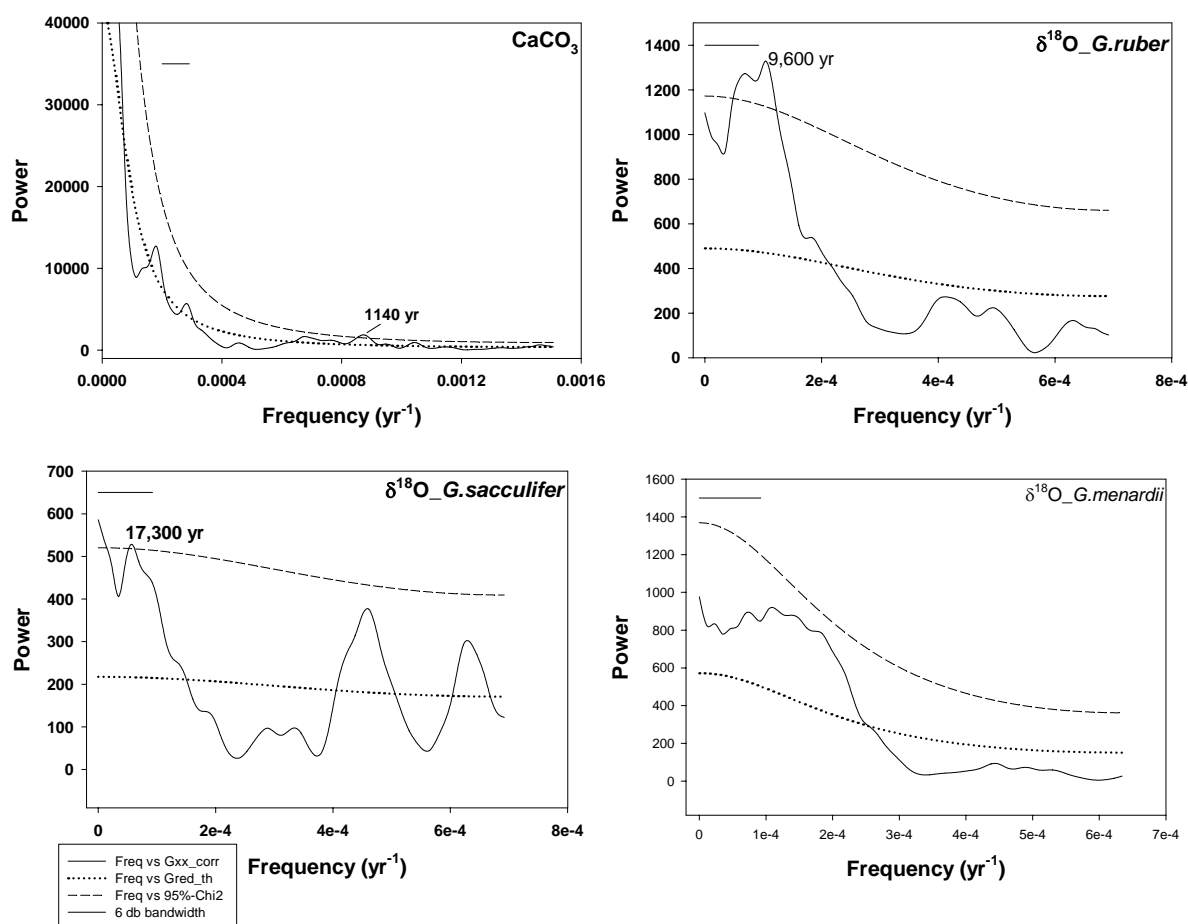


Fig.4.12. Power spectra for various paleoclimatic proxies. Horizontal line at the upper left-hand corner represents 6db bandwidth of the spectral resolution. Gxx_corr denotes amplitude or power of various frequencies; Gred_th shown by dotted line is the background signal; dashed line denotes the 95% significance level calculated using the χ^2 test.

$\delta^{18}\text{O}$ spectrum of the foraminiferal species *G.sacculifer* is dominated by the 17,300 years (y) periodicity, which is very close to the 19,000 y cycle observed for the Earth's precessional cycle. Various other workers like Clemens et al (1991), Rostek et al (1997), Reichert et al (1997), Leuschner and Sirocko (2003) have proposed that in the tropics precessional phase (~ 23 ky) dominates the SW monsoon and associated phenomenon. For example Reichert et al (1997) have shown that C_{org} spectrum is dominated by the 23 ky periodicity while Ti/Al shows both 100 ky and 23

ky periodicities. Beaufort et al (1997) have noticed that the primary productivity record from the equatorial Arabian Sea in the core MD 900963 is strongly dominated by the precession cycles of the 23- to 19 ky periods. This led them to propose that the productivity variation at the core site is mainly governed by the insolation. The $\delta^{18}\text{O}$ spectrum of the *G.ruber* also exhibits a periodicity of $\sim 9,600$ y, which seems to be a sub-cycle of the 19 ky precession cycle. It points towards the fact that SW monsoon (as $\delta^{18}\text{O}$ variations are mainly governed by the evaporation – precipitation budget) is mainly governed by the insolation variations induced by the precessional cycle of the Earth's orbit.

Time series analysis of the CaCO_3 data exhibits a significant periodicity of ~ 1140 y, which is similar to the 1470 ± 500 y periodicity observed in records from different locations around the globe (e.g. Sirocko et al, 1996; Bond et al, 1997; Schulz et al, 1998; Mayewski et al, 1998, Campbell et al, 1998; Sarkar et al, 2000 Agnihotri et al, 2003b). Grootes and Stuiver (1997) have shown that this 1470 y cycle is exhibited by the Dansgaard – Oeschger events in the Greenland ice core's $\delta^{18}\text{O}$ record i.e. D-O events occur every ~ 1400 y. Similar periodicity observed in our equatorial record points towards a common forcing factor, which appears to corroborate a common link between the tropical and north Atlantic climate. Time series analysis of the $\delta^{18}\text{O}$ in *G.menardii* does not yield any periodicity that might be due to the fact that this species dwells in the deeper water and hence is mildly affected by E-P budget, which mainly controls the $\delta^{18}\text{O}$ variations at the core site. It is also not clear why the spectra of *G.sacculifer* and *G.ruber* differ. One possibility is that their abundance peak at different seasons in this site.

4.8. Inferences:

- i. The NE monsoon did not strengthen during the LGM as proposed earlier based on the bulk dating methods. In fact it intensified during the early deglacial period from ~ 19 ka BP to ~ 17 ka BP as shown by our study on three different species of planktonic foraminifera with better age control.
- ii. Oxygen isotope values of all the three species of foraminifera exhibit a good correlation with the GISP2 $\delta^{18}\text{O}$ record on centennial to millennial timescales.

The warm interstadial periods are accompanied by stronger SW monsoon and cooler stadials correspond to reduced SW monsoon. Although during the Holocene, the correlation was not as good.

- iii. The similar variations observed in the tropical/equatorial climate and the North Atlantic climate indicates that tropics were instrumental in bringing about high latitude climatic changes, most probably via atmospheric forcing through greenhouse gases or *vice versa* by albedo feedback.
- iv. Minimum SW monsoon precipitation was observed at LGM based on the oxygen isotope analysis as well as calcareous productivity.
- v. At T IA, an increase in SW monsoon precipitation is observed as evident from the negative $\delta^{18}\text{O}$ values due to influx of Bay of Bengal water, which is of lower salinity due to glacier melting and higher river runoff.
- vi. During the Holocene, SW monsoon intensified uniformly upto the core top as revealed by oxygen isotopes and calcareous productivity.
- vii. Calcareous productivity indicates a decreasing IEW and hence decreasing Indian and east African rainfalls upto LGM with a minimum value at LGM with the maximum El Nino frequency during the last glacial period. Thereafter the IEW strengthened upto 16.5 ka BP after which it fell back sharply to LGM values for a millennium (~15.5 ka BP) indicating a reduction in rainfall. Thereafter IEW exhibit a sharp increase at ~14.5 ka BP that coincides with the Termination IA implying strengthened Southwest monsoon and East African rains.
- viii. Since ~14.5 ka BP to the core top (~2.2 ka BP) including the Holocene, calcareous productivity exhibits a uniformly increasing trend implying a uniformly strengthening IEW and Southern oscillation index and hence

strengthening SW monsoon and east African rains along with a declining El Nino frequency.

- ix. Based on the comparative study from the other two cores from the eastern Arabian Sea, it could be inferred the IEW and SW monsoon winds strengthened and weakened in unison pointing towards a common forcing factor, most probably insolation, at least during the last 35 ka.
- x. Spectral analyses of various proxies indicate that SW monsoon is dominated by the quasi-period of the precessional cycle, which indicates that it is governed by the solar forcing on the Milankovitch timescale. Common periodicity between the equatorial and north Atlantic records points towards a possible common mechanism linking them.
- xi. C_{org} and $\delta^{15}N$ are not useful as productivity indicators in this region because of the very little amount of sedimentary organic matter.
- xii. $\delta^{13}C$ of the foraminifera also is not useful as a productivity indicator in this region as the signal is mixed, caused by two processes *viz.* upwelling and productivity.

Chapter 5

**Western Arabian Sea: SW Monsoon
History since the Last Glacial Maximum**

5.1. Introduction:

The western Arabian Sea is best suited to study the past variations of monsoon, as it experiences intense upwelling during the SW monsoon (Wrytki, 1973; Shi et al, 2000). The upwelling brings up nutrient rich, cold water from deeper levels of the ocean to the sea surface. This causes enhanced productivity (Kabanova, 1968; Codispoti, 1991) and reduces the sea surface temperature by at least 4°C (Haake et al, 1993 a, b). This provides the largest detectable signal for studying the paleomonsoon variations. No wonder a large number of earlier studies are concentrated in this region (Prell et al, 1980; Prell and Kutzbach, 1987; Clemens et al, 1991; Anderson and Prell, 1993; Sirocko et al, 1993; Naidu et al, 1993; Naidu and Malmgren, 1995; Reichart et al, 1997, 1998; Schulz et al, 1998; Anderson et al, 2002; Gupta et al, 2003). We obtained a core SS 4018 G from the western Arabian Sea near the mouth of the Gulf of Aden. The base of the core corresponds to a period when the earth had already experienced the most severe glaciation and was recovering towards a warmer climate. But starting from 15 ka BP to 10 ka BP, the earth's climate fluctuated between extremes that plunged back the earth into the cold, comparable to that of the Last Glacial Maximum, and pulled it out as suddenly to the balmy conditions akin to today. These rapid climate changes took place in a matter of few decades to few centuries. It becomes necessary to assess the behavior of the monsoon during such extreme climatic changes. Furthermore, the variations exhibited by SW monsoon during the Holocene (past 10,000 years) is a matter of debate with some workers favouring decreased monsoon intensity during the Holocene (Sirocko et al, 1993; Gupta et al, 2003) whereas others demonstrating an increasing monsoon for the major part of the Holocene (Sarkar et al, 2000; Agnihotri et al, 2003). This study is based on a large number of AMS radiocarbon dates on planktic foraminiferal separates, and multi-proxy isotopic and chemical analysis of the core will help to resolve this problem.

5.2. Core location:

The core is located at the mouth of the Gulf of Aden near the Red Sea in the Western Arabian Sea. It has been raised from a water depth of 2830 m, which is well above the lysocline in the Western Arabian Sea (~3900 m, Kolla et al, 1976). Refer

Table 2.1 for additional details. Core location is shown in Fig. 5.1 along with other cores with which this study has been compared.

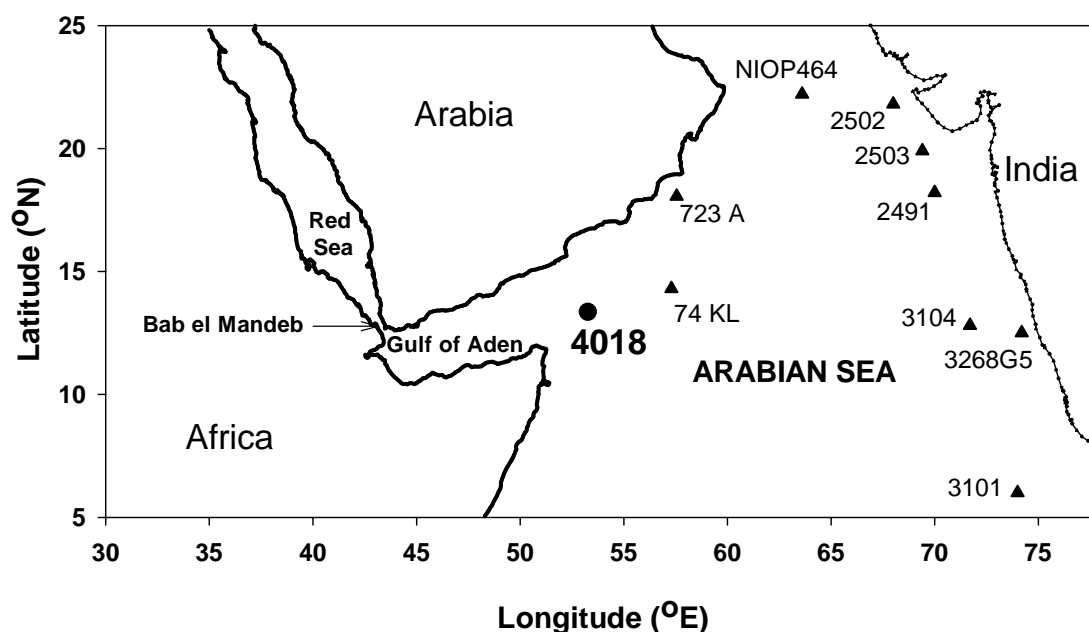


Fig 5.1. Locations of the Core SS 4018G (this study, shown by circle) and other cores with which it has been compared (depicted by triangles)

5.3. Oceanographic conditions at the core site:

There are three kinds of water masses that can be distinguished in the Arabian Sea *viz.* those generated by downwelling, those that are mixtures of other water masses and those that enter from outside. Two shallow subsurface water masses that are present just below the monsoon controlled surface mixed layer and formed due to subduction are Arabian Sea Water (ASW) and Subtropical Subsurface water (SSW) (Schott and McCreary Jr., 2001). ASW or Arabian Sea High- Salinity Water forms in the northern Arabian Sea due to winter cooling during the North East monsoon and spreads southward (Morrison, 1997; Schott and Fischer, 2000) just below the surface layer and upto 100m water depth (Prasanna Kumar and Prasad, 1999). SSW forms in the subtropical gyre of the southern hemisphere as a high salinity water due to excess of evaporation over precipitation. It joins the westward flowing South Equatorial Current (SEC) at 200-250 m water depth and it shoals to 100 m by the time it reaches the

western boundary (Swallow et al, 1988). Thereafter it spreads northward across the equator with the Somali Current, ultimately participating in supplying water to the upwelling off Somalian and Arabian coast (Schott and McCreary Jr., 2001). Another set of high salinity subsurface waters is Persian Gulf Water (PGW) and Red Sea Water (RSW). Persian Gulf Water is a saline water mass that originates due excess of evaporation in the Persian Gulf and enters the Arabian Sea through the Strait of Homruz. It is found at a depth of 200 - 400 m and does not extend far beyond the northern Arabian Sea (Rhein et al, 1997; Prasanna Kumar and Prasad, 1999). Red Sea Water originates in the northern part of the Red Sea and advects into the Arabian Sea through the Strait of Bab el Mandeb as highly saline and warm water mass (Maillard and Soliman, 1986; Woelk and Quadfasel, 1996). RSW occurs at a depth of 100 – 150 m at the Bab el Mandeb and downstream it mixes strongly with the surrounding waters and by the time it reaches Somalian coast off Socotra it sinks to ~800 m water depth (Shapiro and Meschanov, 1991; Woelk and Quadfasel, 1996).

At intermediate depth is found the Antarctic Intermediate Water (AAIW) that enters the basin through the southeastern region (Fine, 1993). It is formed at the subpolar frontal zone and is marked by low salinities because of excess of precipitation over evaporation over there (Schott and McCreary, 2001). The IDW or Indian Deep Water that is specific to northern Indian Ocean occupies the greatest depths. It flows in the density range just above the Circum Polar Deep Water (CDW), and is presumably generated by deep upwelling out of CDW (Mantyla and Reid, 1995).

The surface circulation at the core site is controlled by the seasonal reversal of monsoonal winds. Refer to Figs.1.1 and 1.2 for schematic diagrams of the Indian Ocean circulation during the summer and winter monsoons respectively. The Southeast Trade winds drive the westward flowing South Equatorial Current (SEC) in the latitude range 17 - 22°S. At the tip of Northern Madagascar, about 17°S, SEC splits into two parts that flows northwards and southwards and are called as Northeast Madagascar Current (NEMC) and Southeast Madagascar Current (SEMC). NEMC feeds the northerly flowing East African Coast Current (EACC, Schott and McCreary Jr., 2001). During the summer monsoon the EACC feeds the northward flowing

Somali Current (SC) that develops into various clockwise rotating cells and gyres such as Southern Gyre (SG), Great Whirl (GW) and Socotra Eddy (SE) that develops northeast of Socotra Island (Fig.1.1) (Schott et al, 1990; Brock et al, 1991). It induces intense upwelling along the Somali and Oman coast with upwelling velocities close to 3×10^{-3} cm/sec and an upwelling transport of 1.5 – 2 Sv in the upper 50 m as shown in the Fig. 5.2 (Smith and Bottero, 1977; Shi et al, 2000).

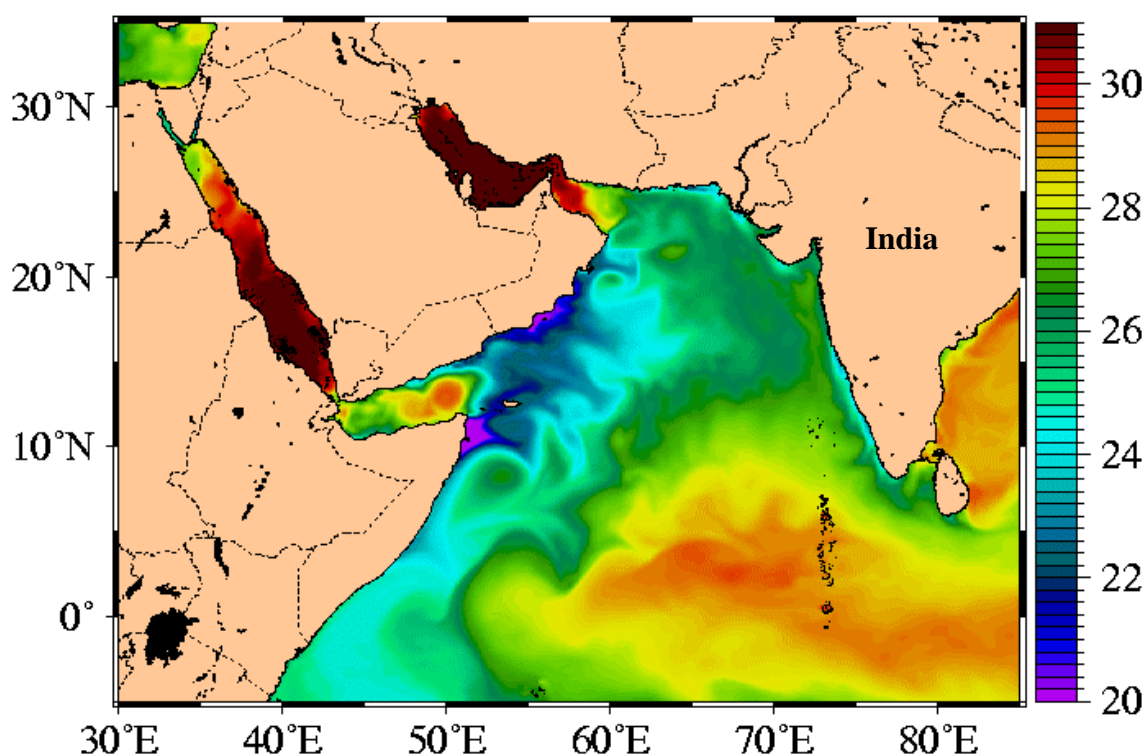


Fig.5.2. SST contours (in $^{\circ}\text{C}$) during August. The upwelling along the Somali and Oman coast is manifested by the reduction in SST due to surfacing of cooler waters from below.

The typical temperature of the upwelled water is $19 - 24^{\circ}\text{C}$ (Schott and McCreary Jr., 2001). The reasons attributed for such intense coastal upwelling is the Ekman divergence due to the flow of strong winds parallel to the coast. As the surface water moves away from the coast, water from below upwells to take its place. The offshore upwelling takes place due to the strong positive wind stress curl to the NW of the axis of the Somali jet, which is a low level cross-equatorial jet (Smith and Bottero, 1977; Shallow, 1984). The central Arabian Sea exhibits a bowl shaped mixed

layer deepening under the effect of Findlater Jet wind-stress forcing and Ekman pumping (McCreary and Kundu, 1989; Rao and Sivakumar, 2000).

During the winter monsoon, the Somali Current reverses its direction and flows southward and meets the EACC at 2-4°S that supplies the eastward flowing South Equatorial Countercurrent (SECC, Dueing and Schott, 1978; Swallow et al, 1991). The cold and dry Northeast monsoon winds accompanied by the Ekman pumping cause subduction of the high salinity surface waters in the northern Arabian Sea (Morrison, 1997; Schott and Fischer, 2000).

5.4. Age – Depth model:

SS 4018G has 15 radiocarbon dates of planktonic foraminiferal separates (see section 2.3). One depth *viz.* 60 - 62 cm was repeated by picking another set of planktic foraminifera and both the samples gave similar result. For this particular sample the two radiocarbon dates obtained are 10364 ± 55 and 10543 ± 60 , which after calibration gave the calendar ages as $11,000 \pm 230$ and $10,930 \pm 380$ respectively that are similar within the error range (errors given are 1 standard deviation). An average of both the values *i.e.* 10965 ± 222 has been taken for the Age – Depth model. This core covers up to ~19,000 calendar years (depth~130cm) and thus possess an average sedimentation rate of $\sim 7\text{cm}/10^3$ years. Although this core is from an open ocean location (water depth: 2830m), it has a high sedimentation rate owing to the high surface productivity. The resolution in this case is 150 years per cm but since the sampling is done at every two cm, the effective resolution becomes ~ 300 years per sample. For the dates in tabular form and other related information, please refer to the Table 2.2.

The radiocarbon dates in this core has been calibrated to calendar ages using the calibration program “Calib 4.1 (INTCAL 98)” (Stuiver et al, 1998) with a reservoir age correction of 563 ± 30 years ($\Delta R = 163 \pm 30$ yr, Dutta et al, 2001). Recently Southon et al (2002) carried out extensive study in the Indian Ocean regarding the oceanic reservoir ages. For the western Arabian Sea they proposed a mean ΔR value of 190 ± 25 yr that is very similar to that of Dutta et al (2001). The Age-Depth model is shown in the Fig.5.3.

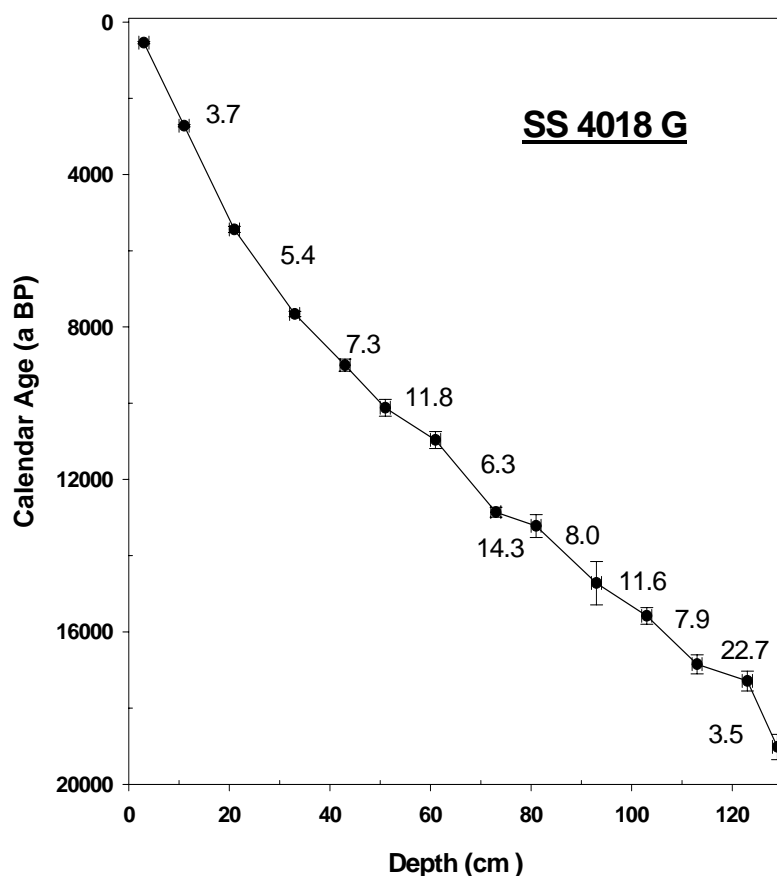


Fig. 5.3. Calibrated radiocarbon ages and sedimentation rates (cm/kyr) for SS4018G.

5.4. Downcore productivity variations in the core SS 4018 G:

Oceanic productivity manifests itself in many forms such as calcareous (foraminifera, coccoliths, pteropods), siliceous (diatoms, radiolarians) and organic productivity. To determine the productivity variation in SS4018 G, various chemical proxies (i.e. CaCO_3 %, C_{org} %) and isotopic proxies (i.e. $\delta^{15}\text{N}$, $\delta^{13}\text{C}$) were measured.

5.4.1. Productivity as manifested by CaCO_3 and C_{org} :

Calcareous productivity (CaCO_3 wt. %) can be taken as an indicator of overhead productivity if the core has been raised above the lysocline and has not

suffered any carbonate dissolution. Moreover it should not have been diluted by the terrestrial input (Sirocko et al, 1993, Naidu et al, 1993). Similarly organic productivity as exhibited by the C_{org} (wt. %) can point towards past productivity variations provided it has not been contaminated by terrestrial organic matter, or wasn't oxidized by oxic bottom waters.

Organic carbon preservation is controlled by the availability of the oxidizing agents and its removal from the diagenetically active layer with complex interplay of many variables such as organic matter composition, bioturbation rates, diffusive openness of the sediments to various oxidizing agents and protective adsorption of organic matter on the mineral surfaces etc. (Hedges and Kiel, 1995). The core has been raised from a water depth of 2830m that is overlain by oxic waters. But the core site experiences high sedimentation rate (~7 cm/kyr) due to the intense productivity occurring over there (Nair et al, 1989). Due to the high sedimentation rate the organic matter rapidly crosses the diagenetically active layer, which is of the order of ~20 cm. Thus the organic matter not only escapes the effect of bioturbation that is more active near the sediment surface but also the dissolved oxidizing agents such as O_2 , NO_3^- , SO_4^{2-} etc. (Heinrichs, 1992). Furthermore several workers have questioned the effect of oxygen availability on diagenesis. Several laboratory and field studies of the relative mineralization rates of bulk organic matter or specific biochemical compounds such as dissolved sugars, amino acids etc. under oxic vs. anoxic conditions have indicated little or no effect of O_2 concentration (Foree and McCarty, 1970; Hansen and Blackburn, 1991; Cowie and Hedges, 1991,1992; Lee, 1992; Hedges and Kiel, 1995). Moreover lack of any relationship between sedimentary organic matter preservation and O_2 concentrations (Pederson et al, 1992; Calvert and Pederson, 1992) or burial efficiencies (Heinrichs and Reeburgh, 1987; Betts and Holland, 1991) has cast doubts on the importance attached to the oxygen availability. Thus many exceptions exist to the oxygen effect and there is no universal pattern (Pederson et al, 1992).

Schulte et al (1999) carried out multi-proxy study on a core near [Maldives raised from a water depth of 2450 m] that has experienced oxic conditions throughout its history. They have conclusively proved that the variation in organic carbon is due to overhead productivity alone and is not affected by the bottom water preservation

characteristics. Similarly Reichert et al (1997) studied a core from the Murray Ridge in the Northern Arabian Sea from a water depth of 1470m (oxic waters) and concluded that C_{org} record is a manifestation of surface water productivity.

Rostek et al (1997) obtained a core from a location adjacent to that of SS4018 G from a water depth of 2490 m. The similar variations exhibited by C_{org} and total alkenone concentration proved that variations in organic matter are related to marine productivity. Following figure shows the downcore variation in the $CaCO_3$ (wt. %) and C_{org} (wt. %) that are controlled mainly by the overhead productivity changes.

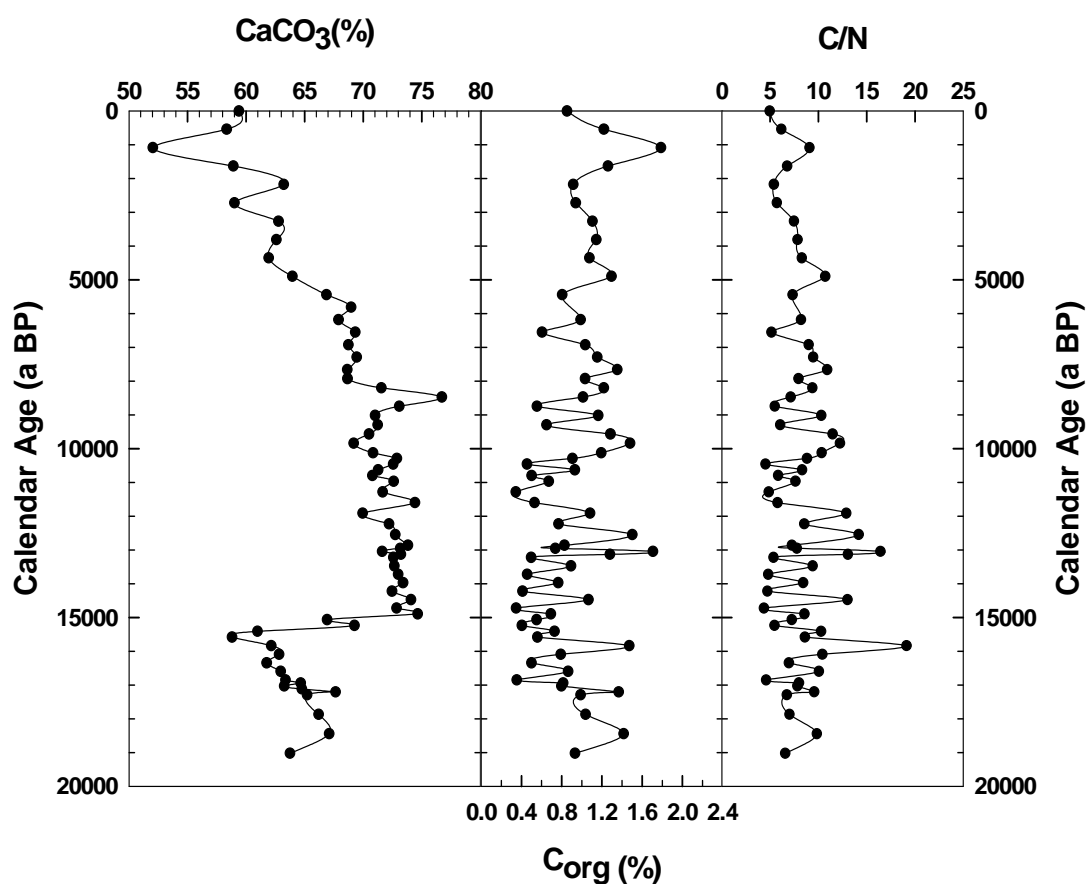


Fig. 5.4. Downcore variations of productivity proxies in the core SS 4018 G

C/N ratio indicates the provenance of the organic matter: recent marine sedimentary organic matter has a typical value of $\sim 8 \pm 2$ and older sediments yield organic matter with a value of ~ 12 to ~ 15 (Mackenzie, 1980). In contrast, the terrestrial organic matter has a C/N ratio of ~ 20 to ~ 100 with an average value of ~ 60

(Premuzic et al, 1982; Meyers, 1994). In this core, the average C/N value is ~9. Prior to Holocene there are some variations but the values still fall well within the range for marine organic matter. Thus the C/N values in this core unequivocally point towards the marine origin of the organic matter with negligible terrestrial input, if any.

The calcareous productivity as evident by the CaCO_3 (wt. %), and the organic productivity (C_{org}) show a decreasing trend upto 15 ka BP indicating a reduced monsoon during the early deglacial period. Thereafter calcareous productivity exhibits an enhancement at 15 ka BP pointing towards an increase in the monsoon intensity that coincides with the major deglaciation episode. Albedo changes associated with melting of Tibetan glaciers (Zahn, 1994) can cause more heating of the Tibetan plateau that can lead to an enhanced monsoon. After 15 ka BP, the CaCO_3 productivity stays more or less uniform upto 9 ka BP where it shows a sudden increase indicating monsoon enhancement. This episode of monsoon enhancement follows just after the maximum summer insolation in the latitude 20°N to 35°N at 10 ka BP (Loutre et al, 1992). Thereafter the calcareous productivity stays uniform upto 6 ka BP after which it shows a decreasing trend. Such a trend was also seen by Sirocko et al (1993) and Gupta et al (2003) in the cores 74 KL and 723A respectively from the nearby regions (Fig.5.1). Sirocko et al (1993) also observed an increase in the monsoon intensity at ~15 ka BP as evident by the increased calcareous productivity at that time and an enhancement at ~9 ka BP. Thereafter they found a decreasing trend in the calcareous productivity which they attributed to the decreasing monsoon intensity during the Holocene (past 10,000 years). Similarly, Gupta et al (2003) have analyzed *G.bulloides* % in the core 723A covering the Holocene. *Globigerina bulloides* is foraminiferal species inhabiting the temperate to sub-polar waters. It occurs in the tropical regions where upwelling takes place due to which cooler water from the deeper levels surfaces. Thus it is an indicator of upwelling, which in turn is governed by the wind strength. More the *G.bulloides* %, more the wind strength. They found a decreasing *G.bulloides* % during the Holocene that they attributed to a weakening wind strength and hence decreasing monsoon intensity. Recently Fleitmann et al (2003) measured $\delta^{18}\text{O}$ in cave stalagmite from southern Oman and attributed its variation to local precipitation changes. They found a sudden increase in precipitation centered at ~10 ka BP and thereafter a high monsoon

precipitation from 9.6 to 5.5 ka BP. Furthermore they maintain that a long term gradual decrease in monsoon precipitation has taken place from ~8 ka BP to 2.7 ka BP after which there is a hiatus in stalagmite deposition.

But the major limitation of these studies was that they were based on a single proxy. When multiple proxies are taken into account then they point towards a different picture. In the present study CaCO_3 % shows a decreasing trend after 8 ka BP (see Fig.5.3). Had this decrease been due to decreasing monsoon and therefore productivity, then C_{org} should also have shown a decrease as it is manifestation of organic productivity. But such a decrease is not seen, which indicates that productivity probably hasn't decreased during the Holocene. This is further supported by the $\delta^{13}\text{C}$, $\delta^{15}\text{N}$ studies carried out on this core.

5.4.2. Productivity as manifested by $\delta^{13}\text{C}$:

Downcore variations in the $\delta^{13}\text{C}$ in the three species of foraminifera viz. *G.ruber*, *G.sacculifer* and *G.menardii* are shown below in Fig.5.4.

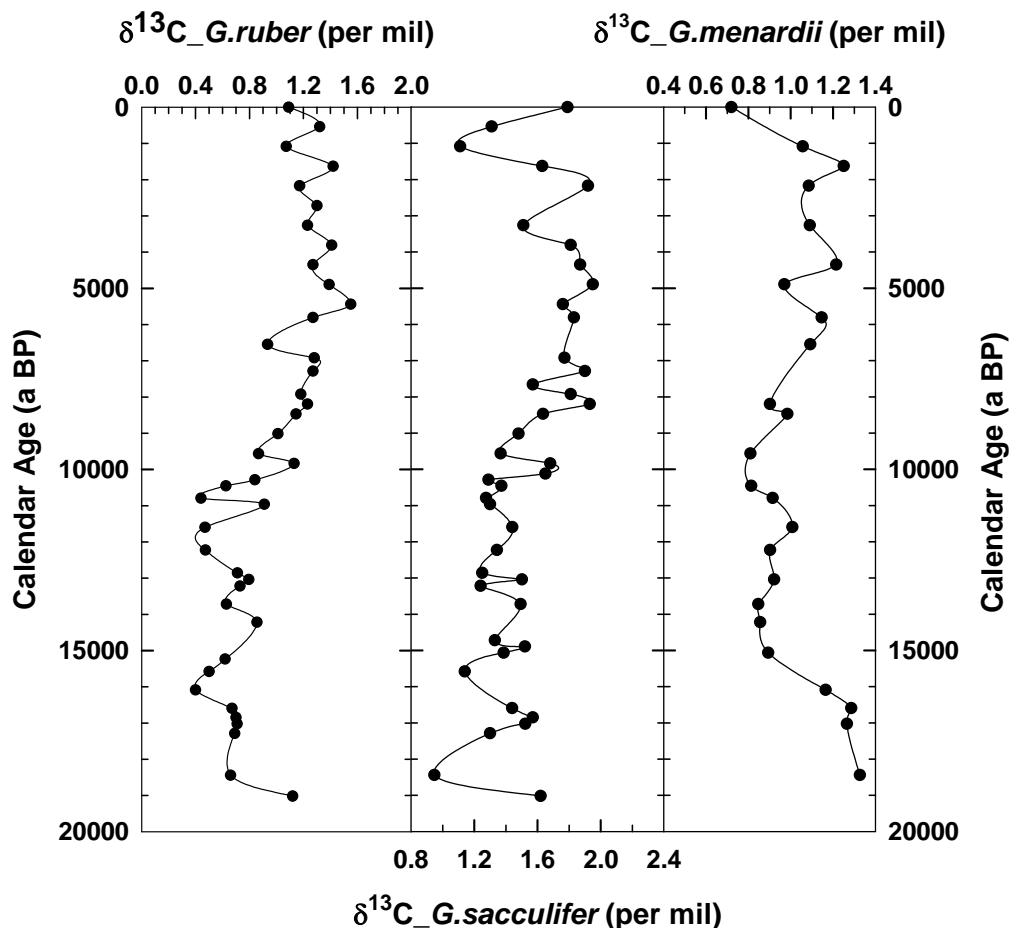


Fig.5.5. Downcore variation of $\delta^{13}\text{C}$ of three species of foraminifera

$\delta^{13}\text{C}$ of calcareous shells of foraminifera are controlled by the carbon isotopic composition of the ambient bicarbonate that in turn is controlled by the organic productivity as discussed in section 2.4.2. During enhanced organic productivity, more of lighter isotope (^{12}C) is taken through photosynthesis, making the calcifying microenvironment enriched in the heavier isotope (^{13}C), the signature of which gets preserved in the calcitic shells of foraminifera. Thus higher $\delta^{13}\text{C}$ in several species indicate enhanced organic productivity. During the Holocene productivity has shown a sharp increase from 10 ka BP to 6 ka BP and thereafter it stays more or less uniform

as evident by the $\delta^{13}\text{C}$ plot of all the three species of the foraminifera. This shows that productivity probably did not decrease during Holocene as hypothesized by earlier workers. It is further supported by the $\delta^{15}\text{N}$ of the sedimentary organic matter.

5.4.3. Productivity as manifested by $\delta^{15}\text{N}$:

The Fig 5.5 shows the downcore variation in the productivity as exhibited by $\delta^{15}\text{N}$ of sedimentary organic matter.

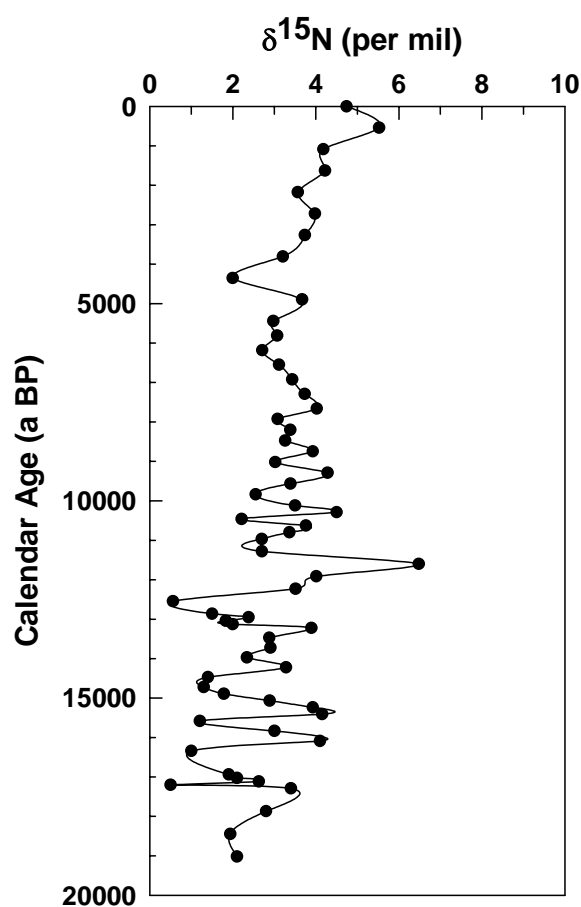


Fig. 5.6. Plot showing the downcore variation of $\delta^{15}\text{N}$ of the sedimentary organic matter in the core SS4018 G

$\delta^{15}\text{N}$ of sedimentary organic matter reflects the surface productivity and the ensuing oxygen depleted conditions as discussed in the section 2.4.3. Higher $\delta^{15}\text{N}$ in general indicates a higher productivity. As evident from Fig.5.5, productivity does not decrease during the Holocene, as revealed by slightly increasing trend seen in $\delta^{15}\text{N}$.

Thus it is apparent that proxies that are manifestation of organic productivity stay more or less uniform or exhibit a slightly increasing trend. This trend in productivity as exhibited by various proxies indicates that monsoon strength did not

decrease during the Holocene. An increase in the monsoon intensity during the Holocene (10 ka –2 ka BP) has also been observed by Agnihotri et al (2003b), Bhushan et al (2001) and Sarkar et al (2000) based on the cores obtained from the eastern continental margin of the Arabian Sea off the western Indian Coast (see Fig. 5.1). But the calcareous productivity in the western Arabian Sea shows a decreasing trend during the Holocene. One way to reconcile these contradictory observations is that increasing monsoon strength favours silicate rather than carbonate production (Naidu et al, 1993; Rixen et al, 1996) and causes cross equatorial transport of the nutrient poor water (Rixen et al, 1996) along the Somali current (Dueing et al, 1980; Schott and Fieux, 1985), which causes further reduction in the productivity.

Haake et al (1993) have shown on the basis of sediment trap data from the Western Arabian Sea that there is enhanced concentration of nitrate and phosphate at around ~30 m water depth, whereas silicate concentration peaks at around ~150 m. During the onset of monsoon, when the monsoon winds just begin to strengthen, upwelling takes place from shallower a depth that enhances the calcareous productivity. But during later stages, as the monsoon wind strength increases upwelling starts from the deeper levels as evident by a further decrease of SST. This injects sufficient silicate into the euphotic zone that leads to diatom blooms causing high siliceous fluxes in the western Arabian Sea (Rixen et al, 1996). Lower sea surface temperatures are associated with high nutrient concentrations (Smith, 1982) that favours diatom blooms (Deuser and Ross, 1980; Deuser et al, 1981). Satellite observations have also shown that plankton blooms that cover the whole northwestern Arabian Sea during the later stages of the SW monsoon (Brock et al, 1991; Brock and McClain, 1992) are diatomaceous (Rixen et al, 1996). Thus it is clear from the above-mentioned observations that increased wind strengths likely lead to enhanced siliceous productivity, rather than calcareous productivity.

Naidu et al (1993) found in a sediment core from the western equatorial Indian Ocean (Somali basin) that $\delta^{13}\text{C}$ of *G.menardii* exhibits enriched values (indicating enhanced organic productivity) in contrast to CaCO_3 % that shows lower values (indicating reduced calcareous productivity) during interglacials. The SW monsoon enhanced during interglacials (Prell and Van Campo, 1986; Clemens et al, 1991) that would have caused increased wind induced surface mixing resulting in higher

productivity. They proposed that the observed anticorrelation between the $\delta^{13}\text{C}$ and CaCO_3 is because of higher biogenic siliceous productivity. Murray and Prell (1991) have also reported higher opal content during interglacials pertaining to increased productivity due to upwelling changes. Naidu et al (1993) further maintain that increased biogenic productivity during interglacials would result in more organic matter degradation that will ultimately cause more CO_2 supply to the bottom waters resulting in enhanced dissolution of CaCO_3 . Similarly Reichart et al (1997) analyzed a core from the northern Arabian Sea namely NIOP464 (shown in Fig. 5.1) covering the past 225 ka and found that high calcareous productivity does not always correspond to enhanced surface productivity as evident by other productivity indicators such as C_{org} . They argued that pelagic carbonate production (including planktonic foraminifera) decreased and was replaced by organic walled and siliceous organisms during enhanced productivity. Enhanced productivity also results in enhanced dissolution of calcite but signs of dissolution such as broken planktonic foraminiferal shells were not found, which implies that the lower CaCO_3 along with high C_{org} is likely due to enhanced siliceous productivity during intense monsoon. The sediments underlying such regions are enriched in silica and organic carbon (Broecker and Peng, 1982) and depleted in calcite. Thus biogenic calcareous productivity might reduce during increased monsoonal wind strengths and is compensated by enhanced biogenic siliceous productivity.

Thus organic productivity has not decreased during the Holocene or at best, has shown a slight increase. But a clear-cut increasing trend is not visible in the productivity proxies. Rixen et al, 1996 observed that during one of the years with the highest monsoon wind strength and minimum SST, the surface productivity was minimum. They attributed this to enhanced cross-equatorial transport of the cold, nutrient poor surface water along the Somali Current. Conkright et al (1994) have shown that waters south of equator are deficient in nutrients as compared to Arabian Sea. The Somali current carries with it the south equatorial waters into the Arabian Sea (Dueing et al, 1980; Schott, 1983; Schott and Fieux, 1985). It flows between the Somalia and Socotra into the upwelling regime off Oman (Fischer et al, 1996). The collapse of the two gyre system (i.e. great whirl and southern gyre) in the later stages of SW monsoon (Evans and Brown, 1981; Schott, 1983) could further strengthen the

cross-equatorial transport along the Somali Current and will control the productivity in the western Arabian Sea. Rixen et al (1996) have proposed that this transport of cold, nutrient poor water is enhanced during higher wind strengths. Such a process could be assumed to take place during the past as well. After the well documented monsoon enhancement at ~9 ka BP, the monsoon strength further increased as evident from the productivity variations in the core SS4018. This further enhancement not only intensified upwelling of nutrient rich waters but also caused increased cross-equatorial transport of nutrient poor waters. These two counterbalancing processes are responsible for the more or less uniform trend seen in various productivity proxies during the Holocene. Monsoon intensification during the Holocene is also supported by the oxygen isotopic analysis as discussed below.

5.5. Oxygen isotopic analysis:

Oxygen isotopic analysis has been carried out on three species of planktonic foraminifera viz. *Globigerinoides ruber*, *Globigerinoides sacculifer*, *Globorotalia menardii* in the core SS4018. *G. ruber* and *G. sacculifer* are surface dwelling species predominantly inhabiting the top ~25m and ~50m respectively. *G. menardii* is a deeper dwelling species found at the top of thermocline at a water depth of 100-150m (Be, 1977). Fig.5.6 (please see the next page) depicts the temporal variation in oxygen isotopic signals in the three species of the foraminifera.

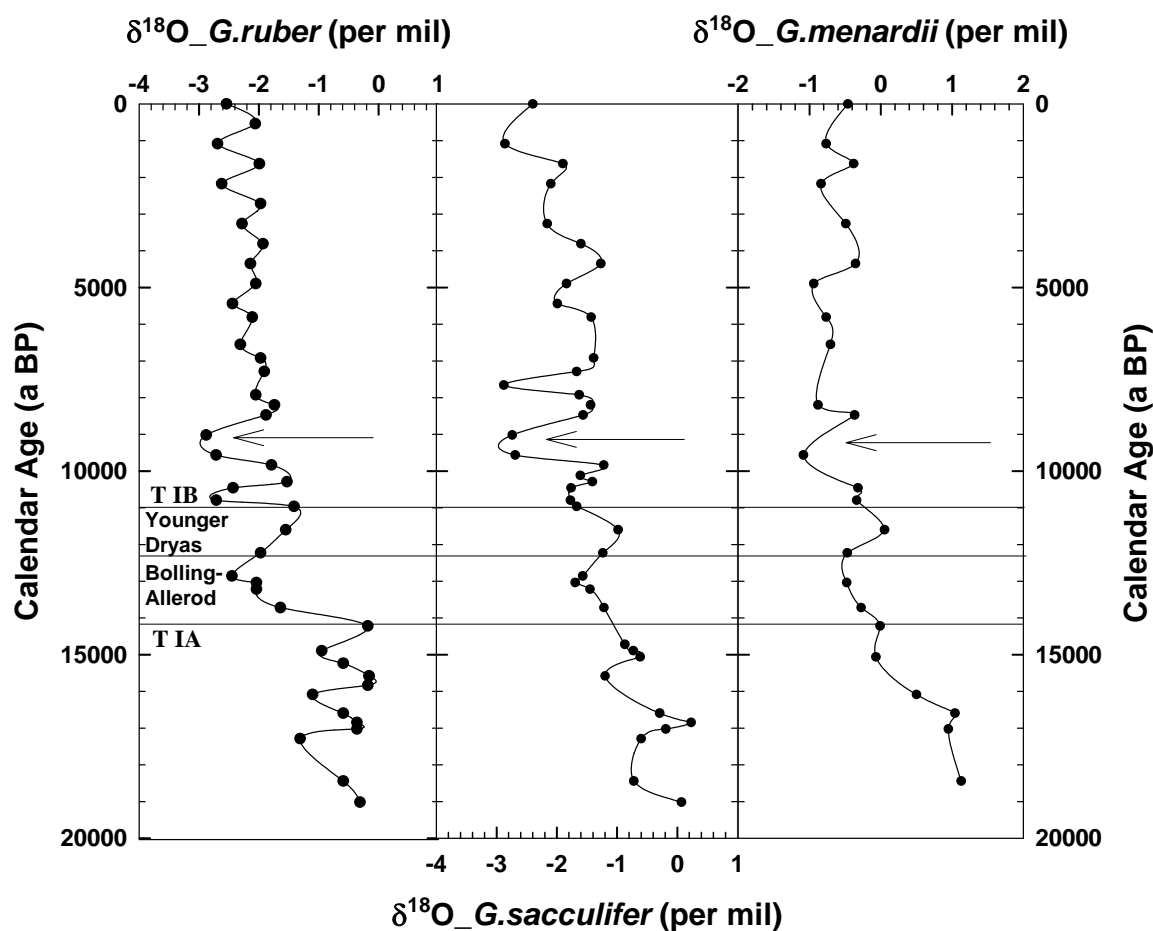


Fig.5.7. Downcore variation in $\delta^{18}\text{O}$ of three species of foraminifera in the core SS4018 G

The calcification temperature and the oxygen isotopic composition of the seawater control the $\delta^{18}\text{O}$ of the calcitic shells of foraminifera as discussed in section 2.4.1. At the present core location, processes that are controlling the oxygen isotopic value of the seawater, at the depths where the studied species dwell are the ice-volume effect and evaporation - precipitation (E - P) balance. The water temperature is controlled by the variation in the upwelling intensity that brings up cold water from deeper levels to the surface. All the three species show more or less the same signals, though a little subdued in the deeper dwelling species *G. menardii*. All the species show higher $\delta^{18}\text{O}$ values during the glacial period than the Holocene. Fairbanks (1989) calculated the global seawater oxygen isotopic curve as governed by the global ice - volume effect. It is based on the sea level curve obtained from Barbados corals

using a factor of 0.011 ‰ per meter change in sea level (Fairbanks and Matthews, 1978).

According to this curve, from LGM to T IA (Termination IA), global seawater $\delta^{18}\text{O}$ decreased by 0.25 ‰. In the core SS4018 G, $\delta^{18}\text{O}$ decrease from LGM to T IA is about 1 ‰. Remaining 0.75‰ decrease is due to seawater water temperature increase due to reduced upwelling as SW monsoon was weak upto 15 ka BP as evident from various productivity proxies discussed earlier. During the later phase of Termination IA global seawater $\delta^{18}\text{O}$ dropped by 0.3‰ (the so called melt water phase, mwp – IA). In the studied core this drop is 1.4 ‰ for *G.ruber*, 0.8 ‰ for *G.sacculifer* and 0.6 ‰ for *G.menardii*, which means that remaining decrease of 1.1 ‰, 0.5 ‰ and 0.3 ‰ respectively are due to local E – P balance. As exhibited by calcareous productivity the SW monsoon intensified at 15 ka BP resulting in enhanced winds and probably precipitation that would cause $\delta^{18}\text{O}$ values to decrease. The highest decrease is found in the surface dwelling species with the amplitude reducing in the deeper dwelling species, consistent with the above interpretation.

During Younger Dryas (13.5 ka BP to 11.5 ka BP) the $\delta^{18}\text{O}$ values increased by 1‰ for *G.ruber*, 0.8 ‰ for *G.sacculifer* and 0.6 ‰ for *G.menardii*. The global seawater $\delta^{18}\text{O}$ fell by 0.15 ‰ during this time, which means that total increase in $\delta^{18}\text{O}$ values of the foraminifera were 1.15 ‰ for *G.ruber*, 0.95 ‰ for *G.sacculifer* and 0.75 ‰ for *G.menardii*. The probable reasons for such a increase can either be enhanced upwelling or E –P balance. If it had been due to enhanced upwelling, then it should have affected all the three species equally. But the surface dwelling species shows the maximum amplitude that indicates a surface phenomenon i.e.. an excess of evaporation over precipitation during that time. During Termination IB (centered at 11ka BP, mwp – IB), again $\delta^{18}\text{O}$ values decreased by ~1.2 ‰ for *G.ruber*, 0.6 ‰ for *G.sacculifer* and 0.4 ‰ for *G.menardii*. The ice – volume effect for this period is 0.2 ‰ decrease. The remaining decrease in the $\delta^{18}\text{O}$ of the foraminifera can be explained by the enhanced precipitation during that time.

Global ice – volume effect is only 0.15 ‰ from 10 – 9 ka BP. But during that period all the species exhibit a sharp reduction in $\delta^{18}\text{O}$ values by ~1 ‰ that points towards copious precipitation (enriched in lighter isotope) and hence monsoon

intensification. This observation is further corroborated by various productivity proxies viz. CaCO_3 , C_{org} and $\delta^{13}\text{C}$ in all the three species of foraminifera that exhibit a sudden enhancement centered at 10 – 9 ka BP. Further enhancement of monsoon results in increased precipitation (enriched in lighter isotope) as well as increased upwelling of colder water that shift the $\delta^{18}\text{O}$ values towards heavier (positive) side. Because of these two counter-balancing processes, the $\delta^{18}\text{O}$ values in all the foraminiferal species stay more or less uniform. Had the monsoon intensity reduced during the Holocene, the $\delta^{18}\text{O}$ should have shown a decreasing trend due to reduced upwelling. But such a decrease is not seen that indicates that SW monsoon intensity did not probably reduce during the Holocene.

In chapter 3 dealing with the core SK145-9, we have compared with the % *G.bulloides* data of the Gupta et al (2003) and inferred that the SW monsoon wind signals obtained in the western Arabian Sea cores are in good agreement with the SW monsoon runoff signals obtained from the eastern Arabian Sea cores. This inference is based on the observation that % *G.bulloides* decline is accompanied by reduced precipitation. But in this chapter, % *G.bulloides* (which is a manifestation of calcareous productivity) decline is attributed to increasing monsoon. It can be explained if we take ***thresholds in the response*** of % *G. bulloides* or the CaCO_3 % in to account. When the abundance of *G. bulloides* was ~28%, further intensification of monsoon brought it down due to reasons discussed earlier in this chapter. However, in the Chapter-3, the values were already low (~10%). Here the intensification of the monsoon may increase rather than decrease the abundance.

5.6. Spectral Analysis:

The periodicities in the time–series data of various proxies has been determined using the REDFIT 3.6 program (Schulz and Mudelsee, 2002). The power spectra obtained for various proxies are given in the Fig.5.7. Out of the productivity proxies, $\delta^{13}\text{C}$ in *G.sacculifer* exhibits a dominant periodicity of ~25,600 years (y), which probably corresponds to the precessional cycle of the earth (~23 kyr) seen by

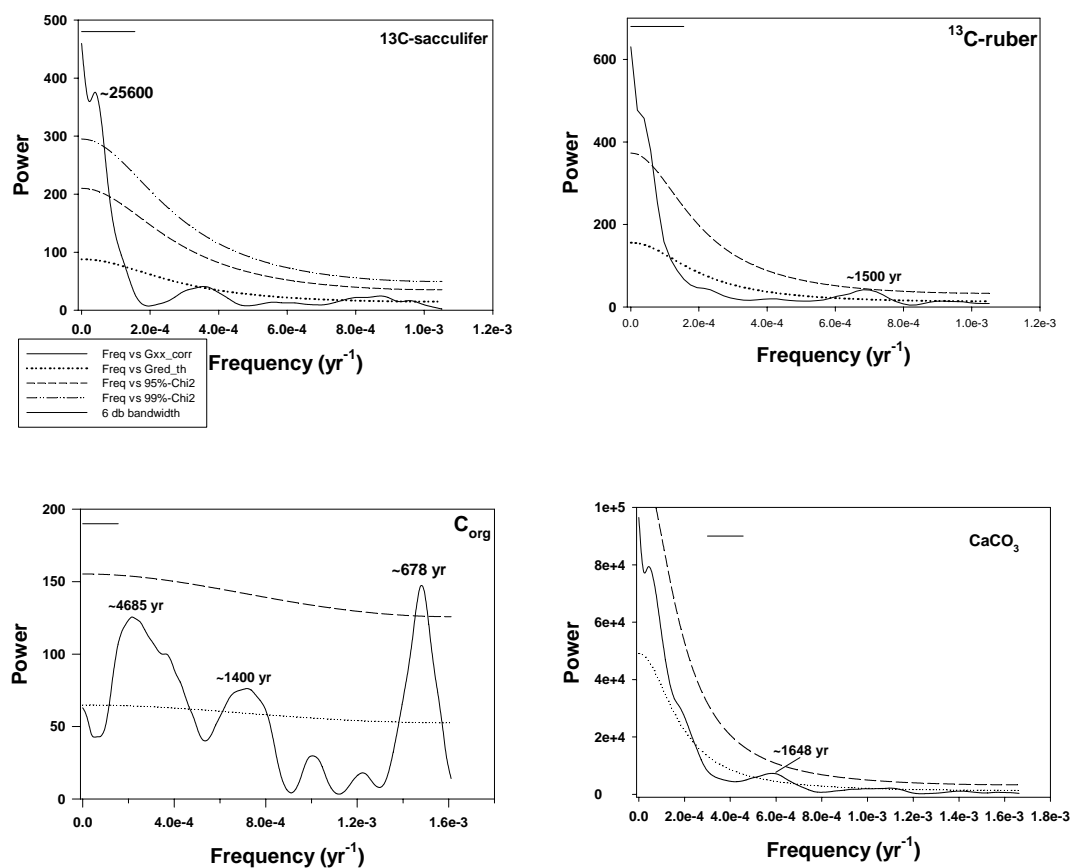
other workers (e.g. Clemens et al, 1991, Leuschner and Sirocko, 2003) in sediment cores from the western Arabian Sea and northern Arabian Sea (Reichart et al, 1997).

Other productivity proxies like $\delta^{13}\text{C}$ in *G.ruber*, C_{org} and CaCO_3 exhibit periodicities of ~1500 y, 1392 y and 1648 y respectively, which are although below the 95% confidence limit but are still above the background. These periodicities are very close to the widely reported 1470 ± 500 y periodicity from various archives (e.g. Bond et al, 1997; Sirocko et al, 1996; Schulz et al, 1998; Mayewski et al, 1998, Campbell et al, 1998; Sarkar et al, 2000 Agnihotri et al, 2003b). The 1470 y cyclicity is exhibited by the Dansgaard–Oeschger interstadials (Grootes and Stuiver, 1997) implying the correlation between low latitude monsoon variations and high latitude changes. $\delta^{18}\text{O}$ in *G.ruber* and *G.sacculifer* also exhibit 1370 y periodicity that is below the 95% confidence limit. The probable reason for these proxies to fall below the 95% confidence limit is the poor temporal resolution which on average is ~500 y except in the case of C_{org} and CaCO_3 where it is ~300 y. Moreover, the $\delta^{18}\text{O}$ values are controlled by many processes such as SST, salinity etc. leading to suppression of the amplitude of frequencies. C_{org} further demonstrate a dominant frequency of ~678 y (above 95% confidence limit) that corresponds very well to ~700 y periodicity seen by Sarkar et al (2000) in the $\delta^{18}\text{O}$ of the planktonic foraminifera (*G.sacculifer*) and Agnihotri et al (2003) in productivity related elements in the sediment cores from the eastern Arabian Sea. Furthermore, Wang et al (1999) report a periodicity of ~775 y from a sediment core from the South China Sea that is being influenced by SE Asian monsoon. These common frequencies might point towards the common forcing factor.

Another productivity indicator $\delta^{15}\text{N}$ exhibit a dominant frequency of ~1982 y that is above even the 99% confidence level. Similar periodicities of ~2028 y and ~2200 y are exhibited by $\delta^{18}\text{O}$ in *G.ruber* and *G.sacculifer* respectively, albeit below the 95% confidence limit due to the reasons discussed earlier. Similar periodicity of 2200 y has been observed by Naidu and Malmgren (1995) in upwelling intensity indices from a core from the Oman margin, Western Arabian Sea. Furthermore, a 2300 y cyclicity (Magny, 1993; Sonnet and Finney, 1990) and a 2050 y periodicity (Damon and Peristykh, 2000) are reported for the atmospheric ^{14}C variations. Based on similar periodicity for oceanic proxy and the ^{14}C variations, Naidu and Malmgren

(1995) proposed that oceanic circulation changes are controlling the ^{14}C periodicities at 2300 y time scale as enhanced oceanic circulation will induce greater vertical circulation that will release ^{14}C depleted CO_2 into the atmosphere. They further argue that thermohaline circulation might influence the Asian monsoon through various complex feedback mechanisms as Street - Perrott and Perrott (1990) have reported the influence of deep-sea circulation on precipitation over northern tropical areas. Our multi-proxy study appears to reinforce the above hypothesis.

$\delta^{18}\text{O}$ and $\delta^{13}\text{C}$ (not shown in the Fig.5.7) in *G.menardii* do not show any significant periodicity, probably due to a coarser sampling resolution (~ 800 y).



Contd...

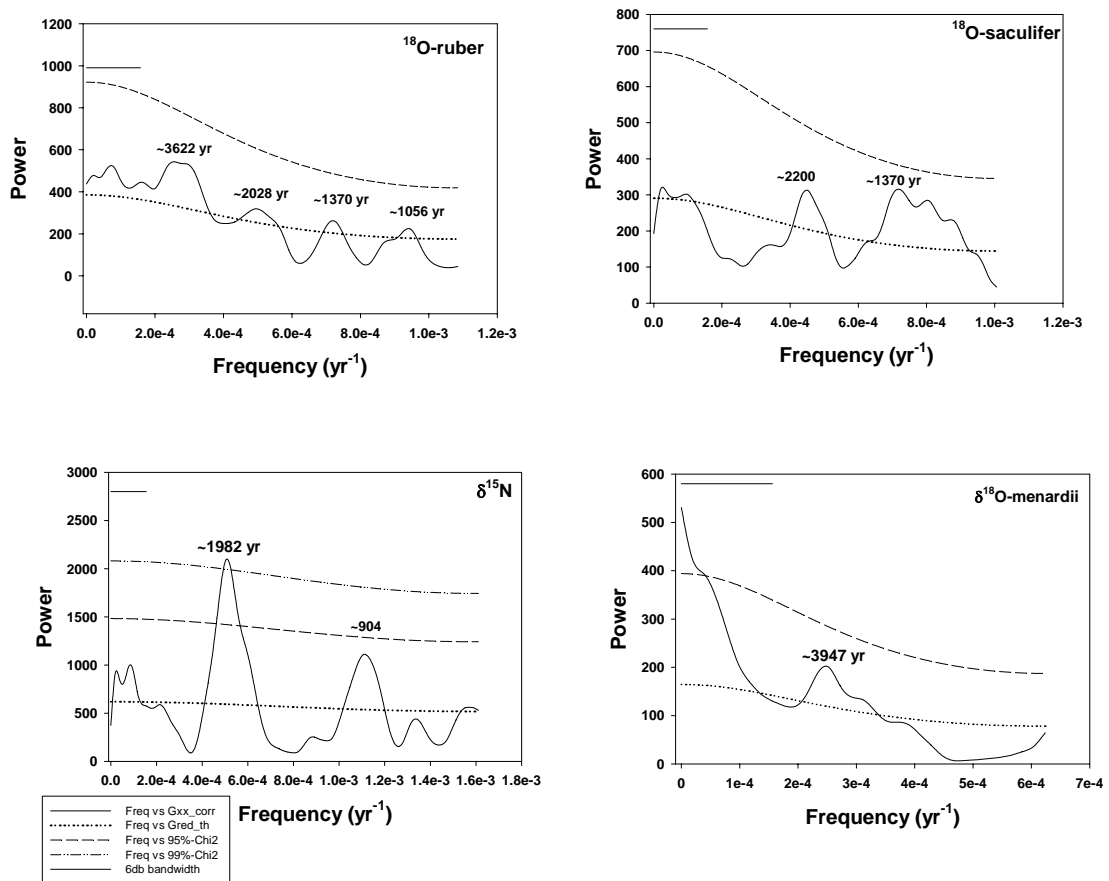


Fig.5.8. Power spectra for various paleoclimatic proxies. Horizontal line at the upper left-hand corner represents 6db bandwidth of the spectral resolution. Gxx_corr denotes amplitude or power of various frequencies; Gred_th shown by dotted line is the background signal; dashed line and dash-dot-dot line denote the 95% and 99% significance levels calculated using the χ^2 test.

5.7. Inferences:

- i. The southwest monsoon was weaker during the early deglacial period as evident from the calcareous productivity and supported by organic productivity (C_{org} and $\delta^{13}C$) and $\delta^{18}O$ analysis carried out on three different species of planktonic foraminifera.
- ii. A sudden intensification of SW monsoon is observed centered at ~14.5 ka BP. It coincides with the first step of deglaciation (T IA) and such a rapid response by the monsoon system can be attributed to albedo changes over central Asia and Tibetan plateau that would enhance the land – sea air pressure difference during summer.
- iii. Monsoon intensity seems to decline during the younger Dryas as evident by excess of evaporation over precipitation. The monsoon again regained its strength during the T IB (centered at 11 ka BP).
- iv. At ~9 ka BP, another episode of monsoon intensification took place just after the maximum tropical summer insolation at 10 ka BP between 20⁰N and 35⁰N.
- v. Thereafter SW monsoon strengthened during the Holocene as observed in the multi-proxy isotopic and chemical data. Monsoon does not appear to have decreased during the Holocene as proposed by some earlier studies in this region.
- vi. Spectral analysis points that on Milankovitch timescale, monsoon is mainly influenced by the precessional cycle of the earth. On shorter timescales the dominant periodicities exhibited by monsoon are

~1400y and 700 y that points towards the correlation with high latitude and thermohaline circulation changes.

Chapter 6

Conclusions

6.1. Major Conclusions:

This study was carried out to document the centennial to millennial scale variations in the monsoon intensity using high-resolution analysis of accurately dated sediment cores from three different locations of the Arabian Sea. Further, it compared the past variations in SW monsoon wind intensity (from the western Arabian Sea) and the SW monsoon precipitation (eastern Arabian Sea) to assess that how different locations/proxies respond to same climatic forcing. It also looked at the past variations in the relative strengths of SW and NE monsoon and compared the proxy record of SW monsoon precipitation with the high latitude climatic fluctuations. Moreover this study made an attempt to look into the intermonsoon period and the related climatic phenomena. The possibility of a solar connection with the SW monsoon has also been explored by the spectral analysis of various SW monsoon proxies. The major conclusions reached are:

6.1.1. Past variations in the SW monsoon intensity:

- I. Starting from ~35 ka BP, the SW monsoon has shown a decreasing trend with minimum precipitation at LGM along with several millennial scale fluctuations to relatively higher values that correspond to the interstadials. During the early deglacial period the SW monsoon was still weak with a major intensification centered around ~14.5 ka BP that matches with Termination IA. This sudden enhancement can be attributed to albedo changes over the central Asia/Tibetan plateau, which can enhance the sea-land temperature (and hence air pressure) contrast during summer that can strengthen the SW monsoon.
- II. The glacial to Holocene transition period is marked with several millennial to centennial scale fluctuations in the SW monsoon precipitation with higher precipitation during periods of global warmth (*viz.* Bolling-Allerod, Termination IA, Termination IB) and reduced precipitation during cooler times (*viz.* Oldest, Older and Younger Dryas).

- III. A sudden increase in SW monsoon intensity took place at ~9 ka BP, following the maximum summer insolation at 10 ka BP between 20°N and 35°N.
- IV. The SW monsoon strengthened during the Holocene as evident from the multi-proxy isotopic and chemical data from both the western as well as equatorial Arabian Sea cores. It does not appear to have decreased during the Holocene as proposed by a few earlier studies.
- V. A high-resolution study has been carried out to document the SW monsoon variations on centennial to subcentennial timescales for the past three millennia in a core from the eastern Arabian Sea. A prominent arid event is observed at 2000 a BP followed by other centennial scale dry events centered at ~1500 a BP, ~1100 a BP, ~850 a BP and ~500 a BP. These arid episodes are also seen in other proxy records such as varved sediments and speleothems from the regions around the Arabian Sea.
- VI. To quantify SW monsoon precipitation variations during the past 3000 years, a parameter *viz.* precipitation – evaporation (P-E) was calculated using an empirical equation. The P-E values ranged from ~100 mm for arid episodes such as during ~ 2000 a BP and ~500 a BP to ~1000 mm for high monsoon events like the ones observed at ~1800 a BP and ~1150 a BP.

6.1.2. NE monsoon intensification:

- I. Based on our high resolution data with better age control and which is from a site nearer to the source of North East Monsoon Current, we infer that the NE monsoon intensified during the early deglacial period (~19 to ~17 ka BP) concurrent with a weaker than present SW monsoon. The NE monsoon does not appear to have strengthened during the LGM as proposed earlier. During the LGM both the SW as well as NE monsoon appear to have declined in tandem. There is no evidence for an episode of NE monsoon strengthening subsequent to the early deglacial period.

6.1.3. Correlation between SW monsoon wind strength and SW monsoon precipitation:

- I. Our measurements on the eastern Arabian Sea core, which records signal of monsoon precipitation over the Western Ghats was compared with the data of Gupta et al (2003) from the western continental margin off the Oman coast. They based their study on the *G.bulloides* abundance variation, which indicates upwelling strength controlled by the SW monsoon winds. Both the wind intensity record (west) and the precipitation signatures (east) match very well on centennial scale, weak winds were accompanied by reduced precipitation. But the relationship appears to be non-linear as precipitation minimum occurred at ~2000 a BP while the wind minimum occurred at ~1500 a BP.

6.1.4. Correlation between SW monsoon precipitation and high latitude climate:

- I. The oxygen isotopic data from the equatorial Arabian Sea core was compared with the $\delta^{18}\text{O}$ record of the GISP2 ice core to verify the correlation between the SW monsoon precipitation changes and the high latitude climate. Oxygen isotope values of all the three species of planktonic foraminifera exhibit a good correlation with the GISP2 $\delta^{18}\text{O}$ record on centennial to millennial timescales. The warm interstadial periods are accompanied by stronger SW monsoon and cooler stadials correspond to reduced SW monsoon.
- II. But the correlation is not that good during the Holocene as the prominent 8200 a BP cooling event observed in the ice record is not observed in the sedimentary record, which might be due to the much poorer resolution of the sedimentary record. Further during the Late Holocene (~5 ka BP to the core top, ~2.2 ka BP) several fluctuations, possibly due to the centennial scale variations in the precipitation were observed in the sedimentary record with no counterparts in the ice record.
- III. In spite of the above mentioned discrepancies, it appears that SW monsoon fluctuations correlate very well with the high latitude climate as even the

rapid events like Dansgaard/Oeschger interstadials, T IA, T IB, Oldest, Older and Younger Dryas have counterparts in the sedimentary record. Similar variations observed in the tropical/equatorial and the North Atlantic climates indicate that tropics were probably instrumental in bringing about high latitude climatic changes, most probably via atmospheric forcing through greenhouse gases or *vice versa* by albedo feedback.

6.1.5. Past variations in the IEW and the relatable SO index, SW monsoon, East African rains and El Nino frequency:

- I. Past productivity variations in the equatorial core, which are governed by the strength of the Indian Ocean Equatorial Westerlies (IEW) has aided in documenting the past variations in the Southwest monsoon and East African rains along with the El Nino frequency. The Southwest monsoon and East African rains have exhibited a declining trend from ~35 ka BP to LGM with the minimum values at LGM as evident from decreasing productivity. It also suggests that El Nino frequency was highest during the last glacial period. Thereafter the IEW strengthened upto 16.5 ka BP after which it fell back sharply to LGM values for a millennium (upto ~15.5 ka BP) indicating reduction in rainfall. Thereafter IEW exhibits a sharp increase at ~14.5 ka BP that coincides with the Termination IA implying strengthened Southwest monsoon and East African rains.

- II. Since ~14.5 ka BP to the core top (~2.2 ka BP) including the Holocene, calcareous productivity exhibits a uniformly increasing trend implying a uniformly strengthening IEW and Southern oscillation index and hence strengthening SW monsoon and east African rains along with a declining El Nino frequency.

6.1.6. Regional Climatic evolution:

- I. To look into the regional climatic evolution the productivity records from the equatorial (this study) and eastern Arabian Sea (Agnihotri et al, 2003 a) were compared. Furthermore the core from the western Arabian Sea (this study) also exhibits similar variations such as sharp increase in SW monsoon wind intensity at ~15 to ~14.5 ka BP and an increasing SW monsoon wind intensity during the Holocene. It appears that the Indian Ocean Equatorial Westerlies and SW monsoon winds strengthened and weakened in unison pointing towards a common forcing factor, most probably insolation, at least during the last 35 ka.

6.1.7. The solar influence:

- I. The $\delta^{18}\text{O}$ record (SW monsoon precipitation signal) from the high-resolution (~50 years) eastern Arabian Sea core was compared with the reconstructed Total Solar Irradiance (TSI) for the past ~1000 years to explore the possibility of a solar influence on SW monsoon on centennial timescales. Broadly, during the periods of lower TSI, the SW monsoon precipitation also reduces whereas during the periods of higher TSI, the precipitation increases. This indicates a possible solar forcing on the SW monsoon on centennial timescale.
- II. Spectral analysis of various SW monsoon proxies indicate that on Milankovitch timescale, it is mainly governed by the insolation variations induced by the precessional cycle of the earth's orbit. On millennial timescales, the dominant periodicity exhibited by the monsoon lies near 1400 ± 500 years that points towards a common forcing factor for the SW monsoon as well as high latitude climatic changes further corroborating the fact that a common link exists between them. Moreover monsoon seems to be influenced by the thermohaline circulation changes as well on millennial timescales. On centennial timescale the solar forcing seems to control the SW monsoon variations as exhibited by the common quasi-periodicity of ~200 yrs in both by monsoon proxies as well as solar activity proxy viz. TSI.

6.1.8. Limitations of C_{org} , $\delta^{15}N$ and $\delta^{13}C$ at the equatorial core site:

- I. In the equatorial region C_{org} and $\delta^{15}N$ are not useful as productivity indicators due to very low amount of sedimentary organic matter present, which makes their measurement imprecise. Moreover in the equatorial region the $\delta^{13}C$ of the foraminifera can not act as a useful productivity proxy as it is distorted by two competing *viz.* upwelling and productivity.

6.2. Recommendation for future studies:

Although this thesis has documented the past variations in monsoon intensity in great detail for the past 35 ka but still additional studies can be helpful to understand various processes that control the vagaries of SW and NE monsoon.

- This study has pointed out that the period of NE monsoon intensification was not the LGM but the early deglacial period. To corroborate this more well-dated cores from the equatorial Arabian Sea should be analyzed with high-resolution.
- We have clearly shown that the SW monsoon strengthened during the Holocene as evident from the multi proxy isotopic and chemical studies in the core from the western and equatorial Arabian Sea in contrast to some of the earlier studies that proposed that SW monsoon declined during Holocene based on single proxy analysis. This indicates the need of multi proxy analyses as in nature various processes are occurring simultaneously and relying on a single proxy might mislead us. To confirm our conclusion more high-resolution cores from different regions of the Arabian Sea employing the multi proxy technique should be analyzed. Also the existence of threshold for the responses of the proxies need to be examined.
- Our study in comparison with another carried out in the western Arabian Sea has shown that the SW monsoon precipitation exhibits good correlation with the SW monsoon wind strength on centennial timescale, but this correlation appears to be non linear. It warrants the study of more well dated cores covering longer

time spans from the eastern and western Arabian Sea that possess comparable resolutions so that the correlation between the wind strength and precipitation can be further elucidated.

- One of the major handicaps in quantifying the past precipitation fluctuations using the foraminiferal $\delta^{18}\text{O}$ is that it is affected by both the salinity and temperature and hence it becomes very important to decouple them. For this purpose alkenone unsaturation index in the sedimentary organic matter and elemental ratios in the foraminiferal calcitic shells should be measured in the same sample. Alkenone unsaturation index ($U^{K'_{37}}$) acts as a Sea Surface Temperature (SST) proxy as certain marine phytoplanktons (e.g. coccolithophorid *Emiliana huxleyi*) respond to water temperature changes by changing the molecular composition of their cell walls (Bradley, 1999). Moreover there are several elements (Sr, Ba, Mn, Cd, Mg) that are chemically similar to Ca, so their trace amount can be incorporated in the calcitic foraminiferal or coralline shells depending on the calcification temperature (Elderfield and Ganssen, 2000; Lea et al, 1999). Thus by measuring their relative concentration (e.g. Sr/Ca, Mg/Ca etc.) we might be able to independently quantify temperature effect.
- Spectral analysis of various SW monsoon proxies along with visual matching with the reconstructed TSI curve has shown that the solar forcing is probably the major governing factor for the SW monsoon precipitation on centennial to millennial timescales. But more studies with annual to decadal scale resolution are needed to understand the full regional variability of SW monsoon and its relation to solar forcing. Such high-resolution records can be obtained from the sedimentary cores from the continental margins that have very high sedimentation rate. Further archives like corals and tree rings can be studied that could provide annual to seasonal resolutions.
- The major debate regarding paleoproductivity proxies such as C_{org} is that whether they are manifestation of overhead productivity or are controlled by

preservation characteristics. To overcome this, various major (Al, Mg, Fe, Ti) and trace (Mn, Cr, V, U) elements can be studied in marine sediments. Al, Mg, Fe, Ti are major components of alumino-silicate minerals and are not affected by redox changes (except Fe that takes part in the redox reactions in the continental margin regions but that is negligible compared to its total abundance) and hence are unaffected by changing preservation characteristics. These elements denote terrestrial inputs relatable to aeolian /alluvial discharge that in turn can be related to the intensity of monsoon precipitation. Similarly downcore variations in the concentrations of trace elements such as Sr, P, Ba, Cu, Ni, Zn that act as micronutrients for marine productivity can be studied to document changes in the paleoproductivity. Downcore variations in Mn, Cr, V, U signify ambient redox conditions as Mn is found to be concentrated in oxic conditions whereas the other three are precipitated in reducing conditions (Bonatti et al, 1971; Piper and Issacs, 1996). Thus the past fluctuations in the redox conditions can throw light on the preservation of productivity proxies such as C_{org} .

REFERENCES

Agnihotri R, Dutta K, Bhushan R, Somayajulu BLK (2002): Evidence for solar forcing on the Indian monsoon during the last millennium. *Earth and Planetary Science Letters*, **198**, 521-527.

Agnihotri R, Sarin MM, Somayajulu BLK, Jull AJT, Burr GS (2003a): Late-Quaternary biogenic productivity and organic carbon deposition in the eastern Arabian Sea. *Palaeogeogr. Palaeoclimat. Palaeoeco.*, **197**, 43-60.

Agnihotri R, Bhattacharya SK, Sarin MM, Somayajulu BLK (2003b): Changes in the surface productivity and subsurface denitrification during the Holocene: a multiproxy study from the eastern Arabian Sea. *The Holocene*, **13**, 5, 701-713.

Aller RC (1994): Bioturbation and remineralization of sedimentary organic matter: effects of redox oscillation. *Chem. Geol.*, **114**, 331-345.

Altabet MA, Francois R (1994): Sedimentary nitrogen isotopic ratios as a recorder for surface ocean nitrate utilization. *Global Biogeochem. Cycles*, **8**, 103-116.

Altabet MA, Francois R, Murray DW, Prell WL (1995): Climate related variations in denitrification in the Arabian Sea from sediment $^{15}\text{N}/^{14}\text{N}$ ratios. *Nature*, **373**, 506-509.

Altabet MA, Murray DW, Prell WL (1999): Climatically linked oscillations in Arabian Sea denitrification over the past 1 m.y.: Implications for the marine N cycle. *Paleoceanography*, **14**, 732-743.

Altabet MA, Higginson MJ, Murray DW (2002): The effect of millennial – scale changes in Arabian Sea denitrification on Atmospheric CO_2 . *Nature*, **415**, 159-162.

Anderson DM, Prell WL (1992): structure of the southwest monsoon winds over the Arabian Sea during the Late Quaternary: observations, simulations, and marine geologic evidence. *J. Geophys. Res.*, **97**, 15481-15487.

Anderson DM, Prell WL (1993): A 300 kyr record of upwelling off Oman during the Late Quaternary: evidence of the Asian Southwest monsoon. *Paleoceanography*, **8**, 193-208.

Anderson DM, Overpeck JT, Gupta AK (2002): Increase in the Asian SW monsoon during the past four centuries. *Science*, **297**, 596-599.

Antony MK (1990): Northward undercurrent along west coast of India during upwelling – Some inferences. *Indian Jour. of Marine Sci.*, **19**, 95-101.

Banse K, McClain CR (1986): Winter blooms of phytoplankton in the Arabian Sea as observed by the Coastal Zone Colour Scanner. *J. Mar. Ecol. Prog. Series*, **34**, 201-211.

Barber RT, Marra J, Bidigare RC, Codispoti LA, Halpern D, Johnson Z, Latara M, Goericke R, Smith SL (2001): Primary productivity and its regulation in the Arabian Sea during 1995. *Deep Sea Research II*, **48**, 1127-1172.

Bard E, Rostek F, Sonzogni C (1997): Interhemispheric synchrony of the last deglaciation inferred from alkenone palaeothermometry. *Nature*, **385**, 707-710.

Bard E (1998): Geochemical and geophysical implications of the radiocarbon calibration. *Geochimica Cosmochimica Acta*, **62**, 2025-2038.

Bard E, Raisbeck G, Yiou F, Jouzel J (2000): Solar irradiance during the last 1200 years based on cosmogenic nuclides. *Tellus*, **52B**, 985-992.

Basu S, Meyers SD, O'Brien JJ (2000): Annual and interannual sea level variations in the Indian Ocean from TOPEX/Poseidon observations and ocean model simulations. *J. Geophys. Res.*, **105**, 975-994.

Be AWH (1977): An Ecological, Zoogeographic and Taxonomic Review of Recent Planktonic Foraminifera. In: *Oceanic Micropaleontology* (ed. ATS Ramsey), Academic Press, London, pp.1-100.

Be AWH (1980): Gametogenic calcification in a spinose planktonic foraminifer, *Globigerinoides sacculifer* (Brady). *Marine Micropaleontology*, **5**, 283-310.

Beaufort L, Lancelot Y, Camberlin P, Cayre O, Vincent E, Bassinot F, Labeyrie L (1997): Insolation cycles as a major control of equatorial Indian Ocean Primary production. *Science*, **278**, 1451-1454.

Beltrando G, Camberlin P (1993): Interannual variability of rainfall in the eastern Horn of Africa and indicators of atmospheric circulation. *International Journal of Climatology*, **13**, 533-546.

Berger WH, Killingley JS, Vincent E (1978): Stable isotopes in deep carbonates: box core ERDC-92, West equatorial Pacific. *Oceanologica Acta*, **1**, 203-216.

Betts JN, Holland HD (1991): The oxygen content of ocean bottom waters, the burial efficiency of organic carbon, and the regulation of atmospheric oxygen. *Palaeogeogr. Palaeoclimat. Palaeoeco.*, **97**, 5-18.

Bhatt US (1989): Circulation regimes of rainfall anomalies in the African-South Asian monsoon belt. *J. Clim.*, **2**, 489-497.

Bhattathiri PMA, Pant A, Sawant S, Gauns M, Matondakar SGP, Mohanraju R (1996): Phytoplankton production and chlorophyll distribution in the eastern and

central Arabian Sea in 1994-1995. *Curr. Sci.* (JGOFS-India Special Section), **71** (11), 857-862.

Bhushan R, Dutta K, Somayajulu BLK (2001): Concentrations and burial fluxes of organic and inorganic carbon on the eastern margins of the Arabian Sea. *Marine Geology*, **178**, 95-113.

Bjerkness J (1969): Atmospheric teleconnections from the equatorial Pacific. *Mon. Weather Rev.*, **97**, 163-172.

Bonatti E, Fisher DE, Joensuu O, Rydell HS (1971): Postdepositional mobility of some transition elements, phosphorous, uranium and thorium in deep sea sediments. *Geochim. Cosmochim. Acta*, **35**, 189-201.

Bond G, Showers W, Cheseby M, Lotti R, Alamas P, deMenocal P, Priore P, Cullen H, Hajdas I, Bonani G (1997): A pervasive millennial-scale cycle in North Atlantic Holocene and glacial climates. *Science*, **278**, 1257-1266.

Bond G, Kromer B, Beer J, Muscheler R, Evans MN, Showers W, Hoffmann S, Lotti-Bond R, Hajdas I, Bonani G (2001): Persistent Solar Influence on North Atlantic Climate During the Holocene. *Science*, **294**, 2130-2136.

Bouvier-Soumagnac Y, Duplessy JC (1985): Carbon and isotopic composition of planktonic foraminifera from the laboratory culture, plankton tows and recent sediment: implications for the reconstruction of paleoclimatic conditions and of the global carbon cycle. *Journal of Foraminiferal Research*, **15** (4), 302-320.

Bradley RS (1999): *In* Paleoclimatology: Reconstructing the climates of the Quaternary, 2nd ed., Harcourt Academic Press, pp. 233-234.

Brock JC, McClain CR, Luther ME, Hay WW (1991): The phytoplankton bloom in the northwestern Arabian Sea during the southwest monsoon of 1979. *Journal of Geophysical Research*, **96**, 20613-20622.

Brock JC, McClain CR (1992): Interannual variability in phytoplankton blooms observed in the northwestern Arabian Sea during the southwest monsoon. *Journal of Geophysical Research*, **97**, 733-750.

Broecker WS, Peng TH (1982): Tracers in the Sea. Eldigio, New York, pp.690.

Brook EJ, Sowers T, Orchardo J (1994): Rapid variations in atmospheric methane concentration during the past 110,000 years. *Science*, **273**, 1087-1091.

Bruce JG, Johnson DR, Kindle JC (1994): A note on the continuance of the Somali eddy after the cessation of the Southwest monsoon. *J. Geophys. Res.*, **99**, 7651-7664.

Burns SJ, Matter A, Frank N, Mangini A (1998): Speleothem-based paleoclimate record from northern Oman. *Geology*, **26**, 499-502.

Cadet D, Reverdin G (1981): Water vapour transport over the Indian Ocean during summer 1975. *Tellus*, **33**, 476-487.

Calvert SE, Pederson TF (1992): Organic carbon accumulation and preservation in marine sediments: How important is anoxia? In *Organic Matter*, Eds. J. Whelan and J.W. Farrington, Univ. Press, New York, NY, pp. 231-263.

Campbell ID, Campbell C, Apps MJ, Rutter NW, Bush ABG (1998): Late Holocene ~1500 yr climate periodicities and their implications. *Geology*, **26**, 471-473.

Capone GD, Zehr JP, Paerl HW, Birgman B, Carpenter EJ (1997): *Trichodesmium*, a globally significant marine cyanobacterium. *Science*, **276**, 1221- 1229.

Carpenter EJ (1983): In “Nitrogen in the Marine Environment”. Eds. E.J. Carpenter and D.G. Capone, Academic Press, New York, 65-103.

Charney JG (1969): The intertropical convergence zone and the Hadley circulation of the atmosphere. Proc. WMO/IUCG Symp. Numer. Weather Predict. Jpn. Meteorol. Agency III: 73-79.

Chester R (2003): Marine Geochemistry, Blackwell publishing, 2nd ed., pp 219-241.

Christensen JP, Murray JW, Devol AH, Codispoti LA (1987): Denitrification in continental shelf sediments has major impact on the oceanic nitrogen budget. *Global Biogeochem. Cycles*, **1**, 97-116.

Clemens S, Prell WL (1991): One million year record of summer monsoon winds and continental aridity: Eolian records from the lithogenic component of deep-sea sediments, *Paleoceanography*, **5**, 109-145.

Clemens S, Prell WL, Murray D, Shimmield G, Weedom G (1991): Forcing mechanisms of the Indian Ocean monsoon. *Nature*, **353**, 720-725.

Clemens S, Murray DW and Prell WL (1996): Nonstationary Phase of the Plio-Pleistocene Asian Monsoon. *Science*, **274**, 943-948.

Cline JD, Kaplan IR (1975): Isotopic fractionation of dissolved nitrate during denitrification in the eastern tropical North Pacific Ocean. *Marine Chem.*, **3**, 271-299.

Codispoti LA (1991): Primary productivity and carbon and nitrogen cycling in the Arabian Sea. In U.S. JGOFS: Arabian Sea Process study. Eds. S.L. Smith, K. Banse, J.K. Cochran, L.A. Codispoti, H.W. Ducklow, M.E. Luther, D.B. Olson, W.T. Peterson, W.L. Prell, N. Surgi, J.C. Swallow & K. Wishner. U.S. JGOFS Planning Report No.13.

Conkright ME, Levitus S, Boyer TP, Bartolacci DM, Luther ME (1994): Atlas of the Northern Indian Ocean. Natl. Oceanogr. Data Center, NOAA, Washington D.C.

Coplen TB, Kendall C, Hopple J (1983): Comparison of stable isotope reference samples. *Nature*, **302**, 236-238.

Cowie GL, Hedges JI (1991): Organic carbon and nitrogen geochemistry of Black Sea surface sediments from stations spanning the oxic: anoxic boundary. In *Black Sea Oceanography*, Eds. E. Izdar and J.W. Murray, Kluwer, Boston, MA, pp. 343-359.

Cowie GL, Hedges JI (1992): The role of anoxia in organic matter preservation in coastal sediments: relative stabilities of the major biochemicals under oxic and anoxic depositional conditions. *Org. Geochem.* **19**, 229-234.

Craig H (1953): The geochemistry of the stable carbon isotopes. *Geochimica et Cosmochimica Acta*, **3**, 53-92.

Craig H (1957): Isotopic standards for carbon and oxygen and correction factors for mass spectrometric analysis of carbon dioxide. *Geochimica et Cosmochimica Acta*, **12**, 133-149.

Cutler AN, Swallow JC (1984): Surface current of the Indian Ocean (To 25⁰S, 100⁰E). *I.O.S. Technical Rept.* 187.

Craig H (1961): Standard for reporting concentrations of deuterium and oxygen-18 in natural waters, *Science*, **133**, 1833-1834.

Damon PE, Peristykh AN (2000): Radiocarbon calibration and application to geophysics, solar physics, and astrophysics. *Radiocarbon*, **42**, 137-150.

Das PK (2002): The Monsoons. National Book Trust, India, pp.87-96.

Deuser WG, Ross EH, Mlodzinska ZJ (1978): Evidence for and the rate of denitrification in the Arabian Sea. *Deep Sea Research*, **25**, 431-445.

Deuser WG, Ross EH (1980): Seasonal change in the flux of organic carbon to the deep Sargasso Sea. *Nature*, **283**, 364-365.

Deuser WG, Ross EH, Anderson RR (1981): Seasonality in the supply of sediment to the deep Sargasso Sea and implications for the rapid transfer of matter to the deep ocean. *Deep Sea Res., Part A*, **28**, 495-505.

Devassy VP, Bhattathiri PMA, Qasim SJ (1978): *Trichodesmium* phenomenon. *Indian J. Mar. Sci.*, **7**, 168-186.

Dueing W, Schott F (1978): Measurements in the source region of Somali current during the monsoon reversal. *Journal of Physical Oceanography*, **8**, 278-289.

Dueing W, Molinari RL, Swallow JC (1980): Somali current: Evolution of surface flow. *Science*, 209, 588-590.

Duplessy JC, Be AWH, Blanc PL (1981): Oxygen and carbon isotopic composition of planktonic foraminifera in the Indian Ocean. *Palaeogeogr. Palaeoclimat. Palaeoeco.*, **33**, 9-46.

Duplessy JC (1982): Glacial to interglacial contrasts in the northern Indian Ocean. *Nature*, **295**, 494-498.

Dutta K, Bhushan R, Somayajulu BLK (2001): ΔR correction values for the northern Indian Ocean. *Radiocarbon*, **43**, 483-488.

Elderfield H, Ganssen G (2000): Past temperature and $d_{18}O$ of surface ocean waters inferred from foraminiferal Mg/Ca ratios. *Nature*, **405**, 442-445.

Emerson S, Hedges JI (1988): Processes controlling the organic carbon content of open ocean sediments. *Paleoceanography*, **3**, 621-634.

Emiliani C (1971): Depth habitats of the growth stages of pelagic foraminifera. *Science*, **173**, 1122-1124.

Emrich K, Ehhalt DH, Vogel JC (1970): Carbon isotope fractionation during the precipitation of calcium carbonate. *Earth and Planetary Science Letters*, **8**, 363-371.

Erez J, Luz B (1983): Experimental paleotemperature equation for planktonic foraminifera. *Geochimica et Cosmochimica Acta*, **47**, 1025-1031.

Evans RH, Brown OB (1981): Propagation of thermal fronts in the Somali Current system. *Deep Sea Res.*, **28**, 521-527.

Fairbanks RG, Matthews RK (1978): The marine oxygen isotope record in Pleistocene coral, Barbados, West Indies. *Quaternary Res.*, **10**, 181-196.

Fairbanks RG, Wiebe PH, Be AWH (1980): Vertical distribution and isotopic composition of living planktonic foraminifera in the western North Atlantic. *Science*, **207**, 61-63.

Fairbanks RG, Sverdlow M, Free R, Wiebe PH, Be AWH (1982): Vertical distribution and isotopic fractionation of living planktonic foraminifera from the Panama Basin. *Nature*, **298**, 841-844.

Fairbanks RG (1989): A 17,000-year glacio-eustatic sea level record: influence of glacial melting rates on the Younger Dryas event and deep ocean circulation. *Nature*, **342**, 637-642.

Faure G (1986): Principles of Isotope Geology. John Wiley and Sons publishers, 2nd ed., pp 497.

Findlater J (1981): An experiment in monitoring cross-equatorial airflow at low levels over Kenya and rainfall of western India during the northern Summer, Monsoon Dynamics, Ed. Sir James Lighthill and R.P. Pearce, Cambridge University, 309-318.

Fine RA (1993): Circulation of Antarctic Intermediate Water in the South Indian Ocean. *Deep-Sea Res. I*, **40**, 2021-2042.

Fischer J, Schott F, Stramma L (1996): Currents and transports of the Great Whirl-Socotra Gyre system during the summer monsoon, August 1993. *Journal of Geophysical Research*, **101**(C2), 3573-3587.

Fleitmann D, Burns SJ, Mudelsee M, Neff U, Kramers J, Mangini A, Matter A (2003): Holocene forcing of the Indian Monsoon recorded in a stalagmite from southern Oman. *Science*, **300**, 1737-1739.

Fleitmann D, Burns SJ, Neff U, Mudelsee M, Mangini A, Matter A (2004): Palaeoclimatic interpretation of high-resolution oxygen isotopes profiles derived from annually laminated speleothems from Southern Oman. *Quaternary Science Reviews*, **23**, 935-945.

Foree EG, McCarty PL (1970): Anaerobic decomposition of algae. *Environ. Sci. Technol.*, **4**, 842-849.

Foucal P (2003): Can slow variation in solar luminosity provide missing link between the sun and climate? *EOS*, **84** (22), 205-208.

Gadgil S (2003): The Indian monsoon and its variability. *Annu. Rev. Earth Planet. Sci.*, **31**, 429-467.

Ganeshram RS, Pederson TF, Calvert SE, Murray JW (1995): Large changes in oceanic inventories from glacial to interglacial periods. *Nature*, **376**, 755-758.

Ganeshram RS, Calvert SE, Pederson TF, Cowie GA (1999): Factors controlling the burial of organic carbon in laminated and bioturbated sediments off NW Mexico: Implications for hydrocarbon preservation. *Geochim. Cosmochim. Acta*, **63**, 1723-1734.

Ganeshram RS, Pederson TF, Calvert SE, McNeill GW, Fontugne MR (2000): Glacial – interglacial variability in the world’s oceans: Causes and consequences. *Paleoceanography*, **15**, 361-376.

Gasse MA, Fontes JC, Fort , Gibert E, Huc A, Bingyan L, Yuanfang L, Qing L, Mlires F, Van Campo E, Fubao W, Qingsong Z (1991): A 13000-year climate record from western Tibet. *Nature*, **353**, 742-745.

Ghosh P (2000): Isotopic and Elemental Studies of Gondwana Carbonates and their Implications. Unpub. PhD thesis, Devi Ahilya Vishwa Vidhyalaya, Indore, pp. 47.

Gonfiantini R (1981): The δ -notation and the mass spectrometric measurement techniques. In “Stable isotope Hydrology: Deuterium and Oxygen-18 in the water Cycle. Technical Reports Series no. 210.” (Gat JR & Gonfiantini R, Eds.), IAEA, Vienna, 35-84.

Gosain AK, **Rao** S (2003): Climate Change and India, vulnerability assessment and adaptation (ed. PR Shukla et al), University Press, Hyderabad, India, 159-192.

Grootes PM, Stuiver M, White JWC, Johnsen S, Jouzel J (1993): Comparison of oxygen isotope records from the GISP2 and GRIP Greenland ice cores. *Nature*, **366**, 552-554.

Grootes PM, Stuiver M (1997): Oxygen18/16 variability in Greenland snow and ice with 10^{-3} to 10^5 year time resolution. *J. Geophys. Res.*, **C102**, 26455-26470.

Grossman EL (1984): Carbon isotopic fractionation in live benthic foraminifera: comparison with inorganic precipitate studies. *Geochimica Cosmochimica Acta*, **48**, 1505-1512.

Grossman EL (1987): Stable isotopes in modern benthic foraminifera: a study of vital effect. *Journal of Foraminiferal Research*, **17** (1), 48-61.

Guilderson TP, Fairbanks RG, Rubenstone JL (1994): Tropical temperature variations since 20,000 years ago: Modulating interhemispheric climate change. *Science*, **263**, 663-665.

Gupta AK, Anderson DM, Overpeck JT (2003): Abrupt changes in the Asian southwest monsoon during the Holocene and their links to the North Atlantic Ocean. *Nature*, **421**, 354-357.

Guptha MVS, Curry WB, Ittekkot V, Murlinath AS (1997): Seasonal variation in the flux of Planktic foraminifera: Sediment trap results from the Bay of Bengal, Northern Indian Ocean. *Jour. of Foraminiferal Res.*, **27**, 5-19.

Haake B, Rixen T, Ittekkot V (1993a): Variability of monsoonal upwelling signals in the deep western Arabian Sea. In *Monsoon Biogeochemistry*, Eds. V. Ittekkot and R.R. Nair, Mitt. Geol. Palaontol. Inst. Univ. Hamburg, **76**, 85-96.

Haake B, Ittekkot V, Rixen T, Ramaswamy V, Nair RR, Curry WB (1993b): Seasonality and Interannual variability of particle fluxes to the deep Arabian Sea. *Deep Sea Res.*, **40**, 1323-1344.

Hansen LS, Blackburn TH (1991): Aerobic and anaerobic mineralization of organic material in marine sediment microcosms. *Mar. Ecol. Prog. Ser.*, **75**, 283-291.

Hastenrath S, Lamb PJ (1979): Climatic Atlas of the Indian Ocean. Part II: the oceanic heat budget. The Univ. Wisconsin Press, pp.93.

Hastenrath SL, de Castro L, Aceituno P (1987): The southern oscillation in tropical Atlantic sector. *Contrib. Atmos. Phys.*, **60**, 447-463.

Hastenrath S, Nicklis A, Greischar G (1993): Atmospheric-hydrospheric mechanisms of climate anomalies in the western equatorial Indian Ocean. *J. Geophys. Res.*, **98** (C 11), 20, 219-20, 235.

Hawser SP, O'Neil JM, Roman MR, Codd GA (1992): Toxicity of blooms of the cyanobacterium *Trichodesmium* to zooplankton. *J. Appl. Phycol.*, **4**, 79-86.

Hedges JI, Kiel RG (1995): Sedimentary organic matter preservation: an assessment and speculative synthesis. *Marine Chemistry*. **49**, 81-115.

Heinrichs SM, Reeburgh WS (1987): Anaerobic mineralization of marine sediment organic matter: Rates and the role of anaerobic processes in the oceanic carbon economy. *Geomicrobiol. J.*, **5**, 191-237.

Heinrichs SM (1992): Early diagenesis of organic matter in marine sediments: progress and perplexity. *Marine Chemistry*, **39**, 119-149.

Hemleben C, Spindler M and Anderson OR (1988): Modern Planktonic Foraminifera. Springer-Verlag publishers, pp 88-111.

Hoefs J (1997): Stable Isotope Geochemistry. Springer-Verlag pub., 4th ed., pp. 27-63.

Houghton et al (2001): Climate Change 2001: The scientific basis, Cambridge University Press, U.K., pp. 881.

Jagadheesha D, Nanjundaiah R, Ramesh R (1999): *Palaeoclimates, Data and Modelling*, **3** (4), 279-301.

Jull AJT, Donahue DJ, Linick TW (1989): Carbon-14 activities in recently fallen meteorites and Antarctic meteorites. *Geochimica Cosmochimica Acta*, **53**, 2095-2100.

Kabanova YG (1968): Primary production in the northern part of the Indian Ocean. *Oceanology*, **8**, 214-225.

Kienast M, Steinke S, Statterger K, Calvert SE (2001): Synchronous tropical South China Sea SST change and Greenland warming during deglaciation. *Science*, **291**, 2132-2134.

Kolla V, Be AWH, Biscaye PE (1976): Calcium carbonate distribution in the surface sediments of the Indian Ocean. *J. Geophys. Res.*, **81**, 2605-2616.

Kroopnick P, Weiss RF, Craig H (1972): Total CO₂, ¹³C, dissolved oxygen – ¹⁸O at GEOSECS II in the north Atlantic. *Earth and Planetary Science Letters*, **16**, 103-110.

Kroopnick P (1974): The dissolved O₂ – CO₂ – ¹³C system in the eastern equatorial Pacific, *Deep sea Research*, **21**, 211.

Kroopnick PM (1985): The distribution of ¹³C of ΣCO₂ in the world oceans. *Deep-Sea Research*, **32**, 75-84.

Kumar S, Ramesh R, Bhosle NB, Sardesai S, Sheshshayee MS (2004): Natural isotopic composition of nitrogen in suspended particulate matter in the Bay of Bengal, *Biogeosciences*, **1**, 63-70.

Kutzbach JE (1981): Monsoon climate of the early Holocene: Climate experiment with the Earth's orbital parameters for 9000 years ago. *Science*, **214**, 59-61.

Labeyrie LD, Duplessy JC, Blanc PL (1987): Deep water formation and temperature variations over the last 125,000 years. *Nature*, **327**, 477-482.

Lane GA, Doyle M (1956): Fractionation of oxygen isotopes during respiration. *Science*, **123**, 574-576.

Lea DW, Mashiotta TA, Spero HJ (1999): Controls of magnesium and strontium uptake in planktonic foraminifera determined by live culturing. *Geochim. Cosmochim. Acta*, **63**, 2369-2379.

Lea DW, Pak DK, Peterson LC, Hughen KA (2003): Synchronicity of tropical and high-latitude Atlantic temperatures over the last glacial termination. *Science*, **301**, 1361-1364.

Lean J, Beer J, Bradley R (1995): Reconstruction of solar irradiance since 1610: Implications for climatic change. *Geophys. Res. Lett.*, **22**, 3195-3198.

Lee C (1992): Controls on organic carbon preservation: The use of stratified water bodies to compare intrinsic rates of decomposition in oxic and anoxic systems. *Geochim. Cosmochim. Acta*, **56**, 3323-3335.

Leuschner DC, Sirocko F (2003): Orbital insolation forcing of the Indian Monsoon—a motor for global climate changes? *Palaeogeo. Palaeoclim. Palaeoeco.*, **197**, 83-95.

Levitus S, Boyer TP (1994): In World Ocean Atlas Vol. 4: Temperature NOAA Atlas NESDIS 3. US Dept. of Commerce, Washington D.C.

Libby WF (1955): Radiocarbon Dating. Univ. of Chicago Press, 2nd ed., pp 175.

Linick TW, Jull AJT, Toolin LJ, Donahue DJ (1986): Operation of the NSF – Arizona facility for radioisotope analysis and results from selected collaborative research projects. *Radiocarbon*, **28**, 522 – 533.

Liu K, Kaplan IR (1989): The eastern tropical Pacific as a source of ¹⁵N-enriched nitrate in seawater off southern California. *Limnol. and Oceanography*, **34**, 820-830.

Loutre MF, Berger A, Blanc PL (1992): Astronomical frequencies for climate research at the decadal to century time scale. *Climate Dynamics*, **7**, 181-194.

Luckge A, Dose-Rolinski A, Khan AA, Schulz H, von Rad U (2001): Monsoonal variability in the northeastern Arabian Sea during the past 5000 years: geochemical evidence from laminated sediments. *Palaeogeog. Palaeoclim. Palaeoeco.*, **167**, 273-286.

Mackenzie T (1980): Global Carbon Cycle: Some minor sinks for CO₂. Reports of a workshop "Flux of organic carbon by Rivers to the Oceans". September 21-25, Massachusetts, Woods Hole.

Madhupratap M, Prasanna Kumar S, Bhattathiri PMA, Dileep Kumar M, Raghukumar S, Nair KKC, Ramaiah N (1996): Mechanism of the biological response to winter cooling in the northeastern Arabian Sea. *Nature*, **384**, 549-552.

Magny M (1993): Solar influences on Holocene climatic changes illustrated by correlations between past lake-level fluctuations and the atmospheric ¹⁴C record. *Quat. Res.*, **40**, 1-9.

Maillard C, Soliman G (1986): Hydrography of the Red Sea and exchanges with the Indian Ocean in summer. *Oceanologica Acta*, **9**, 249-269.

Mann ME, Bradley RS, Hughes MK (1998): Global-scale temperature patterns and climate forcing over the past six centuries. *Nature*, **392**, 779-787.

Mantyla AW, Reid JL (1995): On the origins of deep and bottom waters of the Indian Ocean. *J. Geophys. Res.*, **100**, 2417-2439.

Martarira CH (1990): Drought over Zimbabwe in a regional and global context. *Int. J. Climatol.*, **10**, 609-625.

Martinson DG, Pisias NG, Hays JD, Imbrie J, Moore Jr. TC, Shackleton NJ (1987): Age dating and the orbital theory of the ice ages: Development of a high-resolution 0 to 300,000-year chronostratigraphy, *Quat. Res.*, **27**, 1-29.

Mayewski PA, Meeker LD, Whitlow SI, Twickler MS, Morrison MC, Bloomfield P, Bond GC, Alley RB, Gow AJ, Grootes PM, Meese DA, Ram M, Taylor KC, Wumkes W (1994): Changes in atmospheric circulation and ocean ice cover over the North Atlantic during the last 41,000 years. *Science*, **263**, 1747-1751.

Mayewski PA, Meeker LD, Twickler MS, Whitlow S, Yang Q, Prentice M (1998): Major features and forcing of high-latitude Northern Hemisphere atmospheric circulation using 110,000 year long glaciochemical series. *Journal of Geophysical Research*, **102**, 345-366.

McConnaughey T (1989a): ^{13}C and ^{18}O disequilibrium in biological carbonates.1. Patterns. *Geochimica et Cosmochimica Acta*, **53**, 151-162.

McConnaughey T (1989b): ^{13}C and ^{18}O disequilibrium in biological carbonates.2. In vitro simulation of kinetic isotope effects. *Geochim. Cosmochim. Acta*, **53**, 163-171.

McCrea JM (1950): The isotopic chemistry of carbonates and a paleotemperature scale. *J. Chem. Phys.*, **18**, 849-857.

McCreary JP, Kundu PK (1989): A numerical investigation of sea surface temperature variability in the Arabian Sea. *J. Geophys. Res.*, **94**, 1609-16114.

McCreary JP, Kundu PK, Molinari RL (1993): A numerical investigation of dynamics, thermodynamics and mixed layer processes in the Indian Ocean. *Prog. Oceanogr.*, **31**, 181-224.

McIntyre A, Molino B (1996): Forcing of Atlantic equatorial and subpolar millennial cycles by precession. *Science*, **274**, 1867-1870.

Meese DA, Alley RB, Fiacco RJ, Germani MJ, Gow AJ, Grootes PM, Illing M, Mayewski PA, Morrison MC, Ram M, Taylor KC, Yang Q, Zielinski GA (1994 a): Preliminary depth-age scale of the GISP2 ice core. Special CRREL Report 94-1, US.

Meese DA, Gow AJ, Grootes PM, Mayewski PA, Ram M, Stuiver M, Taylor KC, Waddington ED, Zielinski GA (1994 b): The accumulation record from the GISP2 core as an indicator of climate change throughout the Holocene. *Science*, **266**, 1680-1682.

Mehta V, Lau KM (1997): Influence of solar irradiance on the Indian monsoon-ENSO: Relationship at decadal-multidecadal time scales. *Geophysical Research Lett.*, **24**, 159-162.

Meyers PA (1994): Preservation of elemental and isotopic source identification of sedimentary organic matter. *Chemical Geology*, **114**, 289-302.

Morrison JM (1997): Intermonsoonal changes in the T-S properties of the near-surface waters of the northern Arabian Sea. *J. Geophys. Res. Lett.*, **24**, 2553-2556.

Muller PJ (1977): C/N ratios in Pacific deep-sea sediments – effect of inorganic ammonium and nitrogen compounds sorbed on clays. *Geochimica et Cosmochimica Acta*, **41**, 765-776.

Muller PJ, Suess E (1979): Productivity, sedimentation rate and sedimentary organic matter in the oceans-I: organic carbon preservation. *Deep Sea Res.*, **26**, 1347-1362.

Murray DW, Prell WL (1991): Pliocene to Pleistocene variations in calcium carbonate, organic carbon and opal on the Owen Ridge, northern Arabian Sea. Proc. ODP, *Sci. Res.*, **117**, 343-355.

Naidu PD, Malmgren BA, Bornmalm L (1993): Quaternary history of the calcium carbonate fluctuations in the western equatorial Indian Ocean (Somali basin). *Palaeogeogr. Palaeoclimat. Palaeoeco.*, **103**, 21-30.

Naidu PD, Malmgren BA (1995): A 2,200 years periodicity in the Asian monsoon system. *Geophys. Res. Lett.*, **22**, 2361-2364.

Naidu PD, Malmgren BA (1996): A high-resolution record of late Quaternary upwelling along the Oman margin, Arabian Sea based on planktonic foraminifera. *Paleoceanography*, **11**, 129-140.

Naidu PD, Malmgren BA (1999): Quaternary carbonate record from the equatorial Indian Ocean and its relationship with productivity changes. *Marine Geology*, **161**, 49-62.

Nair RR, Ittekkot V, Ramaswamy SJ, Haake B, Degens ET, Desai BN, Honjo S (1989): Increased particle flux to the deep ocean related to monsoons. *Nature*, **338**, 749-751.

Naqvi SWA (1987): Some aspects of the oxygen deficient conditions and denitrification in the Arabian Sea. *Journal of Marine Research*, **29**, 459-469.

Naqvi SWA, Noronha RJ (1991): Nitrous oxide in the Arabian Sea. *Deep Sea Research*, **38**, 871-890.

Naqvi SWA (1994): Denitrification process in the Arabian Sea. *Proc. Indian Acad. Science*, **103**, 181-202.

Neff U, Burns SJ, Mudelsee M, Mangini A, Matter A (2001): Strong coherence between solar variability and the monsoon in Oman between 9 and 6 kyrs ago. *Nature*, **411**, 290-293.

Niitsuma N, Oba T, Okada M (1991): Oxygen and carbon isotope stratigraphy at Site 723, Oman margin. Proc. of the ODP, Scientific Results, Vol. **117**, 321-341.

O'Brien JJ, Hulbert HE (1974): Equatorial jet in the Indian Ocean: Theory. *Science*, **184**, 1075-1077.

Ogallo LJ, Janowiak JE, Halpert MS (1998): Teleconnection between seasonal rainfall over east Africa and global surface temperature anomalies. *Meteorol. Soc. Jpn.*, **66** (6), 807-821.

Olson DB, Hitchcock GL, Fine RA, Warren BA (1993): Maintenance of the low oxygen layer in the central Arabian Sea. *Deep Sea Res. II*, **40**, 673-685.

Ortiz JD, Mix AC, Rugh W, Watkins JM, Collier RW (1996): Deep dwelling planktonic foraminifera of the northeastern Pacific Ocean reveal environmental control of oxygen and carbon disequilibria. *Geochimica et Cosmochimica Acta*, **60** (22), 4509-4523.

Overpeck J, Rind D, Lacy A, Healy R (1996): Possible role of dust-induced regional warming in abrupt climate change during the last glacial period. *Nature* **384**, 447-449.

Pailler D, Bard E, Rostek F, Zheng Y, Mortlock R, Van Geen A (2002): Burial of redox-sensitive metals and organic matter in the equatorial Indian Ocean linked to precession. *Geochimica et Cosmochimica Acta*, **66** (5), 849-865.

Pant GB, Parthasarathy B (1981): Some aspects of an association between the southern oscillation and Indian summer monsoon. *Arch. Meteorol. Geophys. Biokl., Sr. B.*, **29**, 245-251.

Pearson PN, Ditchfield PW, Singano J, Harcourt-Brown KG, Nicholas JC, Olsson RK, Shackleton NJ, Hall MA (2001): Warm tropical sea surface temperatures in the Late Cretaceous and Eocene epochs. *Nature*, **413**, 481-487.

Pederson TF, Shimmield GB, Price NB (1992): Lack of enhanced preservation of organic matter in sediments under the oxygen minimum on the Oman Margin. *Geochimica et Cosmochimica Acta*, **56**, 545-551.

Perigaud C, Delecluse P (1992): Annual sea level variations in the southern tropical Indian Ocean from geosat and shallow water simulations. *J. Geophys. Res.*, **97**, 20169-20178.

Peterson LC and Prell WL (1985): Carbonate dissolution in the Recent sediments of eastern equatorial Indian Ocean: Preservation patterns and carbonate loss above the lysocline. *Mar. Geol.*, **64**, 259-290.

Piper DZ, Issacs CM (1996): Instability of bottom-water redox conditions during accumulation of Quaternary sediment in the Japan Sea. *Paleoceanography*, **11**, 171-190.

Prasanna Kumar S, Prasad TG (1999): Formation and spreading of Arabian Sea High Salinity Water mass, *Journal of Geophysical Research*, **104**, 1455-1464.

Prell WL, Hutson WH, Williams DF, Bé AWH, Geitzenauer K, Molfino B (1980): Surface circulation of the Indian Ocean during the last Glacial Maximum, approximately 18,000 yr. B.P. *Quaternary Research*, **14**, 309-336.

Prell WL (1984): Variations of monsoon upwelling: A response to changing solar radiation. Geophysical Monograph Series, AGU, **29**, 48-57.

Prell WL, Van Campo E (1986): Coherent response of Arabian Sea upwelling and pollen transport to late Quaternary monsoonal winds. *Nature*, **323**, 526-528.

Prell WL, Kutzbach JE (1987): Monsoon variability over the past 150,000 years. *Journal of Geophysical Research*, **92**, 8411 – 8425.

Premuzic ET, Benkovitz CM, Gaffney JS, Walsh JJ (1982): The nature and distribution of organic matter in the surface sediments of the world oceans and seas: *Organic Chemistry*, **4**, 63-77.

Qasim SZ, (1982): Oceanography of the northern Arabian Sea. *Deep Sea Research*, **29**, 1041-1068.

Ramage CS (1971): Monsoon Meteorology. Int. Geophys. Ser., San Diego, CA: Academic, **15**, pp.296.

Ramesh Kumar MR, Prasad TG (1995), National Institute of Oceanography Goa Report, NIO/TR-4/95, 9-46.

Ramesh R (2001): High resolution Holocene monsoon records from different proxies: An assessment of their consistency. *Current Science*, **81**, 1432-1436.

Rao YP (1976): Southwest Monsoon. Meteorol. Monogr. No.1. India Meteorological Dept., New Delhi, pp.366.

Rao RR, Sivakumar R (2000): Seasonal variability of near-surface thermal structure and heat budget of the mixed layer of the tropical Indian Ocean from a new global ocean temperature climatology. *Journal of Geophysical Research*, **105**, 985-1015.

Rasmusson EM, Carpenter TH (1983): The relationship between eastern equatorial Pacific sea surface temperature and rainfall over India and Sri Lanka, *Mon. Weather Review*, **111**, 517-528.

Redfield AC (1934): On the proportion of organic derivatives in seawater and their relation to the composition of plankton. In *James Johnstone Memorial Volume*, 177-192, Liverpool: Liverpool University Press.

Redfield AC (1958): The biological controls of chemical factors in the environment. *American Journal of Science*, **46**, 205-221.

Reichert GJ, Dulk MD, Visser HJ, van der Weijden CH, Zachariasse WJ (1997): A 225 kyr record of dust supply, paleoproductivity and the oxygen minimum zone from the Murray Ridge (northern Arabian Sea). *Palaeogeogr. Palaeoclimat. Palaeoeco.*, **134**, 149-169.

Reichert GJ, Lourens LJ, Zachariasse WJ (1998): Temporal variability in the Northern Arabian Sea Oxygen Minimum Zone (OMZ) during the last 225,000 years. *Palaeoceanography*, **13**, 607-621.

Reichert GJ, Schenau SJ, de Lange GJ, Zachariasse WJ (2002 a): Synchronicity of oxygen minimum zone intensity on the Oman and Pakistan margins at sub-Milankovitch time scales. *Marine Geology*, **185**, 403-415.

Reichert GJ, Nortier J, Versteegh G, Zachariasse WJ (2002 b): Periodical breakdown of the Arabian Sea oxygen minimum zone caused by deep convective mixing. *In* The Tectonic and Climatic Evolution of the Arabian Sea Region. Geological Society, London, Special Publications, **195**, 407-419.

Reichert GJ, Brinkhuis H, Huiskamp F, Zachariasse WJ (2004): Hyperstratification following glacial overturning events in the northern Arabian Sea. *Paleoceanography*, **19**, PA2013.

Reverdin G, Cadet DL, Gutzler D (1986): Interannual displacement of convection and surface circulation over the equatorial Indian Ocean. *Q. J. R. Meteorol. Soc.*, **112**, 43-67.

Rhein M, Stramma L, Plähn O (1997): Tracer signals of the intermediate layer of the Arabian Sea. *Geophys. Res. Lett.*, **24** (21), 2561-2564.

Rixen T, Haake B, Ittekkot V, Gupta MVS, Nair RR, Schlusser P (1996): Coupling between SW monsoon-related surface and deep ocean processes as discerned from continuous particle flux measurements and correlated satellite data. *Journal of Geophysical Research*, **101** (C12), 28569-28582.

Rixen T, Ittekkot B, Gaye BH, Schafer P (2000): The influence of the SW monsoon on the deep-sea organic carbon cycle in the Holocene. *Deep-Sea Research II*, **47**, 2629-2651.

Ropelewski CF, Halpert MS (1987): Global and regional scale precipitation patterns associated with the El Niño/Southern Oscillation. *Mon. Weather Rev.*, **115**, 1606-1626.

Rosenbaum J, Sheppard SMF (1986): An isotopic study of siderites, dolomites and ankerites at high temperature. *Geochim. Cosmochim. Acta*, **50**, 1147-1150.

Rosenthal Y, Oppo DW, Linsley BK (2003): The amplitude and phasing of climate change during the last deglaciation in the Sulu Sea, western equatorial Pacific. *Geophys. Res. Lett.*, **30** (8), 1428.

Rostek F, Ruhland G, Bassinot FC, Muller PJ, Labeyrie LD, Lancelot Y, Bard E (1993): Reconstructing sea surface temperature and salinity using $\delta^{18}\text{O}$ and alkenone records. *Nature*, **364**, 319-321.

Rostek F, Bard E, Beaufort L, Sonzogni C, Ganssen G (1997): Sea surface temperature and productivity records for the past 240 kyr in the Arabian Sea. *Deep-Sea Research II*, **44**, 1461-1480.

Rupa Kumar K et al (2002): Climate Change and India, issues, concerns and opportunities. Ed. P.R. Shukla et al, 24-75.

Saino T, Hattori A (1987): Geographical variation of the water column distribution of suspended particulate organic nitrogen and its ^{15}N natural abundance in the Pacific and its marginal seas. *Deep Sea Res.*, **34**, 807-827.

Saranghi RK, Chauhan P, Nayak SR (2004): Detection and monitoring of *Trichodesmium* blooms in the coastal waters off Saurashtra coast, India using IRS-P4 OCM data. *Current Science*, **86**, 1636-1641.

Sarkar A, Ramesh R, Bhattacharya SK, Rajagopalan G (1990): Oxygen isotope evidence for a stronger winter monsoon current during the last glaciation. *Nature*, **343**, 549-551.

Sarkar A, Bhattacharya SK, Sarin MM (1993): Geochemical evidence for anoxic deep water in the Arabian Sea during the last glaciation. *Geochim. Cosmochim. Acta*, **57**, 1009-1016.

Sarkar A, Ramesh R, Somayajulu BLK, Agnihotri R, Jull AJT, Burr GS (2000): High resolution Holocene monsoon record from the eastern Arabian Sea. *Earth and Planetary Science Letters*, **177**, 209-218.

Schott F (1983): Monsoon response of the Somali current and the associated upwelling. *Prog. Oceanogr.*, **12**, 357-383.

Schott F, Fieux M (1985): The Somali current in autumn 1984, before the onset of the NE monsoon, *Nature*, **315**, 50-52.

Schott F, Swallow JC, Fieux M (1990): The Somali current at the equator: annual cycle of currents and transports in the 1000m and connection to the neighboring latitudes. *Deep Sea Research*, **37**, 1825-1848.

Schott F and Fischer J (2000): Winter monsoon circulation of the northern Arabian Sea and Somali Current. *Journal of Geophysical Research*, **105**, 6359-6376.

Schott FA, McCreary Jr. JP (2001): The monsoon circulation of the Indian Ocean. *Progress in Oceanography*, **51**, 1-123.

Schrag DP (1999): Effects of diagenesis on the isotopic record of late paleogene tropical sea surface temperatures. *Chemical Geology*, **161**, 215-224.

Schulte S, Rostek F, Bard E, Rullkotter J, Marchal O (1999): Variations of oxygen-minimum and primary productivity recorded in sediments of the Arabian Sea. *Earth and Planetary Science Letters*, **173**, 205-221.

Schulz H, von Rad U, Erlenkeuser H (1998): Correlation between Arabian Sea and Greenland Climate oscillations of the past 110,000 years. *Nature*, **393**, 54-57.

Schulz M, Mudelsee M (2002): Estimating red-noise spectra directly from unevenly spaced paleoclimatic time series. *Computers and Geosciences*, **28**, 421-426.

Shankar D, Shetye SR (1997): On the dynamics of the Lakshdweep high and low in the southeastern Arabian Sea. *J. Geophys. Res.*, **102**, C6, 12551-12562.

Shapiro GI, Meschanov SL (1991): Distribution and spreading of Red Sea Water and salt lens formation in the northwest Indian Ocean. *Deep-Sea Res.*, **38**, 21-34.

Shackleton NJ (1967): Oxygen isotope analyses and Pleistocene temperatures reassessed. *Nature*, **215**, 15-17.

Shetye SR (1984): Seasonal variability of the temperature field off the southwest coast of India. *Proc. Indian Acad. Sci. (Earth Planet. Sci.)*, **93** (4), 399-411.

Shetye SR, Shenoy SSC (1988): The seasonal cycle of surface circulation in the coastal North Indian Ocean. *Proc. of the Indian Academy of Science (Earth and Planetary Sci.)*, **97**, 53-62.

Shetye SR, Gouveia AD, Shenoy SSC, Sundar D, Michael GS, Almeida AM and Santanam K (1990): Hydrography and circulation of the west coast of India during the Southwest monsoon 1987. *Jour. of Marine Research*, **48**, 359-378.

Shetye SR, Gouveia AD, Shenoy SSC, Michael GS, Sundar D, Almeida AM and Santanam K (1991): The coastal current off western India during the Northeast monsoon. *Deep-Sea Research*, **38**, 1517-1529.

Shi W, Morrison JM, Bohm E, Manghnani V (2000): The Oman upwelling zone during 1993, 1994 and 1995. *Deep Sea Res. II*, **47**, 1227-1247.

Singh G, Agrawal DP (1976): Radiocarbon evidence for deglaciation in north-western Himalaya, India. *Nature*, **260**, 232.

Sirocko F, Sarnthein M, Erlenkreuser H, Lange H, Arnold M, Duplessy JC (1993): Century scale events in monsoon climate over the past 24,000 years. *Nature*, **364**, 322-324.

Sirocko F, Sconberg DG, McIntyre A, Molino B (1996): Teleconnections between the subtropical monsoons and high-latitude climates during the last deglaciation. *Science*, **272**, 526-529.

Sirocko F, Schonberg DG, Devey C (2000): Processes controlling trace element geochemistry of Arabian Sea sediments during the last 25,000 years. *Global and Planetary Change*, **26**, 217-303.

Smith SL (1982): The northwestern Indian Ocean during the monsoons of 1979: Distribution, abundance, and feeding of zooplankton. *Deep Sea Res., Part A*, **29**, 1331-1353.

Smith RL, Bottero JS (1977): On upwelling in the Arabian Sea. In *A voyage of discovery*. Ed. M. Angel, Pergamon Press: New York, pp. 291-304.

Somayajulu BLK, Bhushan R, Sarkar A, Burr GS, Jull AJT (1999): Sediment deposition rates in the continental margins of the eastern Arabian Sea using ^{210}Pb , ^{137}Cs , ^{14}C , *The Science of Total Environment*, **237/238**, 429 – 439.

Sonnet CP, Finney SA (1990): The spectrum of Radiocarbon. *Phil. Trans., R. Soc. London*, **330**, 413-426.

Southon J, Kashgarian M, Fontugne M, Metivier B, Yim W-S Wyss (2002): Marine reservoir corrections for the Indian Ocean and Southeast Asia. *Radiocarbon*, **44**, 167-180.

Spencer D, Broecker WS, Craig H, Weiss RF (1982): GEOSECS Indian Ocean Expedition, 6, Sections and Profiles, U.S. Government Printing Office, Washington D.C., pp. 140.

Spero HJ, Lea DW (1993): Intraspecific stable isotope variability in the planktic foraminifera *Globigerinoides sacculifer*: results from laboratory experiments. *Marine Micropaleontology*, **22**, 221-234.

Spero HJ, Bijma J, Lea DW, Bemis BE (1997): Effect of seawater carbonate concentration on foraminiferal carbon and oxygen isotopes. *Nature*, **390**, 497-500.

Staubwasser M, Sirocko F, Grootes PM, Segl M (2003): Climate change at the 4.2 ka BP termination of the Indus valley civilization and Holocene south Asian monsoon variability. *Geophys. Res. Lett.*, **30** (8), 1425-1428.

Street-Perrott FA, Perrott RA (1990): Abrupt climatic fluctuations in the tropics: the influence of Atlantic Ocean circulation, *Nature*, **343**, 607-612.

Stuiver M, Grootes PM, Braziunas T (1995): The GISP2 $\delta^{18}\text{O}$ climate record of the past 16,500 years and the role of sun, ocean, and volcanoes. *Quaternary Research*, **44**, 341-354.

Stuiver M, Reimer PJ, Bard E, Beck JW, Burr GS, Hughen KA, Kromer B, McCormac G, van der Plicht J and Spurk M (1998): INTCAL98 Radiocarbon age calibration, 24,000-0 cal BP. *Radiocarbon*, **40** (3), 1041-1083.

Swallow JC (1984): Some aspects of the physical oceanography of the Indian Ocean. *Deep Sea Research*, **31**, 639-650.

Swallow JC, Fieux M, Schott F (1988): The boundary currents east and north of Madagascar, Part I: Geostrophic currents and transports. *Journal of Geophysical Research*, **93**, 4951-4962.

Swallow JC, Schott F, Fieux M (1991): Structure and transport of the East African Coastal Current. *J. Geophys. Res.*, **96**, 22254-22267.

Swart PK, Burns SJ, Leder JJ (1991): Fractionation of the stable isotopes of oxygen and carbon in carbon dioxide during the reaction of calcite with phosphoric acid as a function of temperature and technique. *Chemical Geology*, **86**, 89-96.

Takahasi T, Broecker WS, Langer S (1985): Redfield ratio based on chemical data from isopycnal surfaces. *Journal of Geophysical Research*, **90**, 6907-6924.

Thamban M, Rao VP, Schneider RR, Grootes PM (2001): Glacial to Holocene fluctuations in hydrography and productivity along the southwestern continental margin of India. *Palaeogeogr. Palaeoclimat. Palaeoeco.*, **165**, 113-127.

Urey HC (1947): The thermodynamic properties of isotopic substances. *J. Chem. Soc.*, **1947**, 562-581.

Van Campo E, Duplessy JC, Rossignol-Strick M (1982): Climatic conditions deduced from a 150-kyr oxygen isotope–pollen record from the Arabian Sea. *Nature*, **296**, 56-59.

Van campo E, Gasse F (1993): Pollen- and diatom-inferred climatic and hydrological changes in Sumxi Co Basin (western Tibet) since 13000 yr BP. *Quaternary Research*, **39**, 300-313.

Van Heerden J, Terblancke E, Schulze GC (1988): The southern oscillation and south African rainfall. *J. Climatol.*, **8**, 577-597.

Vinot-Bertouille AC, Duplessy JC (1973): Individual isotopic fractionation of carbon and oxygen in benthic foraminifera. *Earth and Planetary Science Lett.*, **18**, 247-252.

Vogel (2002): Textbook of Quantitative Chemical Analysis (eds. Mendham J, Denney RC, Barnes JD, Thomas MJK). Pearson Education publ., 6th ed., pp. 381-382.

Von Rad U, Schaaf M, Michels KH, Schulz H, Berger WH, Sirocko F (1999): A 5000-yr record of climate change in varved sediments from the oxygen minimum zone off Pakistan, Northeastern Arabian Sea. *Quaternary Research*, **51**, 39-53.

Wachter EA, Hayes JM (1985): Exchange of oxygen isotopes in carbon dioxide – phosphoric acid systems. *Chemical Geology*, **52**, 365 – 374.

Walker TN (1990): Links between South African summer rainfall and temperature variability of the Agulhas and Benguela current systems. *J. Geophys. Res.*, **95** (C3), 3297-3319.

Wang L, Sarnthein M, Erlenkeuser H, Grimalt J, Grootes P, Heiling S, Ivanova E, Kienast M, Pelejero C, Pflaumann U (1999): East Asian monsoon climate during the Late Pleistocene: high resolution sediment records from the south China Sea, *Mar. Geol.*, **156**, 245-284.

Weber JN, Woodhead PJJ (1970): Carbon and oxygen isotope fractionation in the reef building corals. *Chemical Geology*, **6**, 93 – 117.

Webster PJ (1987): The elementary monsoon. In *Monsoons*, Ed. JS Fein, PL Stephens, New York: Wiley, pp. 3-32.

Wefer G, Berger WH (1991): Isotope paleontology: growth and composition of extant calcareous species. *Marine Geology*, **100**, 207 – 248.

Woelk S, Quadfasel D (1996): Renewal of deep water in the Red Sea during 1982-1987. *Journal of Geophysical Research*, **101**, 18155-18165.

Wyrтки K (1971): *Oceanographic Atlas of the International Indian Ocean Expedition*. National Science Foundation Publication, OCE/NSF 86-00-001 Washington, DC, pp.531.

Wyrтки K (1973): Physical oceanography of the Indian Ocean. In *The Biology of the Indian Ocean*. Ed. B. Zeitzschel, Springer-Verlag, New York, pp. 18-36.

Yadava MG, Ramesh R (2005): Monsoon reconstruction from radiocarbon dated tropical Indian speleothems. *The Holocene*, **15**, 50-62.

You Y, Tomczak M (1993): Thermocline circulation and ventilation in the Indian ocean derived from water mass analysis, *Deep Sea Res.*, **40**, 13-56.

Zahn R (1994): Fast flickers in the tropics. *Nature*, **372**, 621-622.

Zonneveld KAF, Ganssen G, Troelstra S, Verstheegh GJM, Visscher H (1997): Mechanisms forcing abrupt fluctuations of the Indian Ocean summer monsoon during the last deglaciation. *Quaternary Sci. Rev.*, **16**, 187-201.